DOE/NBB-0067
DOE/NASA/0143-1
NASA CR-174813

2185

147 pages

9983

6-6
11-20

Research and Development of Neat Alcohol Fuel Usage in Automobiles

June 1984

Prepared for
National Aeronautics and Space Administration
Lewis Research Center
Under Grant No. NAG 3-143

for
U.S. Department of Energy
Assistant Secretary for Conservation
and Renewable Energy
Office of Vehicle and Engine R&D
Under Interagency Agreement DE-A101-77CS51044

DOE
Alcohol
Fuels
Program

Alternative
Fuels
Utilization
Program

DISCLAIMER

This report has been reproduced directly from the best available copy.

Available from the National Technical Information Service, U. S. Department of Commerce, Springfield, Virginia 22161.

Price: Printed Copy A08
Microfiche A01

Codes are used for pricing all publications. The code is determined by the number of pages in the publication. Information pertaining to the pricing codes can be found in the current issues of the following publications, which are generally available in most libraries: *Energy Research Abstracts, (ERA); Government Reports Announcements* and Index (*GRA* and I); *Scientific and Technical Abstract Reports (STAR);* and publication, NTIS-PR-360 available from (NTIS) at the above address.

DOE/NBB-0067
DOE/NASA/0143-1
NASA CR-174813
Distribution Category UC-926, UC-96

Research and Development of Neat Alcohol Fuel Usage in Automobiles

June 1984

Prepared by:
R.K. Pefley, Project Director
Co-Authors: L. Browning, S. Espinola,
B. Pullman, R. Gururangan, N. Saito

Mechanical Engineering Department
University of Santa Clara
Santa Clara California 95053
Under Grant No. NAG 3-143

Prepared for
National Aeronautics and Space Administration
Lewis Research Center
Cleveland, Ohio 44135

for
U.S. Department of Energy
Assistant Secretary for Conservation
and Renewable Energy
Office of Vehicle and Engine R&D
Washington, D.C. 20585

DOE
Alcohol
Fuels
Program

Alternative
Fuels
Utilization
Program

INDEX

List of Figures

List of Tables

CHAPTER I
INTRODUCTION

This grant has provided a unique opportunity to start the bridge between researching the basic feasibilities of alcohol (methyl, known hereafter as methanol and ethyl, known as ethanol) and commercializing these fuels as extenders and supplanters of petroleum in the transportation industry. A bridge is suggested because the research at Santa Clara started in 1968 with a National Air Pollution Control Agency (NAPCA) project investigating the clean burning aspects of methanol to reduce photochemical smog and ranged in 1979 to DOE sponsored alcohol fueled vehicles being demonstrated at the DOE Contractors Coordination Meeting in Detroit; on Capital Hill and at the DOE, Forrestal Building, Washington, D.C. in November of 1979. During that time frame four international alcohol fuel symposia as well as domestic meetings clearly established methanol and ethanol as the most likely near term alternatives to petroleum. They were shown to allow common power plants to continue to be produced throughout the transportation world. (the spark ignited, SI, and compression ignited, CI, engines) yet, allow a large number of countries to preserve or restore their liquid energy independence because they can be produced for coal, natural gas, tar sands, residual crude, shale oil and biomass.

This grant ranges in objectives from nearly basic research in the form of computer modeling of reactive thermofluid mechanics to commercial aspects where after-market conversion kits were engineered to change Post Office vehicles from gasoline to methanol and ethanol fuels. During this time frame pure alcohol fleet vehicle numbers have grown in the U.S from the range of 1-10 through the range of 10-100 and now are in the range of 100-1000.

While alcohol fuels have moved towards commercialization, two problems have not been satisfactorily resolved. These are: cold-start, warm-up driveability and corrosion and wear of fuel system and engine parts. Additionally, environmental factor assessments must continuously be made if the public is to be assured that the alcohols are more beneign than petroleum in terms of environmental, health, and safety factors.

This report is a synopsis of the work designed to push the alcohols along the path of acceptance, for it is believed that properly engineered they will allow the world finally to balance its transportation energy requirements with the energy harvested from the sun, thereby freeing transportation energy from petroleum and oppressive prices associated with monopolies.

The report is heavily keyed to the references which include all of the publications associated with the grant. In effect, it is a summary of this evidence which may be found in greater detail elsewhere in the literature.

CHAPTER II

COMPUTER MODELING OF ENGINE PROCESSES

Computer modeling of complex engine processes has been successfully used in research investigations at the University of Santa Clara to provide a better understanding of trends in engine performance and pollutant emissions produced from our laboratory tests and found in the literature. By using a mix between theory and empiricism, these models have greatly added to our knowledge about various aspects of utilizing alcohols in automotive engines. Unless noted otherwise, all modeling is based on the physical dimensions of the 2.3 liter engine as found in Ford Pinto vehicles.

II.1 COMPUTER AIDED DESIGN STUDY FOR POST OFFICE PROTOTYPE ALCOHOL VEHICLES

A computer model that simulates the second-by-second driving cycles, such as the Federal Test Procedure, was used in this study to examine the effects of changes in fuel type, compression ratio, rear axle ratio and reduction of parasitic loads on energy economy and exhaust emissions. Three driving cycles were defined for this study: the urban driving cycle, the highway driving cycle and the Post Office delivery cycle. Steady-state performance and emissions maps taken from our engine-dynamometer facility were used as inputs to this model. The model, however, does not consider engine warm-up periods or transient performance. The model has been shown to yield economy figures comparable to actual vehicle tests; however, the emissions figures are most useful when compared to other simulated runs [II.1].*

II.1a Fuel Type Comparisons

Three fuels, methanol, ethanol and gasoline, were compared for all three driving cycles. Methanol showed substantial improvements in energy economy over gasoline in all tests. At an average equivalence ratio** of 0.9, methanol showed 18%, 14% and 26% improvement over gasoline for the urban, highway and

---

* [ ] Denotes references at the end of the Chapter.

** Stoichiometric air/fuel (A/F) ratio divided by actual air/fuel ratio.

Post Office driving cycles respectively. Ethanol showed 11%, 12% and 11% improvement over gasoline for the same comparisons. The engine exhaust NO_x emissions from methanol were considerably lower than for gasoline under the same conditions while the other emissions remained about the same. Ethanol, however, showed a substantial increase in hydrocarbon emissions and a substantial decrease in CO emissions while NO_x emissions remained about the same as for gasoline.

II.1b Compression Ratio Comparisons

Increasing the compression ratio seemed to have little effect on energy economy for methanol. Raising the compression ratio from 8.5 to 11.3 increased the energy economy 9%, 14% and 5% for the urban, highway and Post Office Driving cycles. Since raising the compression ratio increases power, a lower throttle setting must be used to maintain the same power level at a given speed. By doing this, the engine is forced to operate at a lower thermal efficiency due to increased exhaust dilution which can offset thermal efficiency gains from raising the compression ratio. Due to the faster burn rate of the 11.3 compression ratio engine, NO_x emissions were shown to be 31% lower than the 8.5:1 engine [2], due to MBT timing closer to TDC and less time at high temperatures and pressures for NO_x formation. Hydrocarbon emissions however rose 118% over the standard 8.5:1 engine.

II.1c Rear Axle Ratio Comparisons

As stated in the previous section, raising compression ratio without increasing the load on the engine results in decreased efficiency. By lowering the rear axle ratio while raising compression ratio, the load on the engine is increased for the same power output at the wheels. Using methanol in the 11.3 compression ratio engine, it was found that lowering the rear axle ratio from 3.08 to 2.73 gave an additional fuel savings of 5%, 12% and 7% respectively for the urban, highway and Post Office driving cycles.

II.1d Reduction of Parasitic Cooling Loads

Since the alcohols have much higher heats of vaporization than gasoline, the internal cooling effects of fuel vaporization in the cylinders is much greater. With this in mind, an alcohol engine can be designed with a smaller cooling system thereby reducing the parasitic cooling loads. The easiest way of accomplishing this would be to disconnect the cooling fan and water pump from the engine and drive them electrically, on an as-needed basis. In order to see the effects of this modification, the model was run with and without the cooling fan and water pump in the accessory loads. Again using the 11.3 compression ratio engine with methanol, 6%, 5% and 3% gains in energy economy can be realized on the urban, highway and Post Office driving cycles respectively by removal of the fan only, while an 8%, 7% and 5% gain can be realized for removal of the fan and water pump.

II.1e Summary

The computer-aided design study presented here indicates gains in fuel economy and reductions in emissions by all of the alcohol conversions considered. The computer model suggests that conversion to methanol yields the best energy economy. Raising compression ratio shows substantial fuel economy benefits but results in a HC emission penalty. The rear axle ratio change and removal of the engine cooling components shows slight fuel economy and emissions benefits but should be weighed against conversion costs.

In the future, alcohol fueled engines will be smaller than their gasoline counterparts enabling them to more effectively exploit the properties of the alcohols and derive the anticipated fuel economy.

As a last word of caution, it should be noted that the data taken for the driving cycle simulations was taken from a fully warm, dynamometer-mounted engine operated at steady-state conditions and did not include transient engine behavior or warm-up performance and emissions. These factors need to be taken into account before a final decision is made on the modification package for a vehicle with a gasoline engine.

II.2 NO_x CONTROL TECHNIQUES FOR METHANOL FUELED SI ENGINES

While alcohol fuels are generally clean burning fuels, air pollution problems existing in major cities throughout the world will eventually require emissions controls on all combustion sources. Since oxides of nitrogen (NO_x) emissions are fundamental in the formation of photochemical smog and the hardest emissions to control, a review of NO_x control techniques is presented. With this study, NO_x control methods can be considered without large penalties in performance or other exhaust emissions and experimental costs.

The method used to study these NO_x control techniques is a fundamental spark ignition (SI) engine computer model. This approach is used since the interaction between engine design and operating variables is sufficiently complex that a fundamental model is essential in interpreting performance and emissions results from a spark ignition engine. A fundamental model employs current knowledge and semi-empirical formulations of combustion and pollutant formation processes occurring during an SI engine cycle to predict, in a reasonably expedient and low-cost fashion, the results of various changes in engine design and operating variables. The results from this kind of study can be used to guide experimentalists in interpreting their results and engine designers in screening various concepts in engine design prior to expensive hardware development and testing.

II.2a The Computer Model

The computer model used in this study has been under continuous development for the past ten years and uses methanol as a fuel. During this time, various highlights of this model have been presented in the literature [II.2,3,4,5,6]. The model is a combination of two submodels, the kinetic Otto cycle submodel and the kinetic exhaust submodel. The kinetic Otto cycle submodel includes both thermodynamic and chemical kinetic considerations of processes occurring during the intake, compression, combustion and expansion phases of the actual SI engine cycle [II.2]. Modifications to the model to incorporate squish chamber cylinder head geometry are outlined in Ref. 3. This model uses a detailed high-temperature chemical kinetic reaction mechanism [II.5] to define methanol

oxidation, and pollutant emissions formation of carbon monoxide (CO) and NO_x during the combustion and expansion phases of the engine cycle.

The kinetics exhaust submodel is a one-dimensional fluid mechanics model of the exhaust port and manifold which applies a detailed low-temperature kinetics reaction mechanism [II.5] to predict unburned fuel (UBF) and aldehyde (ALD) formation during the exhaust event [II.6].

Further refinements to the kinetic exhaust submodel stem from theories found in recently published papers on the hydrocarbon quench layer [II.7,8,9]. These studies suggest that under normal operating conditions, wall quenching is not an important source of exhaust hydrocarbons. This is due to rapid diffusion and burn-up of quenched hydrocarbons on a millisecond time scale without formation of significant aldehydes [II.8]. These studies suggest that exhaust hydrocarbons result from ring crevice storage and absorption-desorption of hydrocarbons in the lubricating oil. Earlier studies by Wentworth have shown up to 74% reductions in exhaust hydrocarbon concentrations by eliminating the ring crevice [II.10]. Thus a submodel utilizing ring crevice storage was formulated to calculate input hydrocarbon concentrations for the kinetic exhaust model. This ring crevice storage model assumes that half of the unburned fuel existing in the ring crevice at the end of combustion exits the crevice during the expansion stroke and is subsequently burned in the bulk cylinder gases before the exhaust valve opens. It is also assumed that 10% of the unburned fuel in the ring crevice does not exit the engine cylinder during the exhaust event. The remaining 40% exits the cylinder under the following assumptions. One-half of the exiting unburned fuel is evenly entrained in the bulk cylinder flow during the time 90% of the cylinder charge (minus exhaust residual) is exhausted from the cylinder. The remaining half exits the cylinder with the remaining 10% of the bulk cylinder charge but at five times the concentration level. These assumptions result in exiting hydrocarbon concentration profiles similar to those found in experimental studies [II.11,12].

The method above was used in calculating input hydrocarbon levels for the exhaust model in all but the exhaust gas recirculation (EGR) study. In this part of the study, additional sources of unburned fuel emissions needed to be considered. One such source resulted from reducing manifold vacuum as EGR was

added to maintain the same volumetric efficiency. This tends to increase fuel flow through the cylinder during the valve overlap period due to scavenging. Also as EGR is added, there is a general degradation from good burns to slow burns [II.13], thereby increasing unburned fuel emissions. Calculations using only ring crevice volume resulted in decreasing input hydrocarbon concentrations with increasing EGR. Thus for this part of the study, the input hydrocarbon concentration was calculated for the no EGR case using the ring crevice model and then used for all EGR addition cases as well.

Run times for the entire engine cycle simulation were typically 1100 seconds on a CDC 7600 computer. This provided the best compromise between computer time and numerical accuracy. A discussion of model tuning can be found in Ref. 5.

II.2b Spark Retard Effects

In a spark ignition engine, spark timing has a large influence on the combustion process and, thus, on power, thermal efficiency and emissions. As shown in Fig. II.1, NO_x emissions decrease rapidly as the spark is retarded from MBT (minimum spark advance for best torque) due to burning later in the cycle and, thus, at lower peak temperatures and pressures. The CO emissions tend to decrease with spark retard due to higher temperatures during the expansion stroke. Unburned fuel emissions also tend to decrease with spark retard due to higher exhaust temperatures. Aldehydes, however, peak slightly retarded of MBT, then decrease with more retard. While the increasing exhaust temperatures tend to react more unburned fuel into aldehydes as the spark is retarded, the amount of unburned fuel in the ring crevice decreases with spark retard due to lower peak pressures. The later becomes the overriding effect for the spark slightly retarded from MBT, thereby causing the aldehyde emissions to drop as the spark is retarded further. Pischinger [II.14] found similiar results for lean mixtures, but found a steady increase in aldehyde emissions with spark retard for rich mixtures.

II.2c Compression Ratio Effects

Due to the high octane number of methanol, higher compression ratios can be used without engine knock. In conventional engines, squish chamber combustion

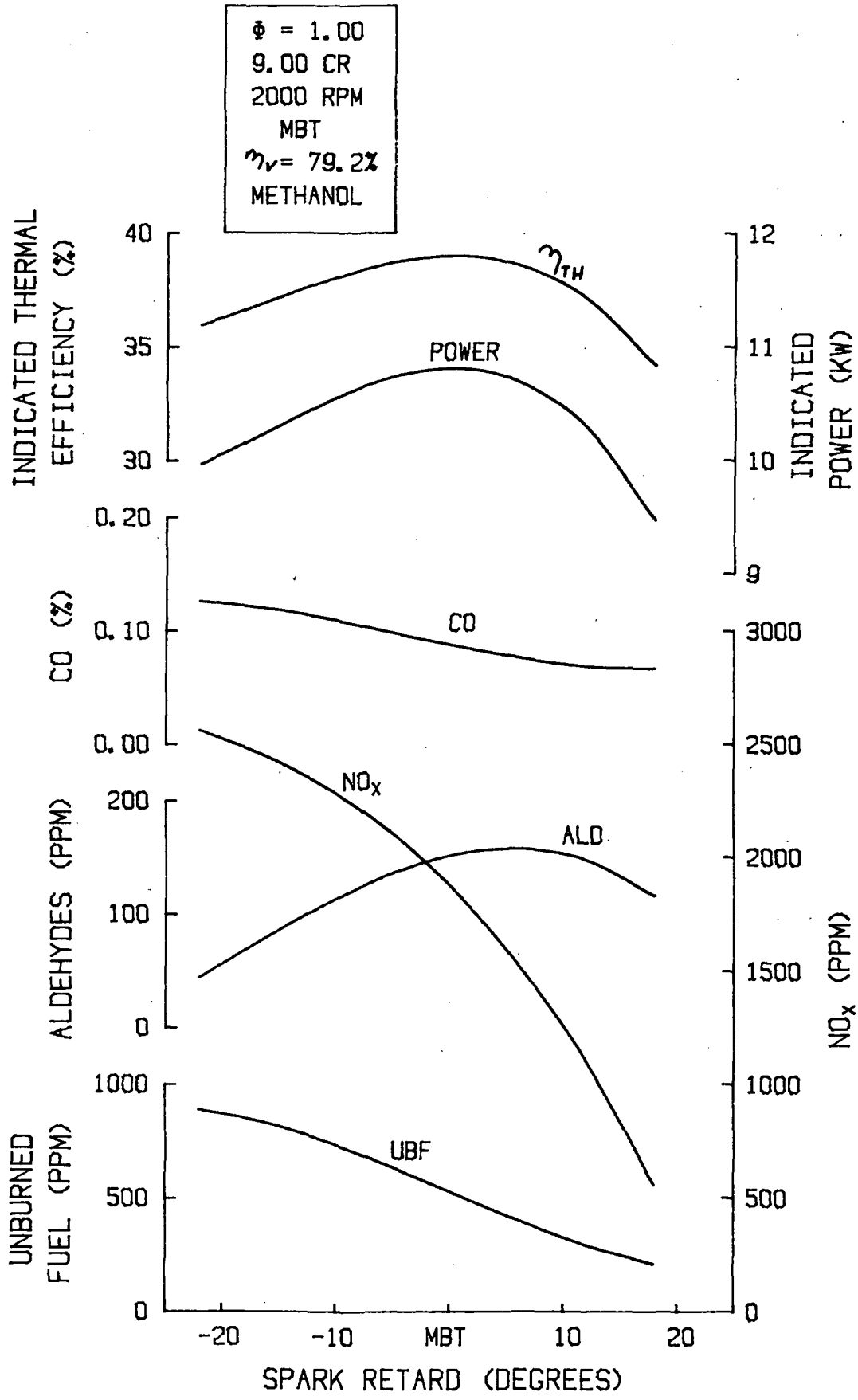

FIGURE II.1: SPARK RETARD EFFECTS

chamber geometry is used to minimize knock by reducing pressure rise rates at the end of combustion and increasing surface area for heat transfer to occur. Near the end of combustion the slower burning rates due to squish and the increased heat transfer to the unburned gas minimizes end gas heating and thus knock.

In this study, two methods of raising compression ratio are examined. The first method maintains the same open-to-squish chamber volume ratio at top dead center (TDC) while compression ratio is raised. This maintains the same relative squish velocities with varying compression ratio and would have relatively the same effect on power and emissions as raising the compression ratio in a flat head engine. This method is best accomplished by piston crown redesign. The second method maintains the same squish chamber clearance height while compression ratio is raised. Thus, compression ratio is increased by lowering only the open chamber height. This results in increased squish velocities as compression ratio is raised (in comparison to method one), thereby reducing the overall in-cylinder turbulence levels. This method is normally accomplished by milling the cylinder head.

With the first method, NO_x increased 29.6% by increasing the compression ratio from 9:1 to 15:1 due to higher peak pressures and temperatures as shown in Fig. II.2. Unburned fuel emissions rose 108.5% for the same comparison due to increased ring crevice storage and decreased exhaust temperatures. Aldehyde emissions, however, decreased 43.9% due to the lower exhaust temperatures, thereby reacting less unburned fuel during the displacement flow period of the exhaust when aldehyde emissions are generally formed [II.5]. The CO emissions rose 14.7%.

Using the second method, the increased turbulence levels and burning rate tended to limit the increase in NO_x and CO emissions as shown in Fig. II.3. By raising the compression ratio from 9:1 to 15:1 by this method, NO_x emissions rose 21.8%, UBF emissions rose 109.8% and CO emissions rose 25.3%. Aldehyde emissions, however, decreased only 19.3%. The trends of aldehyde emissions with compression ratio shown in Fig. II.3 are similar to the trends found by Pischinger [II.14] using a similar method to raise compression ratio. Power and thermal efficiency rose 15% for the same compression ratio increase.

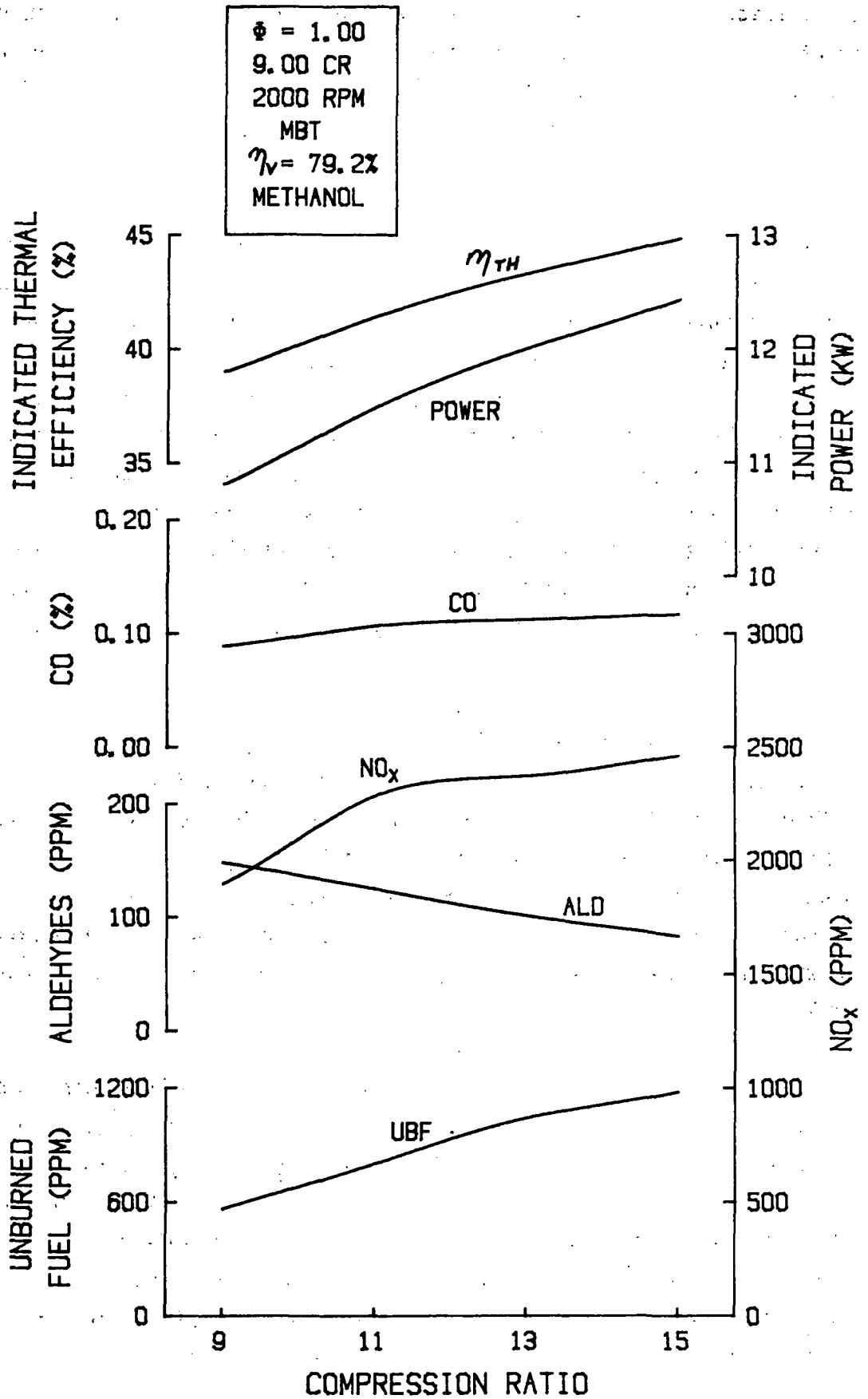

FIGURE II.2: COMPRESSION RATIO EFFECTS CONSTANT OPEN-TO-SQUISH VOLUME RATIO

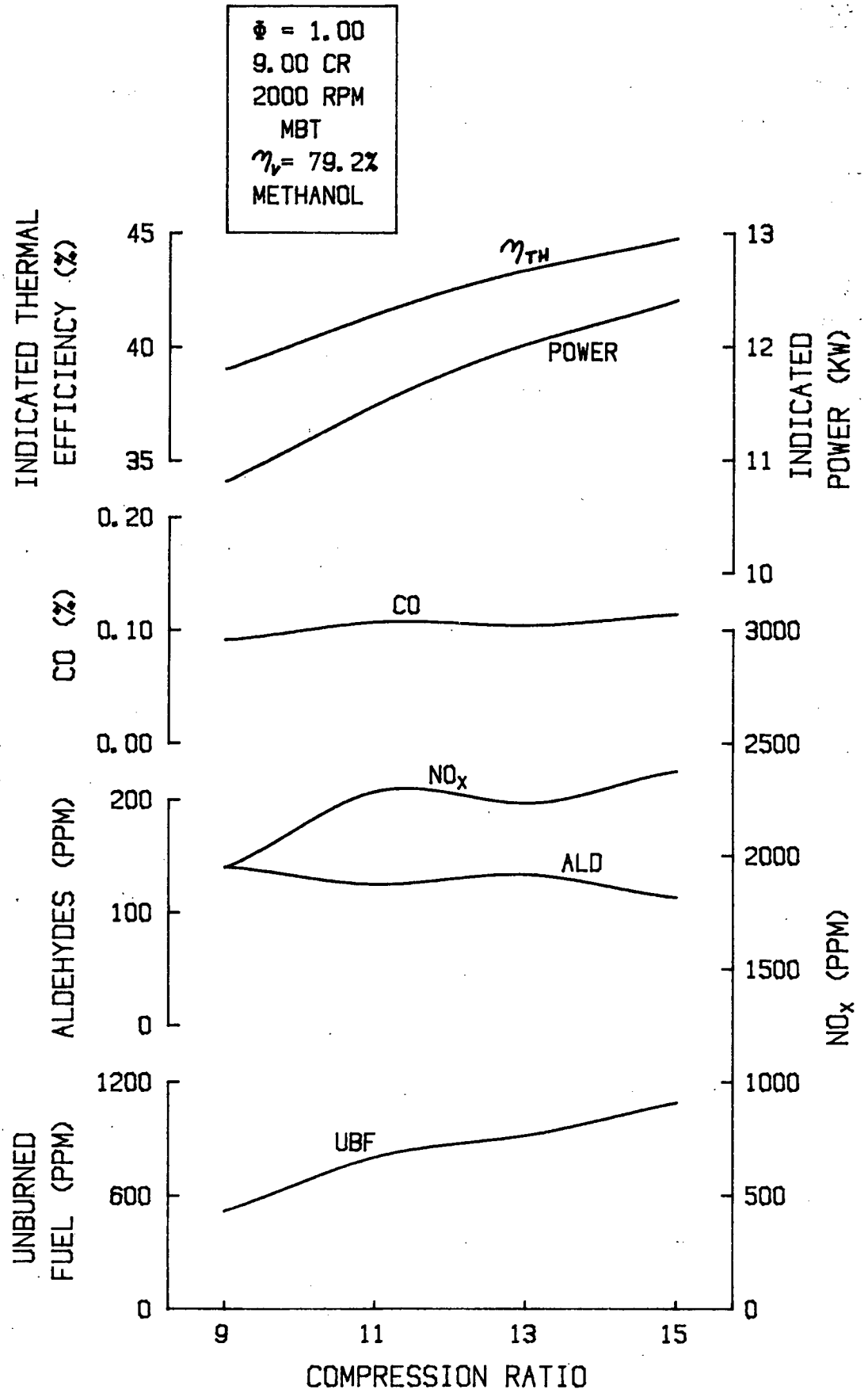

FIGURE II.3: COMPRESSION RATIO EFFECTS CONSTANT SQUISH CLEARANCE HEIGHT

II.2d EGR Effects

In the EGR study, volumetric efficiency was maintained as EGR was added. A throttled condition was chosen for this study to compensate for the increased cylinder charge due to holding the volumetric efficiency constant while adding EGR. Furthermore, the inlet charge temperature was allowed to rise with EGR addition due to the mixing of the hot exhaust ($600^{o}K$) with the cold incoming charge ($289^{o}K$). This raised the inlet temperature substantially from $298^{o}K$ for the no EGR case to $392^{o}K$ for the 30% EGR addition at the 65% volumetric efficiency condition. The increase in inlet temperature as EGR was added more than compensated for the decreased burning velocities, thereby raising both power and thermal efficiency as shown in Fig. II.4. Power and thermal efficiency rose 8.5% with 30% EGR over the no EGR case, while NO_x emissions dropped substantially showing a 97.2% reduction for the above comparison due to lower peak cylinder temperatures and pressures. These results are consistent with other investigators [II.1,15]. Unburned fuel emissions increased 55.8% for the above comparison due to decreasing exhaust temperatures and oxygen concentration. This matches trends found in our laboratory [II.1]. The EGR effect reduced aldehyde emissions 88.3% and CO emissions dropped 70.7% for the same comparison. Another interesting point was observed. As the exhaust temperature decreases, more of the NO is converted to NO_2. For the no EGR case, only 8.2% of the NO_x is NO_2, while 30% EGR yields 49% of the NO_x as NO_2.

It is evident that EGR is an effective method of reducing NO_x emissions without large increases in UBF emissions.

II.2e Summary

A thermokinetic computer model was used to study the effects of simple NOx control techniques on performance and exhaust emissions. A ring crevice storage model was also formulated for predicting unburned fuel emissions. The study showed spark retard to be an effective method of reducing NO_x, CO and UBF emissions at the expense of power, thermal efficiency and aldehyde emissions. It was also shown that upon raising the compression ratio in a squish chamber engine, the rise of NO_x and CO emissions could be limited, but not without an aldehyde penalty. Exhaust gas recirculation, however, was shown to be a very

effective method for reducing NO_x, CO and aldehyde emissions with only a slight UBF emission penalty. It appears from the studies that use of EGR in high compression methanol fueled engines with increased turbulence to reduce cycle-to-cycle variations will both maximize power and thermal efficiency while minimizing harmful exhaust emissions.

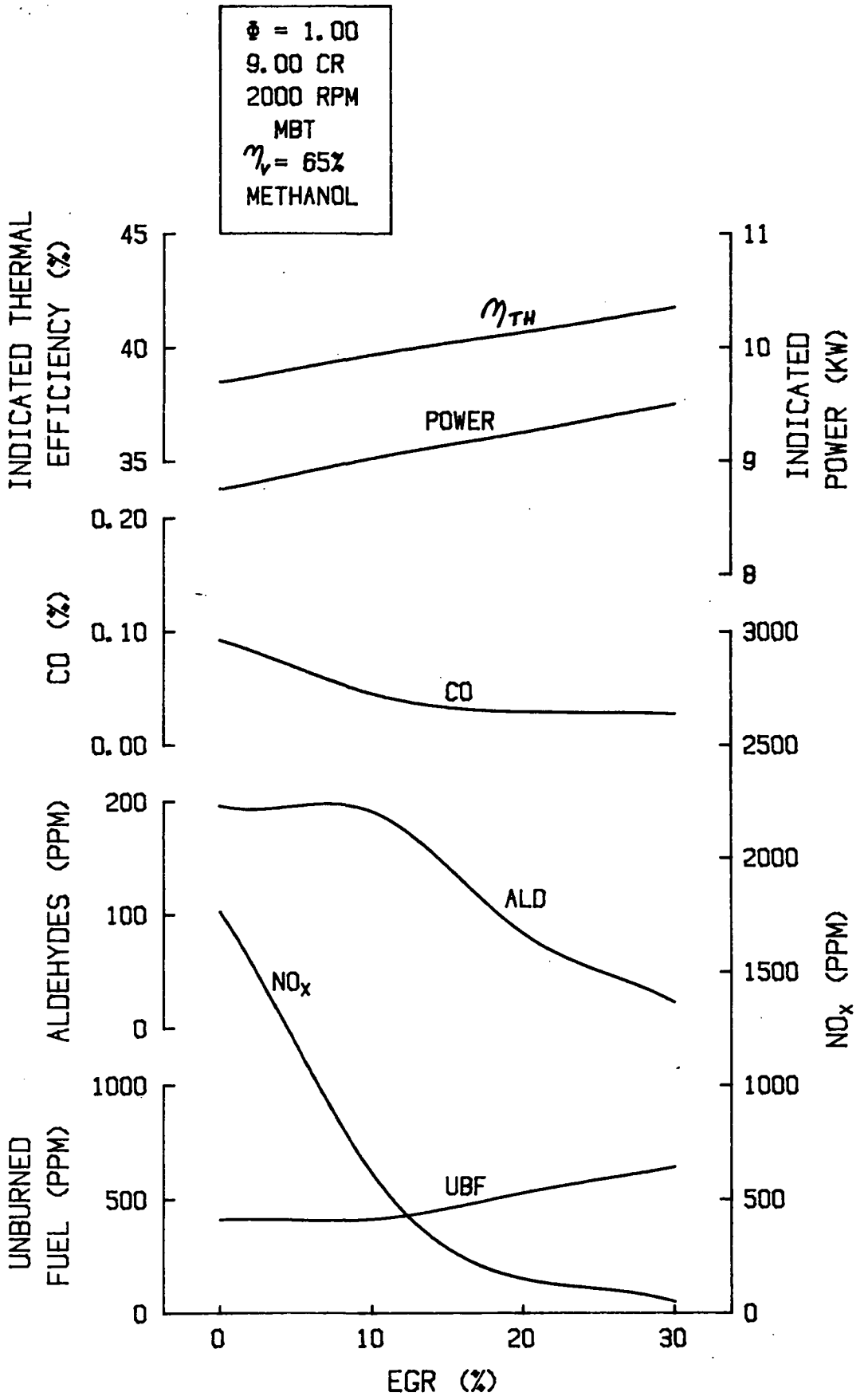

FIGURE II.4: EGR EFFECTS

II.3 COLD START ENGINE PROCESS MODELING

Cold startability of an alcohol fueled vehicle is a vital issue since the methods used to improve cold starting can affect warm-up driveability, emissions and engine wear. As seen in Figs. II.5 and II.6, one of the cold starting problems with alcohol fuels involves their low vapor pressures. If methanol is inducted into a manifold at one atmosphere, the saturated vapor/air equivalence ratio moves outside the lean flammability limit at a temperature of $12^{o}C$ while ethanol moves outside the lean flammability limit at $14^{o}C$. Under hard choking conditions (0.67 atm manifold pressure) methanol moves outside the lean flammability limit at $5^{o}C$ while ethanol moves outside the lean flammability limit at $8^{o}C$. Thus vaporization of alcohols in the intake manifold cannot be relied upon for cold weather starting.

Current technology in alcohol fueled vehicles utilizes auxiliary starting aids for enhancement of cold starting [II.16,17]. These aids are generally fuel additives, auxiliary fuels, electric heat addition and dissociation or reformation of alcohol. While all these methods will provide a cold start at low ambient temperatures, there is a short period of time following the cold start in which intake manifold temperatures drop instead of rise and smooth operation is difficult to obtain. It is this period which requires more than the one-shot approach of auxiliary fuel devices which can provide starting. Such systems must be capable of supplying auxiliary fuel during part of the warm-up, but this complicates the necessary cold start hardware. Electric heat addition will assist in cold starting and warm-up in mild climates [II.3], however the amount of electrical energy necessary to vaporize enough fuel for even idle conditions can become prohibitive [II.17]. Dissociation or reformation of alcohols is a very attractive method of providing cold starting enhancement since the hydrogen gas it produces will allow starting at almost any temperature and the gas will not recondense. However, large amounts of heat are necessary to dissociate the alcohol and it is difficult to produce enough dissociated gases for the warm-up period [II.3]. Finally alcohols can be tailored with such fuel additives as butane, iso-pentane, gasoline and di-methyl-ether, to start at low ambient temperatures, but these additives increase the cost, safety hazards and emissions of the fuel. With these facts in mind, it can be concluded that the ultimate solution to the cold starting problem has not yet been developed.

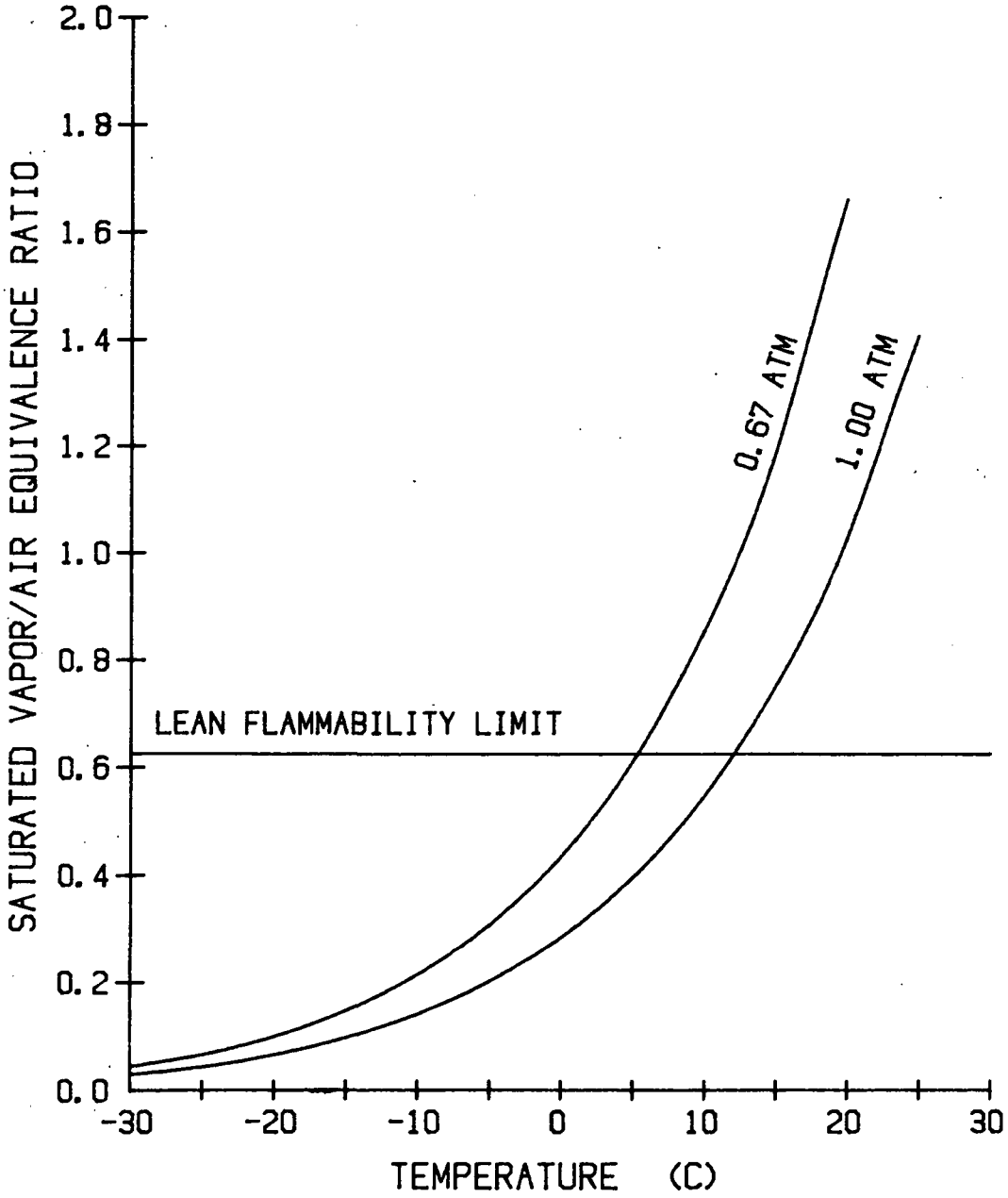

FIGURE II.5: SATURATED VAPOR/AIR EQUIVALENCE RATIO VERSUS TEMPERATURE FOR METHANOL

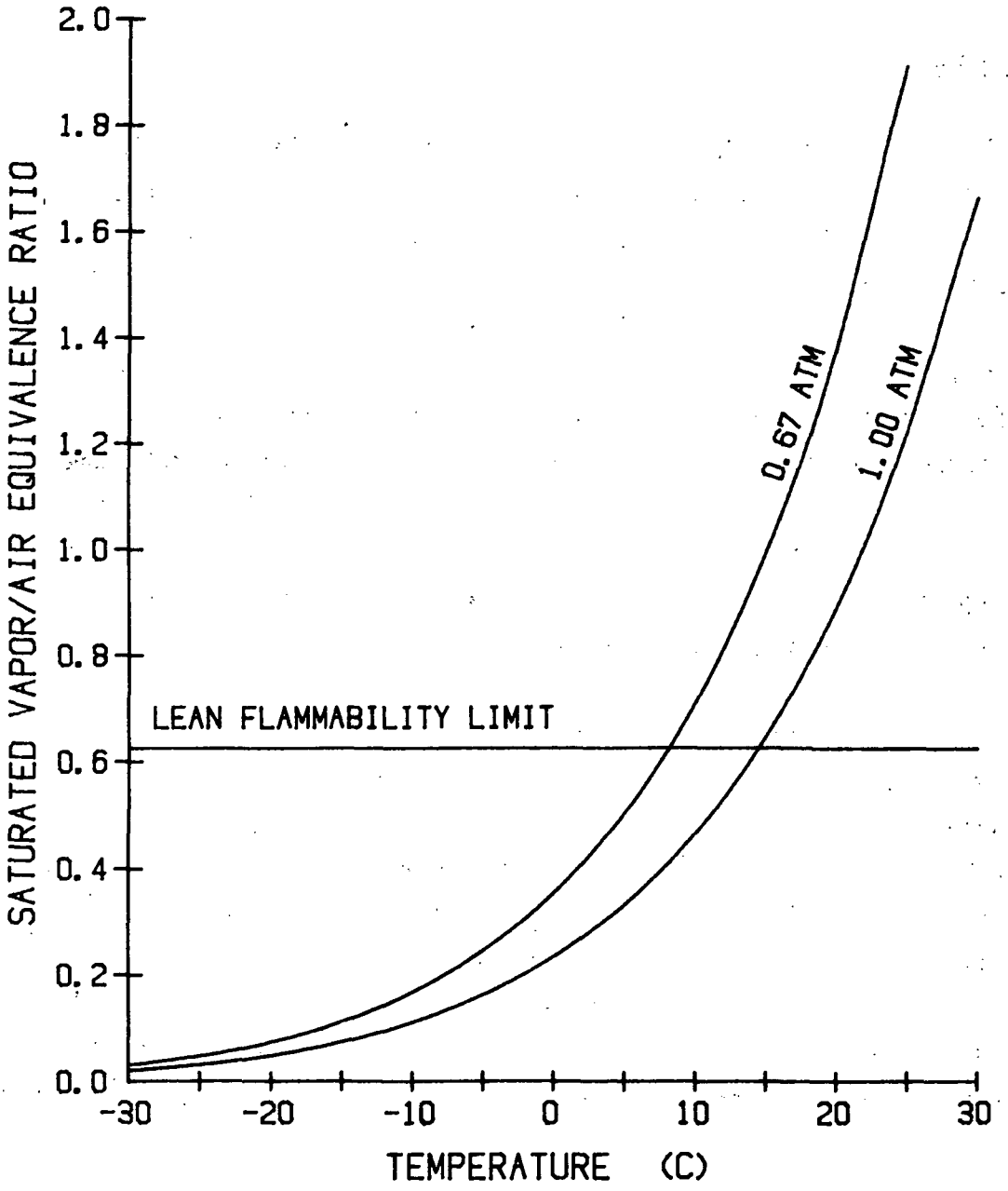

FIGURE II.6: SATURATED VAPOR/AIR EQUIVALENCE RATIO VERSUS TEMPERATURE FOR ETHANOL

Part of the solution to the cold starting problem with alcohol fuels could be more effective fuel transport and vaporization as they mix with the air. If enough fuel can be inducted into the cylinder in a finely atomized fog, the work of compression might vaporize enough fuel to provide a flammable mixture at the end of the compression stroke [II.3]. The object of this study is to provide a theoretical analysis of droplet transport and fuel evaporation in the intake manifold and engine cylinder during the intake and compression strokes and to identify certain important design parameters affecting these phenomena. This has been accomplished through a series of three separate models, the Droplet Fall-Out and Sling-Out Model, the Compression Process Model and the One-Dimensional, Two-Phase Cold Start Engine Model.

II.3a Droplet Fall-Out and Sling-Out Model

A simple fluid dynamics model, shown in schematic form in Fig. II.7, was formulated to study the effects of droplet size and air stream velocity on the transport of a droplet along a two dimensional intake runner. This model assumes that there is no droplet vaporization in the intake runner, the air stream velocity is constant and uniform throughout the runner (plug flow) and the droplets are uniformly dispersed and do not interact. Dimensions for the runner model are from a Ford 2.3 liter four cylinder engine intake manifold. The droplet momentum equation is solved in Lagrangian form for both the x and y directions and can be found in Ref. 18. At the start of the calculations, the droplets enter the center of the runner with no initial velocity. The aerodynamic drag forces on the droplet from the moving air stream and gravity act on the droplet as it moves along the runner.

In Fig. II.8, an air stream velocity of 275 cm/sec was used to simulate a cranking speed of 200 RPM. Droplet trajectories for various sized droplets are plotted within the intake runner. As can be seen from this figure, the 10 and 30 micron ( ) droplets will enter the cylinder while a 50 droplet can fall out of the air stream before entering the cylinder. The 100 droplet is shown to be slung out in the manifold corner. The larger droplets, having lower surface to volume ratios react more to gravitational than aerodynamic forces and the higher downward momentum during their travel in the down-draft section of the intake runner cannot be overcome. Shortening of this down-draft section did not

INTAKE MANIFOLD DROPLET FALL-OUT AND SLING-OUT MODEL

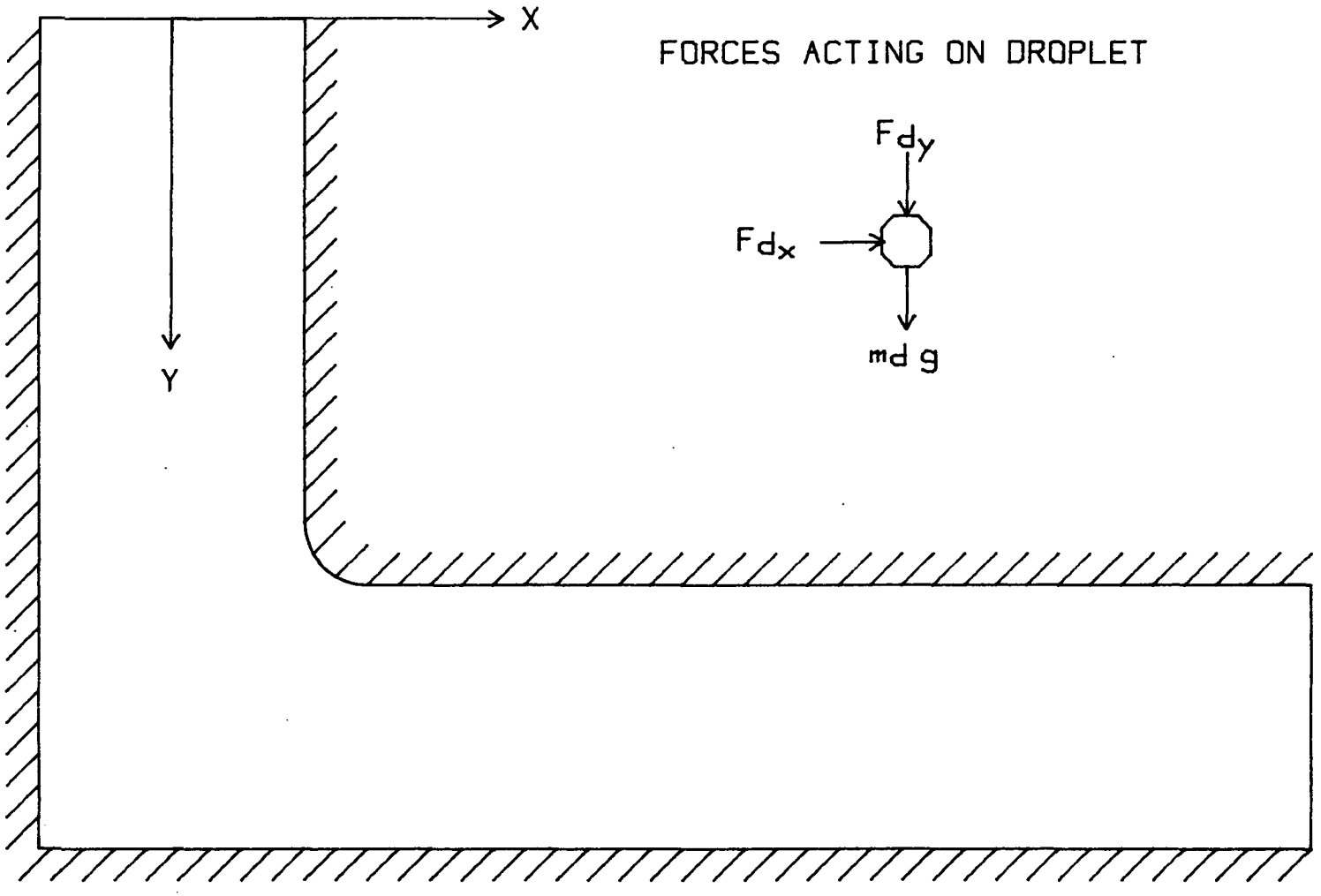

FIGURE II.7: DROPLET FALL-OUT AND SLING-OUT MODEL SCHEMATIC

INTAKE MANIFOLD DROPLET FALL-OUT AND SLING-OUT MODEL
AIR STREAM VELOCITY 275 CM/SEC

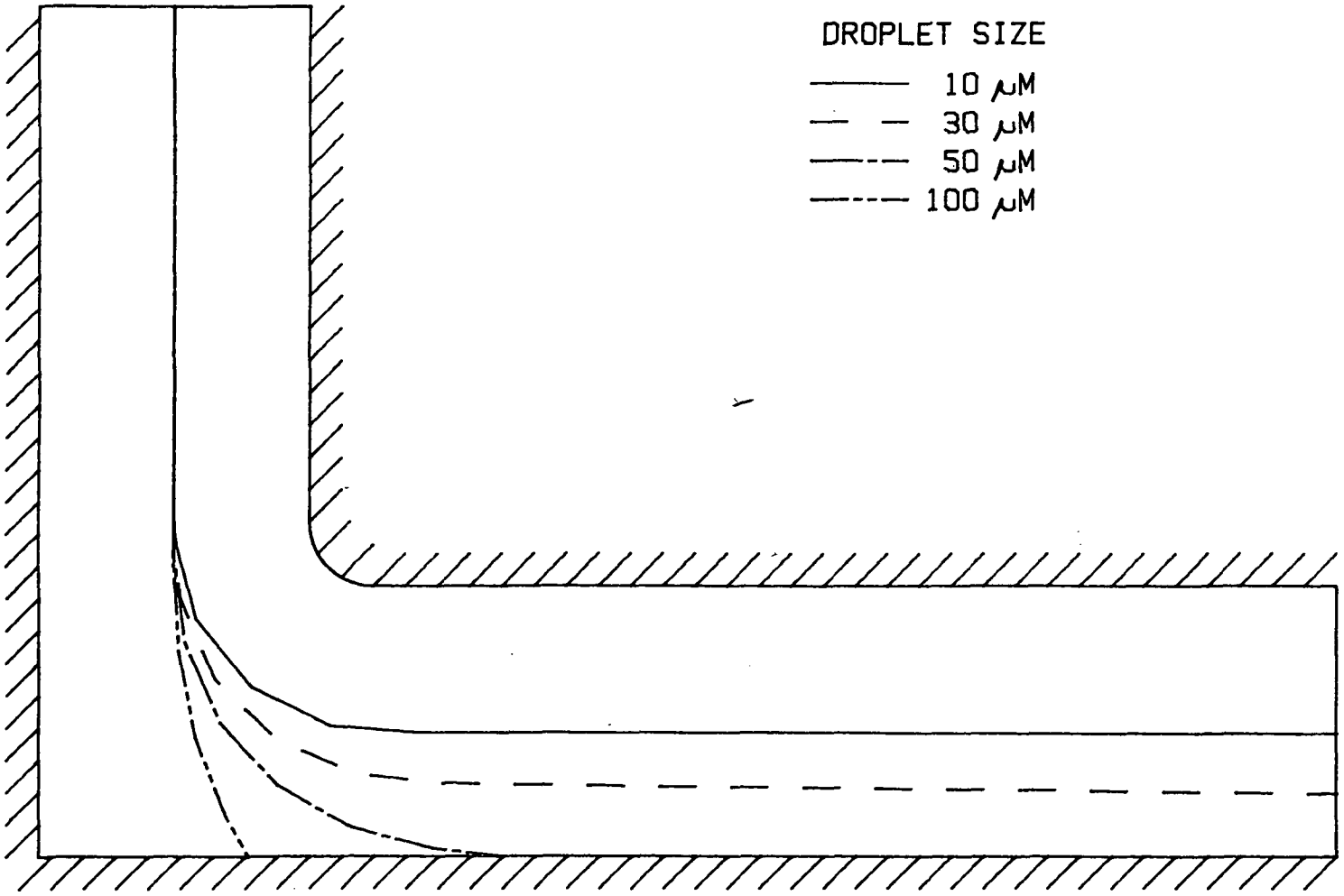

FIGURE II.8: DROPLET SIZE EFFECTS ON DROPLET TRAJECTORY

have much effect on this problem as the larger droplets reach terminal velocities in very short distances.

Figure II.9 shows the effect of air stream velocity (or cranking speed) on the trajectory of a 50 droplet moving in a horizontal plane. As can be seen from this figure, the slower the air stream velocity (slower cranking speeds), the larger the chance of the droplet entering the cylinder. This implies that the centrifugal force is the the significant effect in droplet fall-out. For the 275 cm/sec case, the centrifugal force is over 25 times the gravitational force indicating gravitational forces can be neglected in manifold design for this droplet size and air speed range.

II.3b Compression Process Model

The compression process model examines the fate of droplets in the cylinder during the compression process. The following assumptions are made to simplify the analysis: (1) well stirred cylinder fluids, (2) all the fuel is in droplet form at the beginning of the compression stroke, (3) an ideal mixture of air and fuel vapor, (4) all droplets are of the same size and temperature, (5) all droplets are in suspension during the compression stroke and (6) all cylinder surface areas remain at a constant temperature.

The conservation equations are derived separately for the droplets and for the gaseous mixture of fuel vapor and air and are listed in Ref. 18. Minimum engine starting temperatures for methanol and ethanol are defined here to be the temperatures at which the end of compression vapor/air equivalence ratio is at the lean flammability limit (LFL) of 0.63 [II.19].

The compression process model was first used to examine the effects of fuel vaporization on cylinder pressure and temperature. Using starting conditions of 298.15^{o}K, manifold pressure of 0.775 atmospheres and a stoichiometric mixture of 50 liquid fuel droplets and air at the intake valve closing point of 60 degrees after bottom dead center (ABDC), a compression ratio of 10 to 1 and a cranking speed of 200 RPM, Fig. II.10 shows a comparison of cylinder pressures during the compression stroke for air only, air plus methanol, and air plus ethanol. As can be seen from this figure, there is a substantial reduction in final cylinder

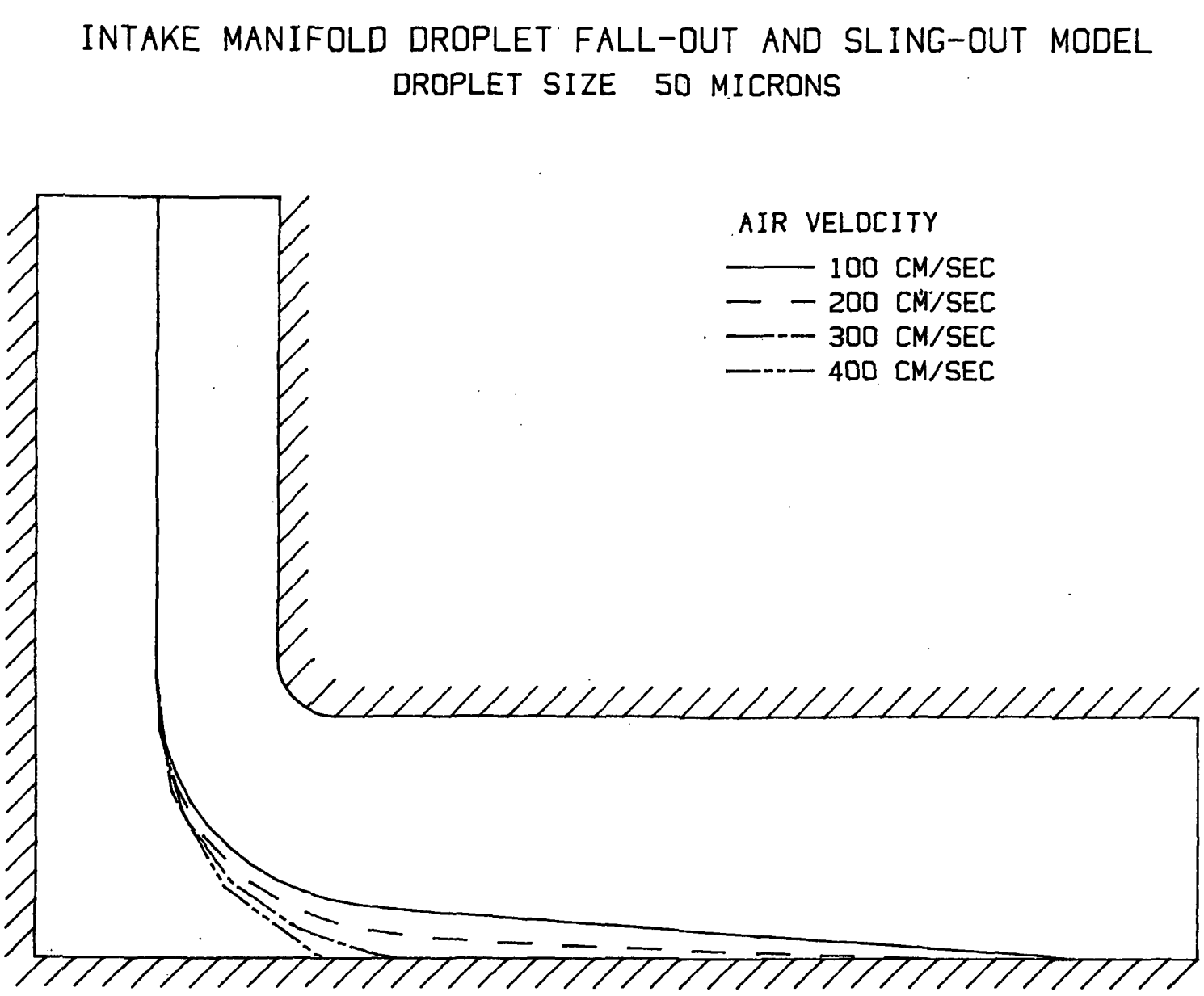

FIGURE II.9: CRANKING SPEED EFFECTS ON DROPLET TRAJECTORY

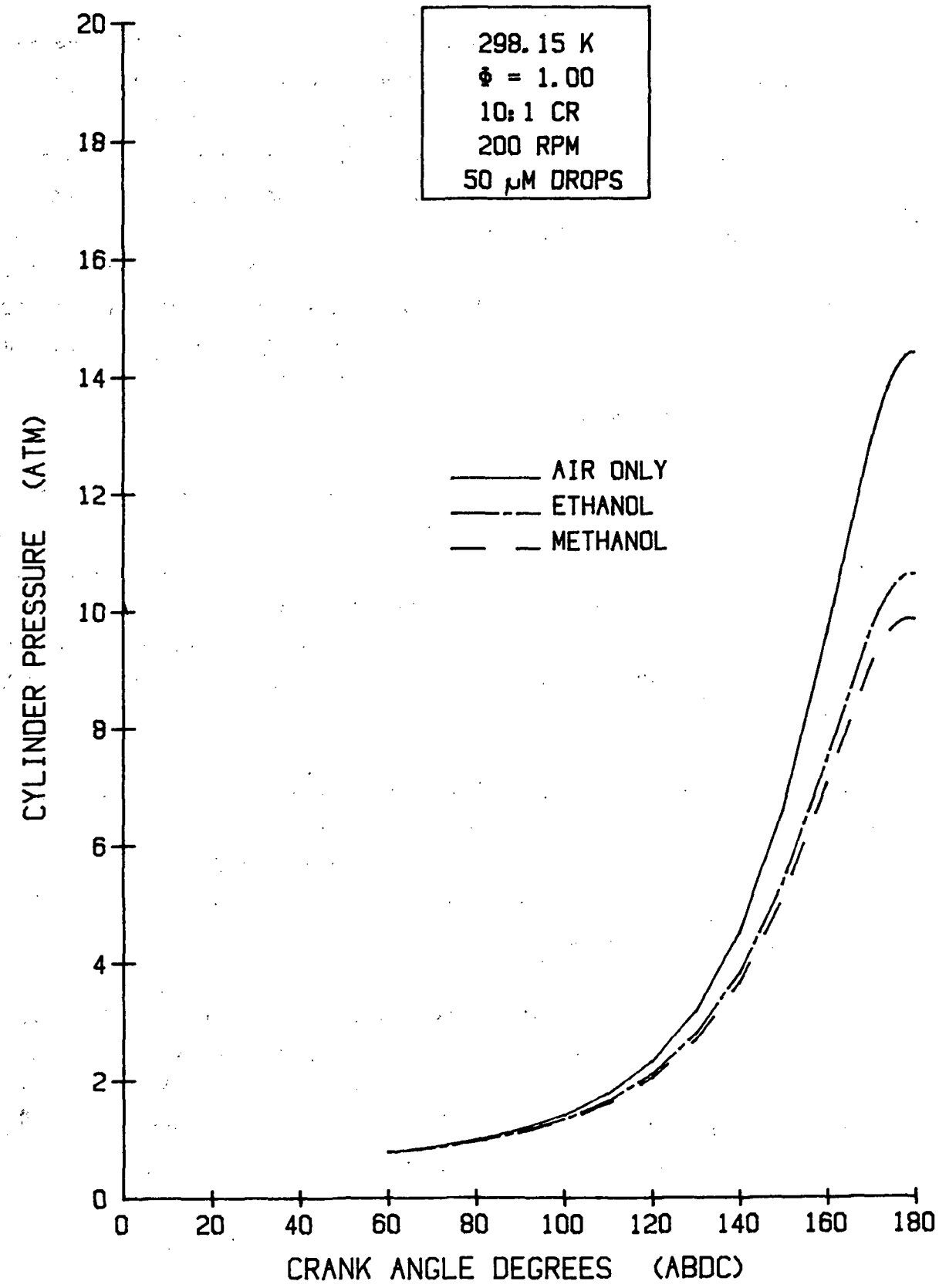

FIGURE II.10: CYLINDER PRESSURE FOR ROOM TEMPERATURE CRANKING

pressure due to fuel vaporization in the air plus fuel cases. As expected, methanol shows the greater reduction in final cranking pressure due to its high latent heat and its larger fuel mass for a stoichiometric mixture in comparison to ethanol.

Figure II.11 shows the cylinder temperature versus crank angle for the same comparison. As expected, methanol shows the greater reduction in final cylinder temperature due again to its high heat of vaporization and increased fuel mass. Fig II.12 shows the fuel vapor/air equivalence ratio (lower curves) and droplet size (upper curves) during the compression process for the above comparison. As can be seen, both methanol and ethanol exceed the lean flammability limit (vapor/air equivalence ratio of 0.63) at the end of compression stroke for room temperature starting conditions. It also shows that ethanol droplets vaporize more readily due to its lower heat of vaporization and decreased mass for the same equivalence ratio. It should be noted that mass/ heat transport rates and not vaporization saturation control the final values.

Fig. II.13 shows the end of compression fuel vapor/air equivalence ratio versus starting temperature for methanol and ethanol holding all other starting conditions constant. As can be seen from this graph, methanol has a minimum cold starting temperature of $18^{o}C$ for 50 drops while ethanol has a minimum cold starting temperature of $-12^{o}C$. Since methanol presents a much harder challenge in cold starting based on this modeling study, the following study is limited to methanol only.

Fig. II.14 shows the effect of droplet size on minimum starting temperature. As can be seen from this figure, droplet size plays an important role in the startability of an alcohol engine. As droplet size is decreased from 100 microns to 10 microns, the minimum starting temperature drops from $55^{o}C$ to $-15^{o}C$. A 30 droplet will allow starting above $3^{o}C$.

The effect of inducted liquid fuel/air equivalence ratio is shown in Fig. II.15. This figure shows that the amount of liquid fuel inducted into the engine cylinder directly affects the slope of the end of compression vapor/air equivalence ratio versus temperature curve by increasing the number of droplets, hence, surface area for evaporation. The greater the amount of inducted liquid

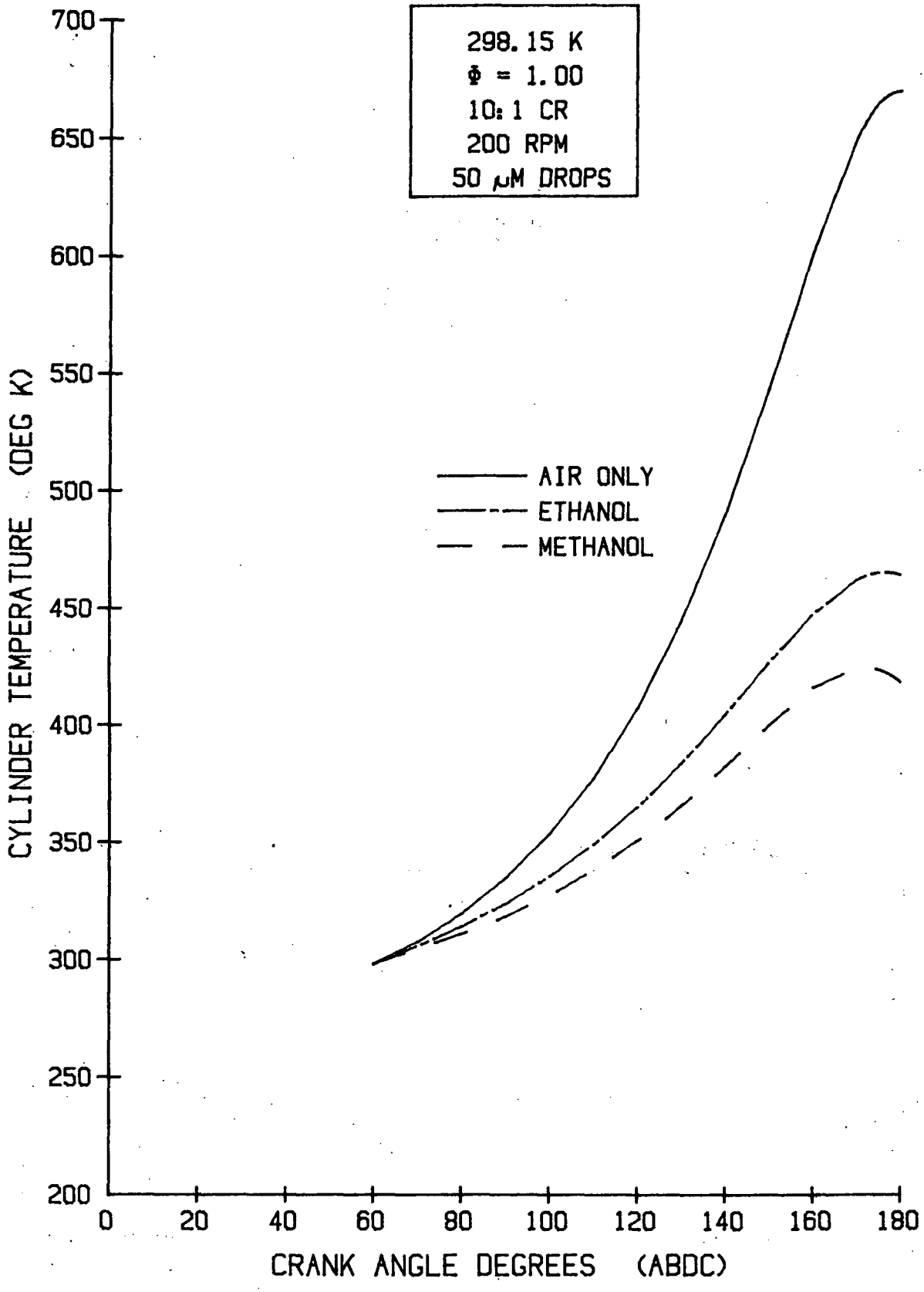

FIGURE II.11: CYLINDER TEMPERATURE FOR ROOM TEMPERATURE CRANKING

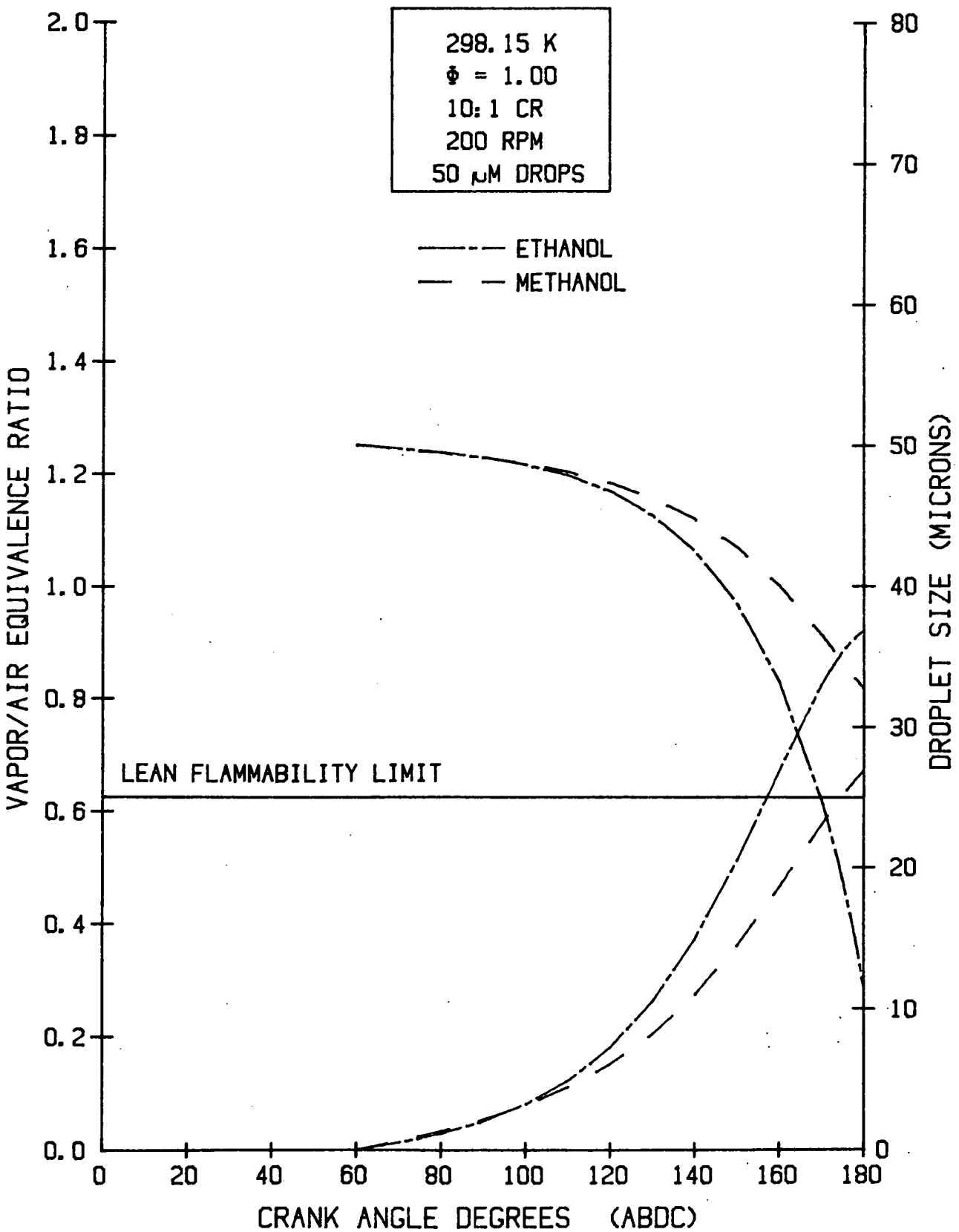

FIGURE II.12: FUEL EFFECTS FOR ROOM TEMPERATURE CRANKING

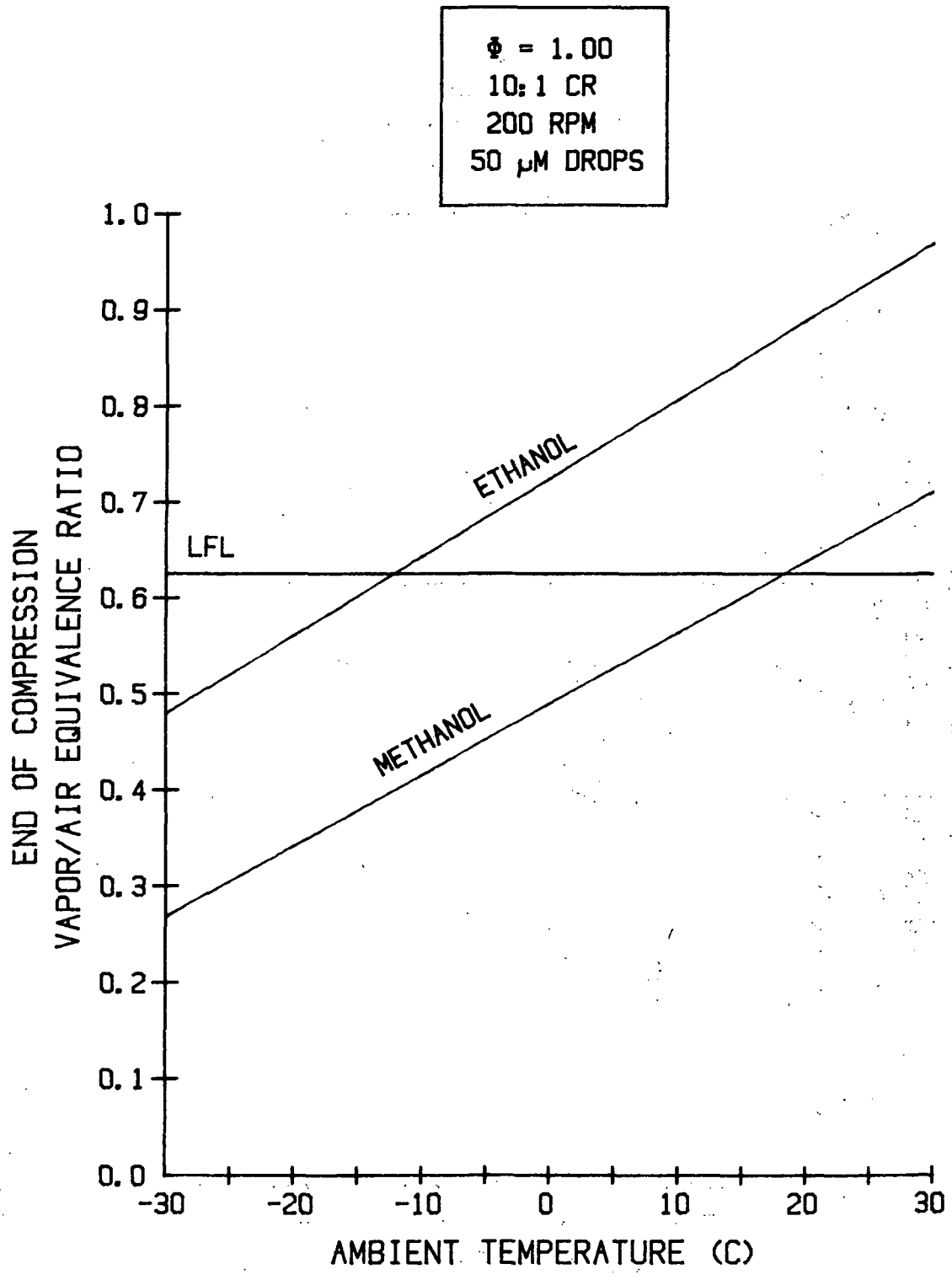

FIGURE II.13: FUEL EFFECTS ON MINIMUM STARTING TEMPERATURE

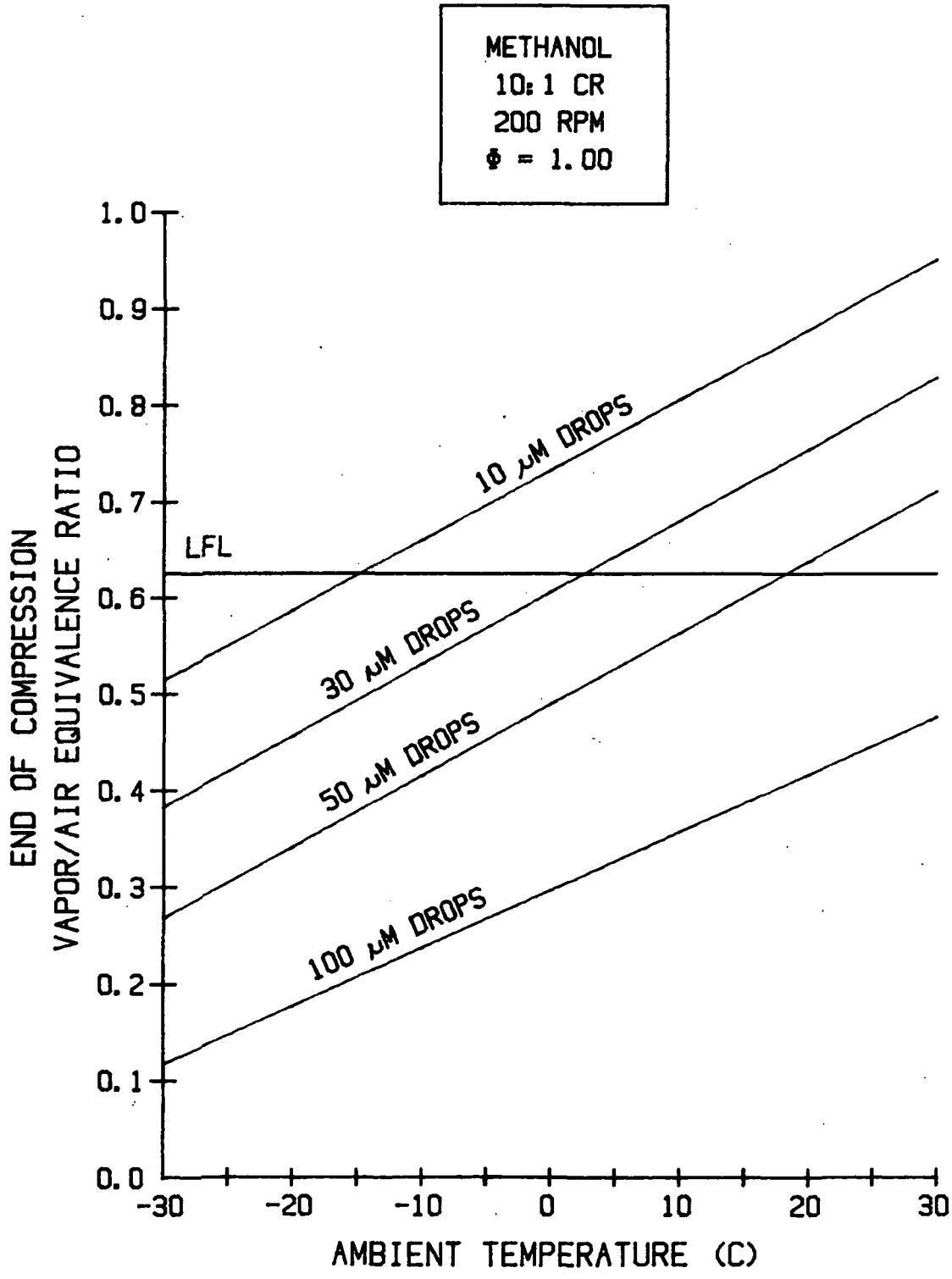

FIGURE II.14: DROPLET SIZE EFFECTS ON MINIMUM STARTING TEMPERATURE

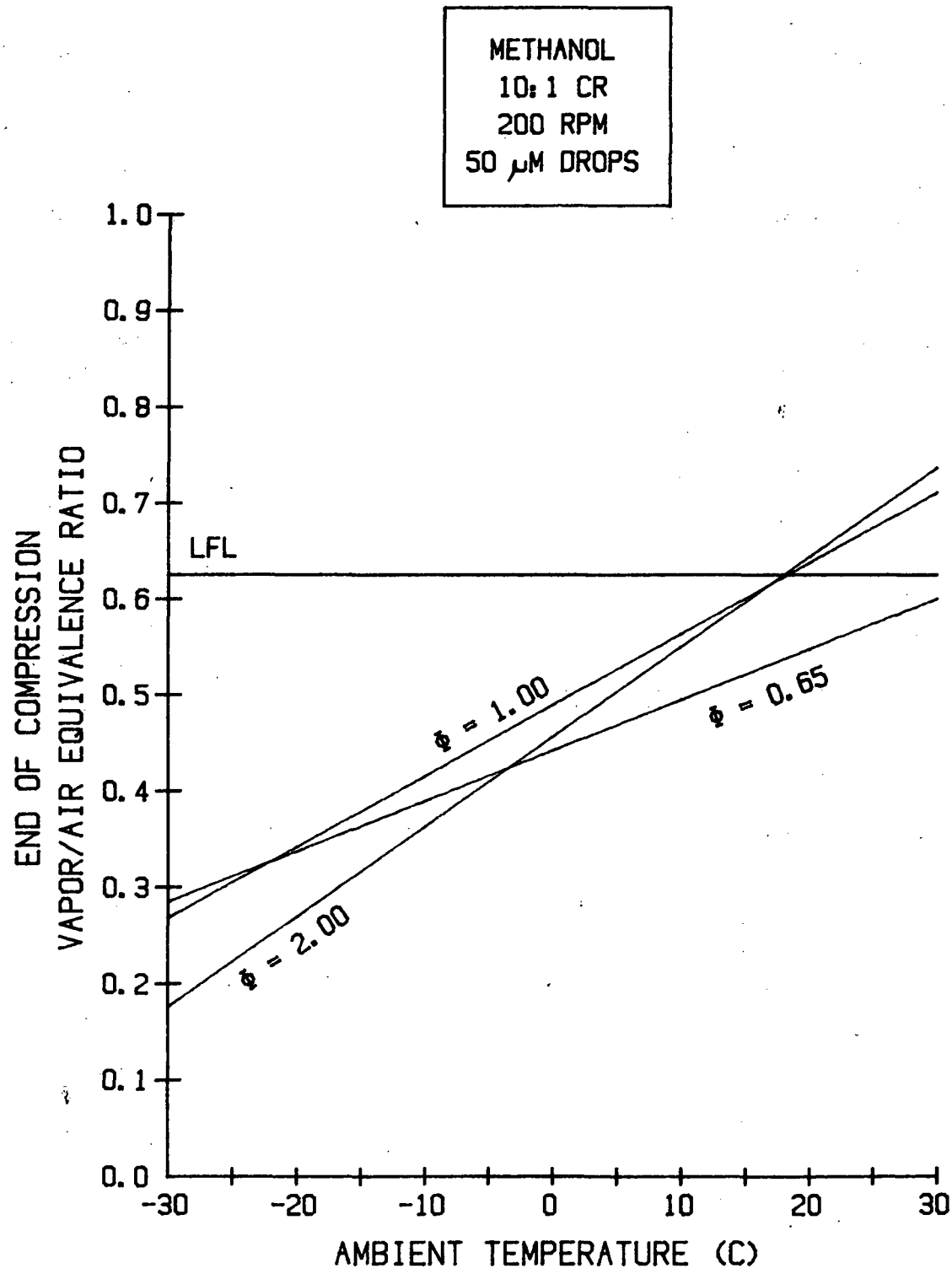

FIGURE II.15: INDUCTED EQUIVALENCE RATIO EFFECTS ON MINIMUM STARTING TEMPERATURE

fuel, the steeper the slope of the curve. This trend however is offset by the fact that more inducted fuel reduces the relative position of compression vapor/air equivalence ratio curve as shown in the figure. Using the data shown in the figure, the optimum inducted equivalence ratio would be approximately 1.5 which would result in a minimum starting temperature of approximately 16 ^{o}C.

In Fig. II.16, the effect of cranking speed on droplet vaporization is shown. As can be seen from this figure, the slower the cranking speed, the more time available for droplet vaporization and therefore the lower the minimum starting temperature. Decreasing cranking speed from 300 rpm to 100 rpm reduces the minimum starting temperature from 24^{o}C to 10^{o}C for 50 micron methanol droplets. In this cranking speed range wall heat transfer does not play a significant role and of course cylinder leakage has been neglected.

Fig. II.17 shows the effect of compression ratio on the startability of a methanol mixture of 50 drops and air. This figure shows that small changes in compression ratio have only slight effects on final vapor/air equivalence ratio. However, raising the compression ratio from 10:1 to 20:1 enhances the minimum starting temperature by dropping it from 18^{o}C to -12^{o}C for 50 methanol droplets.

In Fig. II.18, the effect of manifold vacuum or choking is shown. Reducing the starting cylinder pressure from 0.775 atm to 0.575 atm only reduces the minimum starting temperature by 3^{o}C. This can be anticipated when it is recognized that fuel vapor pressure in all instances considered here is well below saturation pressure.

II.3c One-Dimensional, Two-Phase Cold Start Engine Model

The one-dimensional, two-phase cold start engine model combines droplet transport and vaporization in the intake and exhaust manifolds with vaporization/condensation of droplets during the compression and expansion processes of cold start cranking. The following assumptions are made to simplify the analysis: (1) a well stirred cylinder, (2) an ideal mixture of air and fuel vapor, (3) all droplets are in suspension in the runners and cylinder and (4) all engine surface areas are at constant temperature. In this model cylinder blow-by to the crankcase is also considered.

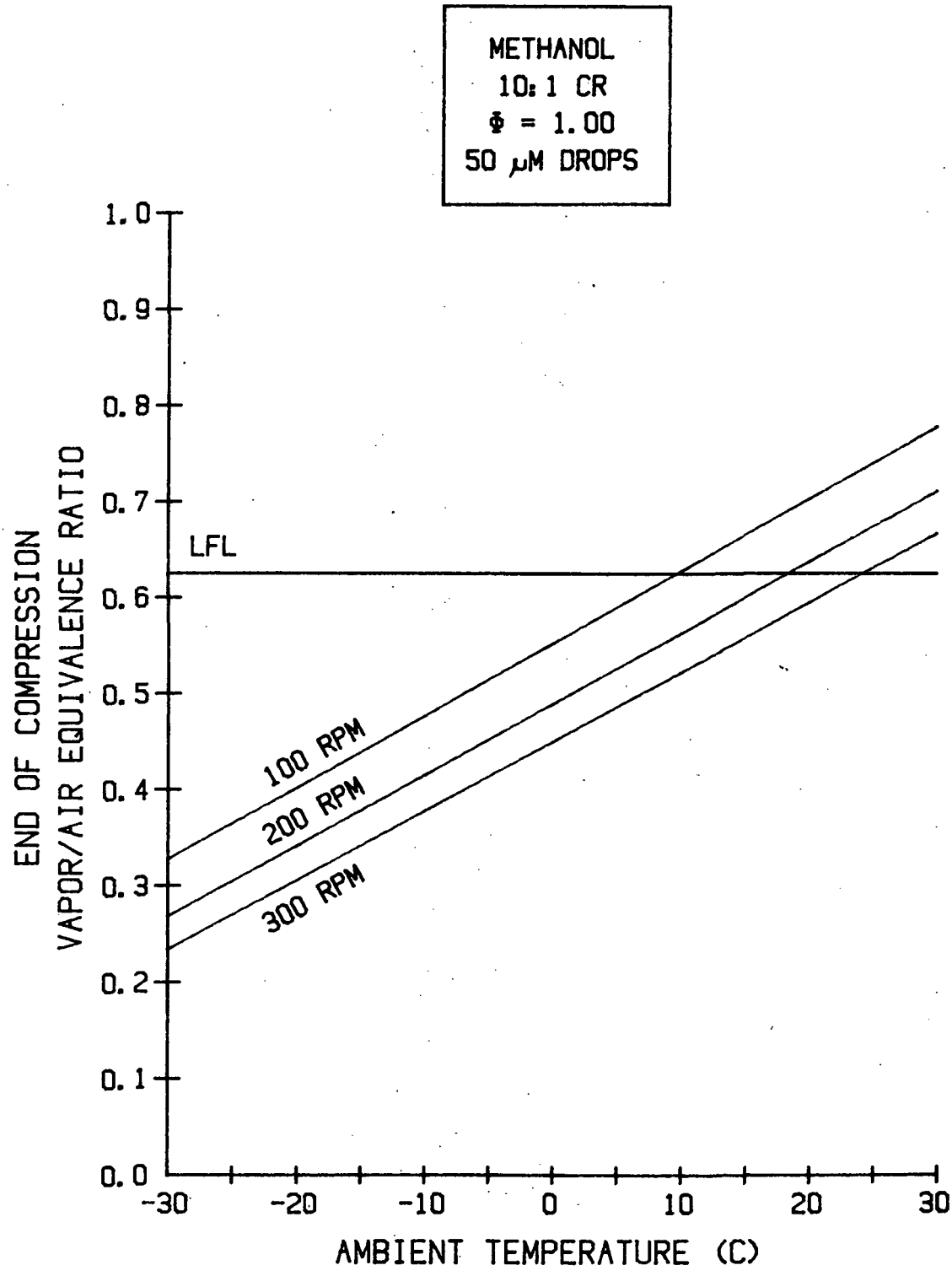

FIGURE II.16: CRANKING SPEED EFFECTS ON MINIMUM STARTING TEMPERATURE

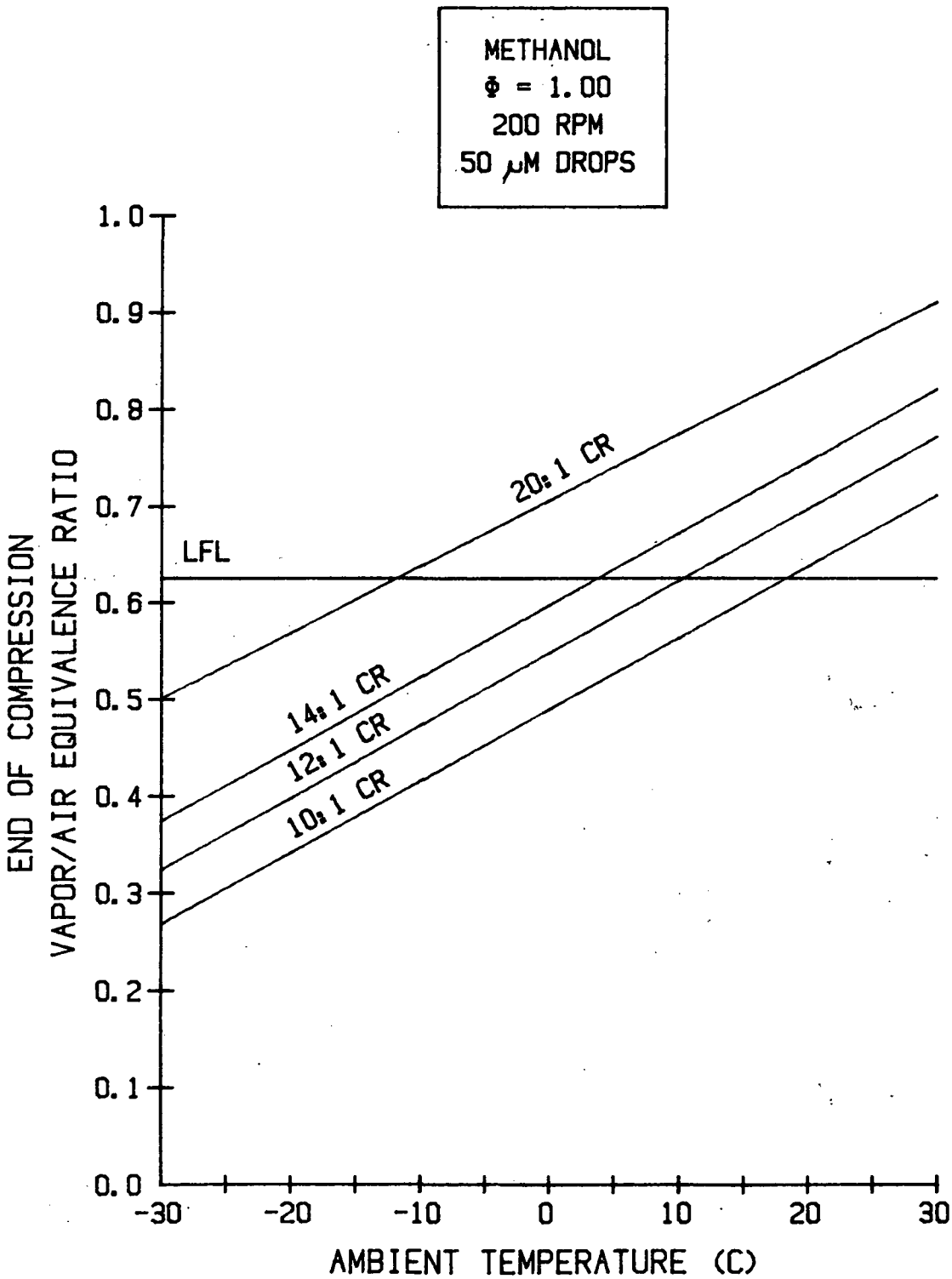

FIGURE II.17: COMPRESSION RATIO EFFECTS ON MINIMUM STARTING TEMPERATURE

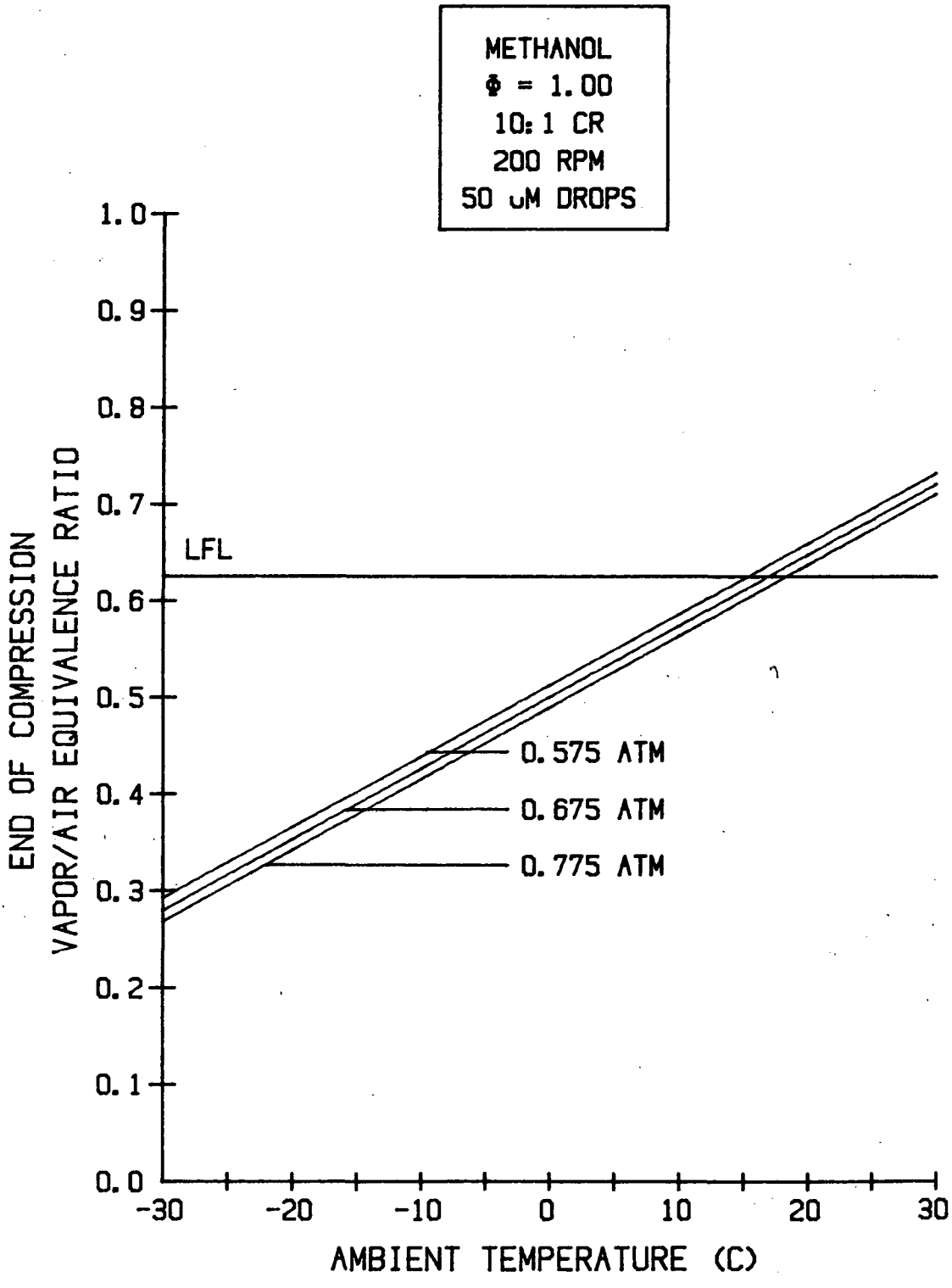

FIGURE II.18: MANIFOLD VACUUM EFFECTS ON MINIMUM STARTING TEMPERATURE

As before the conservation equations are derived separately for droplets and the gaseous mixture in the cylinder as well as all nodes within the intake and exhaust runners. The engine is cranked for three consecutive cycles and the fuel vapor/air equivalence ratio at the end of the cranking is examined for flammability. A color graphics output from this model is also used to study fuel transport and vaporization in the cylinder and runners during the cranking process. While this model is still under development, it has been shown to produce reasonable trends when compared to actual engine data produced by the experimental cold start engine (see Chapter III).

Initial study results from the model visually show the advantages of smaller droplet size, electric heaters in the intake manifold, choking and dissociating* part of the liquid fuel for cold starting. Fig. II.19 shows the vapor/air equivalence ratio versus crank angle for three consecutive cranking cycles for 50 droplets injected into the air stream at an equivalence ratio of 2.0 (to insure enough fuel enters the cylinder) for starting temperatures of 25°C and 0°C. The 10:1 compression ratio engine was cranked at 150 rpm for all runs. Under these conditions with no manifold heat, the final vapor/air equivalence ratio in the cylinder at the time of ignition (end of the third cycle) was 0.79 for the 25°C case and 0.57 for the 0°C case. Since a vapor/air equivalence ratio of 0.63 is needed for ignition, a methanol engine under these conditions could not be started by the third crank at 0°C. Decreasing the droplet size injected to 30 increased the final vapor/air equivalence ratio to 0.70 at the end of the third crank (flammable). Electric heat addition and placement were also found to have significant effects. Placing a 200 watt electric heater under the carburetor raised the final vapor/air equivalence ratio to 0.69 while placing it in the intake port area raised it to 0.96 due to reduced heat transfer to the cold intake manifold walls. Even at -20°C, with the heater in the intake port area, the final vapor/air equivalence ratio was 0.78 (flammable). By choking at these conditions, the final vapor/air equivalence ratio was raised to 0.89 at -20°C.

---

* Dissociating assumes that part of the methanol has been reformed into its composing compounds: $CH_3OH \rightarrow CO + 2H_2$.

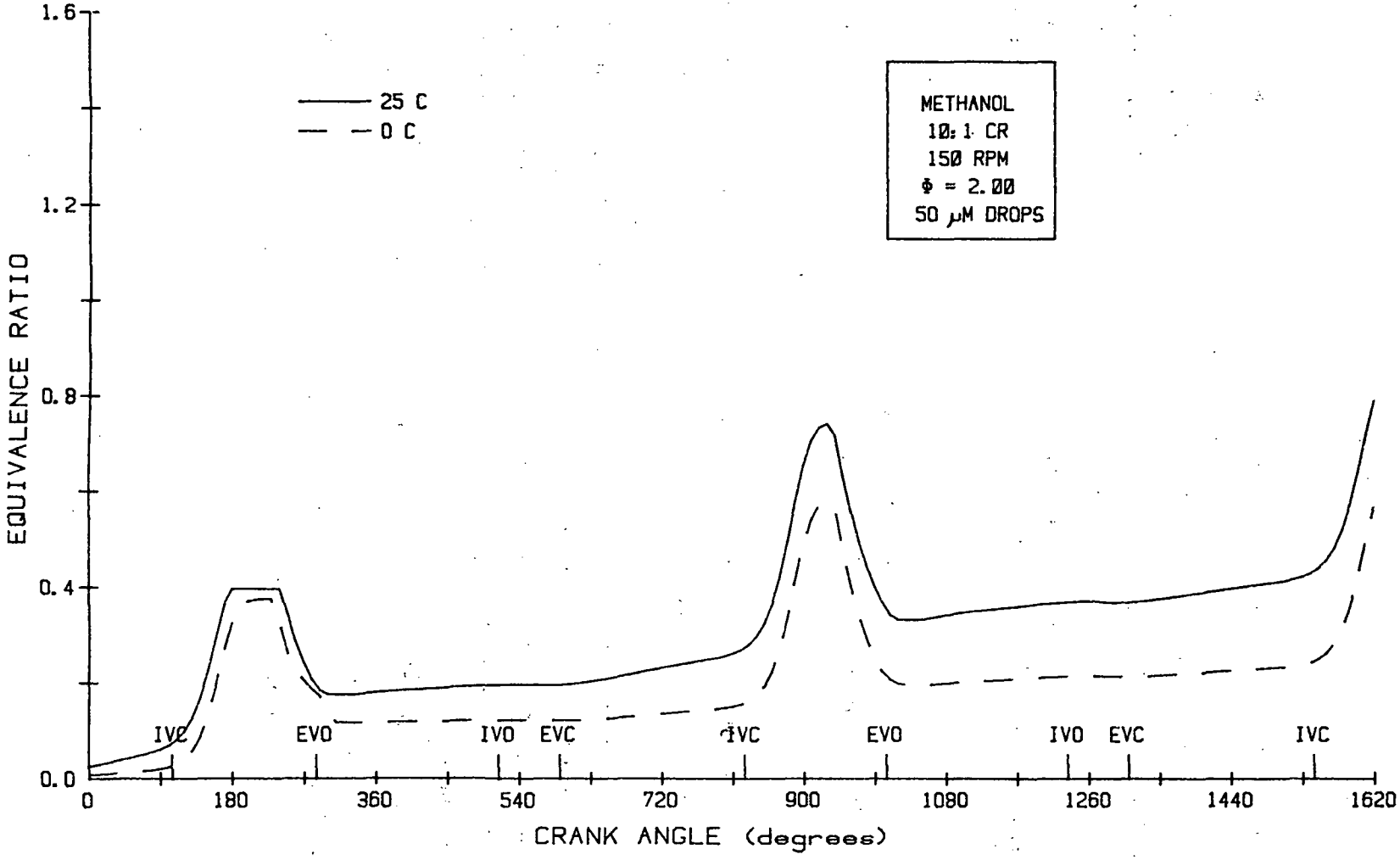

FIGURE II.19: STARTING TEMPERATURE EFFECTS

Dissociation of methanol is another effective way of increasing cold startability of an alcohol engine. If the amount of dissociated gas can be minimized, this method can also be very attractive. By dissociating 15% of the liquid fuel with a droplet size of 50 for the 0°C case, the final vapor/air equivalence ratio was 0.65. Replacing 30% of the fuel with dissociated gases raised the final vapor/air equivalence ratio to 0.72.

II.3d Summary

Three computer models were developed and are available for parametric study of alcohol fuel transport, vaporization and ignitability in a cranking engine. From the first model it is found that droplets must be smaller than 50 to assure entering the cylinder under cranking conditions without being centrifuged to the intake manifold wall. Since typical carburetors meter 100 to 500 droplets, cold starting without additional starting aids on alcohols becomes a problem well above 0°C. This modeling study conclusion is consistent with actual experience. Use of high pressure atomizing fuel injectors, however, can atomize droplets and provide the fine mist of 50 droplets that can be carried into the cylinder during the intake stroke. Well nebulized in-cylinder fuel injection is the ultimate in cold starting as the fuel does not have to travel through a curved intake runner.

The second model found that the heat of compression could be used to vaporize enough fuel for starting under room temperature conditions. Ethanol was shown to vaporize more readily than methanol due to ethanol's lower stoichiometric mass and heat of vaporization. Stoichiometric ethanol mixtures of 50 micron droplets and air were found to allow cold starting to -12°C while methanol under similar conditions has a starting limit of 18°C. Droplet size was found to be the most significant parameter in this study. A stoichiometric methanol mixture of 10 micron droplets and air has a starting limit of -15°C. Very high compression ratios also aid cold starting showing marked reductions in cold starting temperatures. All other variables, for the ranges examined by this study (inducted equivalence ratio, manifold vacuum and cranking speed), showed very little effect on cold startability of a methanol engine.

The third model showed that manifold heating, particularly in the intake port area, was an effective means of increasing the cold startability of an alcohol engine. Furthermore choking and small amounts of dissociated fuel were found to aid cold startability. The color graphics output from this model was used to study the details of the cold starting problem and solutions with much success.

It can be concluded from this study that fine droplet atomization and high compression ratios will aid cold starting of alcohol engines and minimize the amount of other cold starting aids. Furthermore, electric heat in the intake port area greatly helps cold starting. The evidence produced here adds focus to the historical question: is it more cost effective to convert a diesel by adding a spark plug or a gasoline engine by adding injectors to produce an alcohol engine or by blending volatile components into the methanol?

II.4 REFERENCES

II.1 R.K. Pefley, L.H. Browning, et al., "Research and Development of Neat Alcohol Fuel Usage in Automobiles," Six Months Progress Report, NASA-Lewis Contract No. NAG 3-143, University of Santa Clara Report No. ME-81-2, July, 1981.

II.2 R.K. Pefley, L.H. Browning, et al., "Characterization and Research Investigation of Methanol and Methyl Fuels," ERDA Contract No. EY-76-S-02-1258, University of Santa Clara Report No ME-77-2, 1977.

II.3 R.K. Pefley, L.H. Browning, et al., "Characterization and Research Investigation of Alcohol Fuels in Automobile Engines," Final Report, DOE Contract No. DE-AC03-78CS, University of Santa Clara Report No. ME-81-1, 1981.

II.4 L.H. Browning, "A Thermokinetic Combustion Process Simulation for a Methanol Fueled Spark Ignition Engine," Engineer's Degree Thesis, Stanford University, Stanford, California, 1978.

II.5 L.H. Browning and L.A. Argenbright, "An Analytical Investigation of NO_x Control Techniques for Methanol Fueled Spark Ignition Engines," presented at the Fifth International Symposium on Alcohol Fuels Technology, Aukland, New Zealand, May 1982.

II.6 L.H. Browning and R.K. Pefley, "An Analytical Study of Aldehyde formation During the Exhaust Stroke of a Methanol Fueled SI Engine," presented at the Fourth International Symposium on Alcohol Fuels Technology, Guaruja, Brazil, October 1980.

II.7 R. Bergner, H. Eberius and H. Pokorny, "Flame Quenching and Exhaust Hydrocarbons in a Combustion Bomb as a Function of Pressure, Temperature and Equivalence Ratio for Methanol and Other Alcohols," presented at the Third International Symposium on Alcohol Fuels Technology, Asilomar, California, May 1979.

II.8 C.K. Westbrook, A.A. Adamczyk and G.A. Lavoie, "A Numerical Study of Laminar Wall Quenching," presented at the Western States Section Combustion Institute Meeting, Berkeley, California, October 1979.

II.9 J.A. LoRusso, E.W. Kaiser and G.A. Lavoie, "Quench Layer Contribution to Exhaust Hydrocarbons from a Spark-Ignited Engine," Combustion Science and Technology, Vol. 25, pp 121-125, 1981.

II.10 J.T. Wentworth, "Effects of Combustion Chamber Shape and Spark Plug Location on Exhaust Nitric Oxide and Hydrocarbon Emissions," SAE Paper No. 740529, SAE Transactions, Vol 83, 1974.

II.11 W.A. Daniel and J.T. Wentworth, "Exhaust Gas Hydrocarbons--Genesis and Exodus," SAE Paper No 686b, SAE Transactions, Vol 70, 1962.

II.12 R.J. Tabaczynski, J.B. Heywood and J.C. Keck, "Time Resolved Measurements of hydrocarbon Mass Flowrate in the Exhaust of a Spark-Ignition Engine," SAE Paper No 720112, SAE Transactions, Vol 81, 1972.

II.13 W.G. Rado and W.J. Johnson, "Significance of Burn types, as Measured by Using Spark Plugs as Ionization Probes, with Respect to the Hydrocarbon Emissions Levels in S.I. Engines," SAE Paper No. 750354, 1975.

II.14 F.F. Pischinger and K. Kramer, "The Influence of Engine Parameters on the Aldehyde Emissions of a Methanol Operated Four-Stroke Otto Cycle Engine," presented at the Third International Symposium on Alcohol Fuels Technology, Asilomar, California, May 1979.

II.15 J.A. Harrington, "Application of a New Combustion Analysis Method in the Study of Alternate Fuel Combustion and Emission Characteristics" presented at the Symposium on Future Automotive Fuels, General Motor Research Laboratories, Warren, Michigan, October 1975.

II.16 L.H. Browning, J.F. Nebolon and R.K. Pefley, "Research Investigation of Alcohol Usage in Spark Ignition Engines," SAE paper, presented at the 1982 ATD/CCM Conference, October 1982.

II.17 J. Nebolon, K.C. Chan, L.H. Browning and R.K. Pefley, "Multi-Point Injection of Alcohol Vapor as a Cold Starting Aid for Neat Alcohol Fueled Vehicles," presented at the Fifth International Symposium on Alcohol Fuels Technology, Aukland, New Zealand, May 1982.

II.18 L.H. Browning, "Alcohol Cold Starting--A Theoretical Study," presented at the 18th IECEC, August 1983.

II.19 T. Yano and K. Ito, "Minimum Ignition Energies and Quenching Distances of Methanol Blends," Bulletin of the Faculty of Engineering, Hokkaido University, Japan, No. 94, 1979.

CHAPTER III

ENGINE COLD STARTING BY EXPERIMENTATION

In Chapter II cold starting is identified as one of the major problems impeding the full use of pure alcohols as alternate automobile fuels. This problem has attracted the attention of several research groups in the world yet their efforts have met with only modest success with the pure alcohols below 5°C [III.1,2,3,4].

III.1 COLD START PROBLEM ELEMENTS

There are three aspects to the cold start problem. The first involves the low vapor pressure of the pure alcohols, which limits the unassisted starting temperatures under fully choked conditions to 12 °C and 14 °C, for methanol and ethanol repectively, according to Section II.3. Once the engine has started the higher heats of vaporization of the alcohols and the higher flow rate of these fuels cause significant temperature suppression in the intake manifold particularly in cold weather conditions near and below 0 °C . Under these conditions it is reasonable to expect the fuel to condense on the intake manifold walls as well as be present in both liquid droplet and vapor form. As vapor is needed for ignition, this effect aggravates cold starting and idling. Additionally, the suspended droplets and vapor when deposited between the cold spark plug electrodes can act as an electrical conduit and prevent any further ignition, making it very difficult to restart an alcohol fueled engine immediately after a successful cold start if it fails to continue idling.

The second aspect of the cold start problem is related to the transportation of the suspended fuel droplet through the intake manifold. The computer modeling studies reported in Chapter II indicate that droplets above 50 microns may not make it into the cylinder under normal cranking conditions. This is a very important conclusion and it calls for better fuel preparation which is a relatively unexplored area of the alcohol engine cold start solution strategy [III.5]. Assuming that the droplets do make it to the cylinder, the third aspect appears: What fraction of the liquid fuel can be vaporized during the compression stroke, what is the fuel vapor to air ratio at the end of compression and what are the factors that adversely affect this vaporization. These

are the fundamental questions that have to been studied, both analytically and experimentally, as prerequisites for designing and optimizing suitable cold starting systems.

The third aspect of the cold start problem pertaining to the vaporized fuel fraction has been an area of experimental and modeling study over the past several years [III.1]. The amount of fuel vaporized during compression is the important element in this study because the gaseous fuel component determines the flammability of the air fuel mixture present at the time of ignition and the task in the design of all cold start aids is to improve this number beyond the lean flammability limit for all engine starting conditions. An efficient design solution demands a fundamental understanding of the fuel vaporization process and the experimental investigation conducted toward reaching this goal is described in the following sections. The experimental approach taken here also helps to validate and fine tune the computer model discussed in Chapter II.

III.2 EXPERIMENTAL APPROACH

During the compression stroke, the pressure and temperature of the gas inside the cylinder increase. The high pressure forces some gas in the cylinder to escape through the valves and rings (called blow-by) and the temperature elevation establishes some heat flow to the cylinder walls. These two factors combine to produce cylinder pressure and temperature values less than predicted for reversible adiabatic conditions. If the fluid in the cylinder is a mixture of air and methanol fuel in fine droplet form, the pressure in the cylinder tends to increase due to the addition of methanol vapor to the air but at the same time the cylinder gas temperature tends to decrease due to the extraction of heat from the surrounding air for the vaporization process. As alcohols are volatile fuels with relatively high heats of vaporization, the pressure reduction due to temperature reduction predominates the pressure increase due to the addition of vapor to the air resulting in a lesser magnitude of peak cylinder pressure during compression of an air and fuel mixture compared to that of air with no fuel (AIR-ONLY). The magnitude of this pressure suppression depends on the mass of fuel vaporized during the compression process and this quantity is influenced by the type of fuel used, the ambient air conditions, the diameters of the fuel droplets and the droplet diameter distribution.

The magnitude of gas leakage past the rings and valves depends on the leak area and the pressure difference hence, this process can be modeled as flow through an orifice. The leak area can be determined experimentally as explained later. The magnitude of heat transfer depends on the temperature gradient, the gas Reynolds number and the shape of the combustion chamber (swirl etc). Although much work has been done on the measurement and correlation of heat transfer during cranking, none of the correlations can be considered universal. For this reason it is necessary to experimentally determine the heat transfer and this is best done by the analysis of the AIR-ONLY pressure data in which, once the leak rate is determined, the only unknown quantity is the heat transfer to the walls. By correcting for leakage and then determining heat transfer for the air only case, the AIR & FUEL pressure data can be analyzed to obtain the rate of vaporizaton and the mass of fuel vaporized during compression as functions of crank angle. As a result the total mass of fuel available in the vapor state and the air to fuel vapor ratio can be calculated at the time of ignition or at the end of the stroke [III.6].

III.3 THE EXPERIMENTAL HARDWARE

The experimental engine for this study is the same 2.3 L Ford Pinto engine as used in the Chapter II modeling study. It is mounted in a cold chamber test cell (Fig. III.1). The engine head is suitably instrumented to receive a Quartz crystal pressure transducer and a 0.005" diameter thermocouple (K-Type) in the first cylinder. Figure III.1 shows the experiment set-up and Fig. III.2 shows the head instrumentation and the location of the pressure transducer. An optical transducer that encodes each degree of crank rotation is coupled to the crank shaft through a flexible coupling (Fig. III.3). Thermocouples are located suitably to measure the temperatures of the intake manifold air, oil, coolant, engine head, exhaust, and ambient air. A pressure tranducer is located at the intake manifold to measure the manifold vacuum. These pressure and temperature signals are suitably amplified and transmitted along with the pulses from the shaft encoder through a high quality cable to the computer sampling ports.

A PDP 11/03 computer is used in the data acquisition process (Fig. III.4). This computer is programmed to record the gas pressure in the first cylinder for each degree of crank rotation during a compression stroke, to sample the temperature

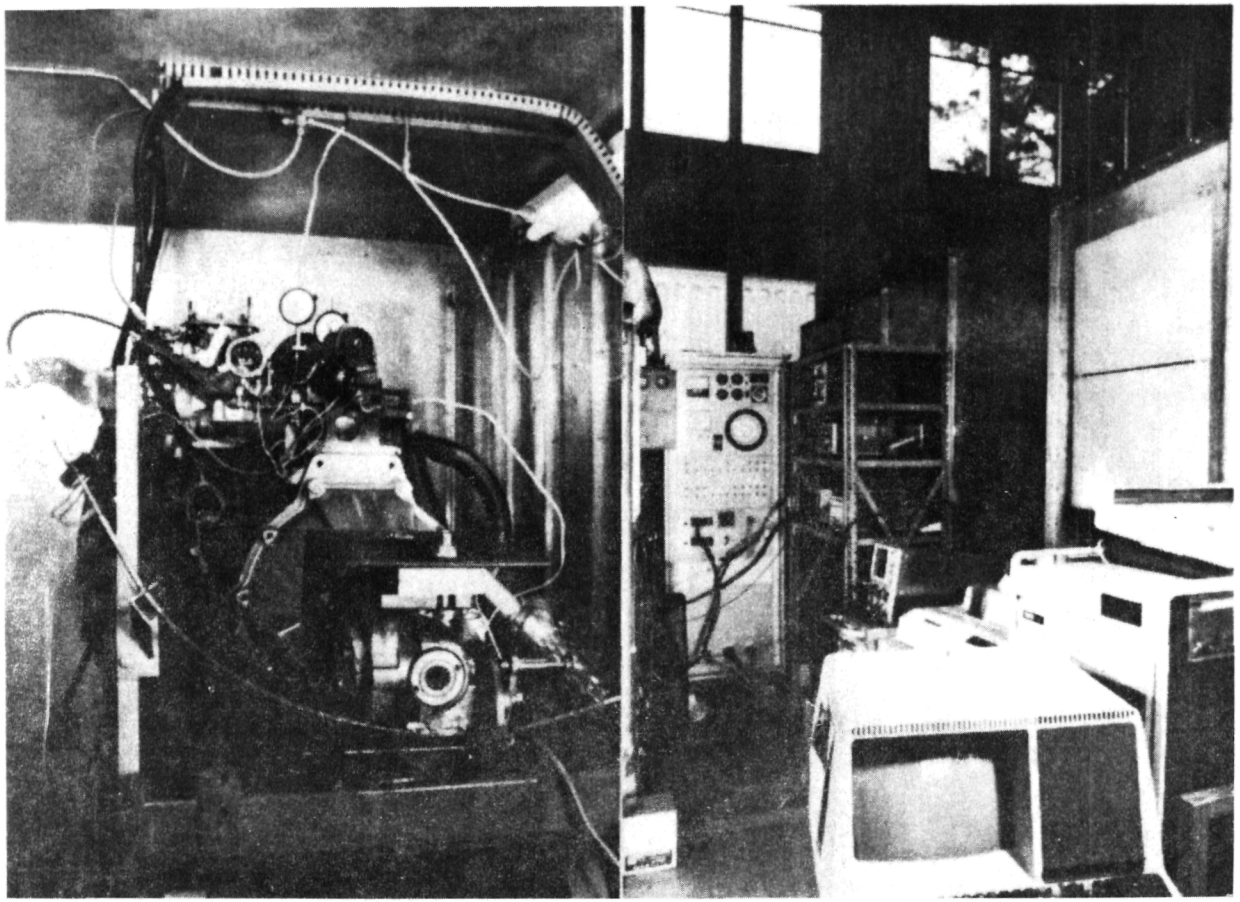

FIGURE III.1: COLD START EXPERIMENTAL SET-UP

ENGINE, INSTRUMENT CABINET AND PDP11/03 COMPUTER

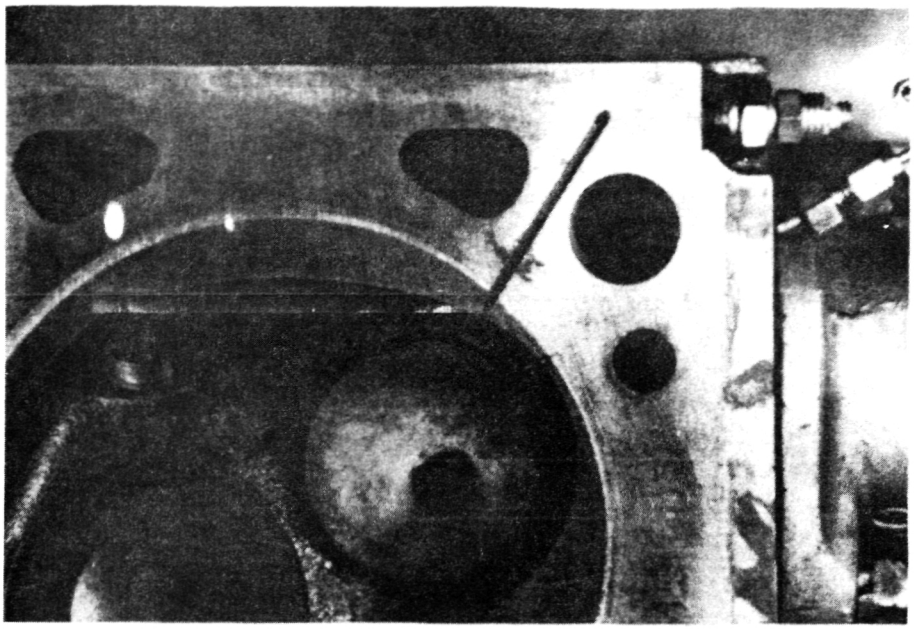

FIGURE III.2: HEAD INSTRUMENTATION

LOCATION OF PRESSURE TRANSDUCER & THERMOCOUPLE

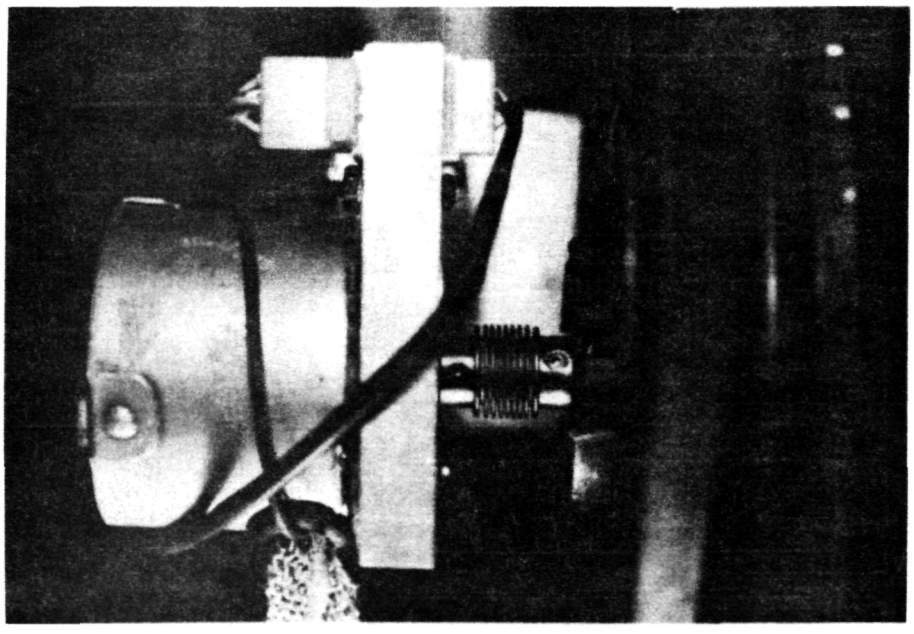

FIGURE III.3: SHAFT ENCODER ASSEMBLY

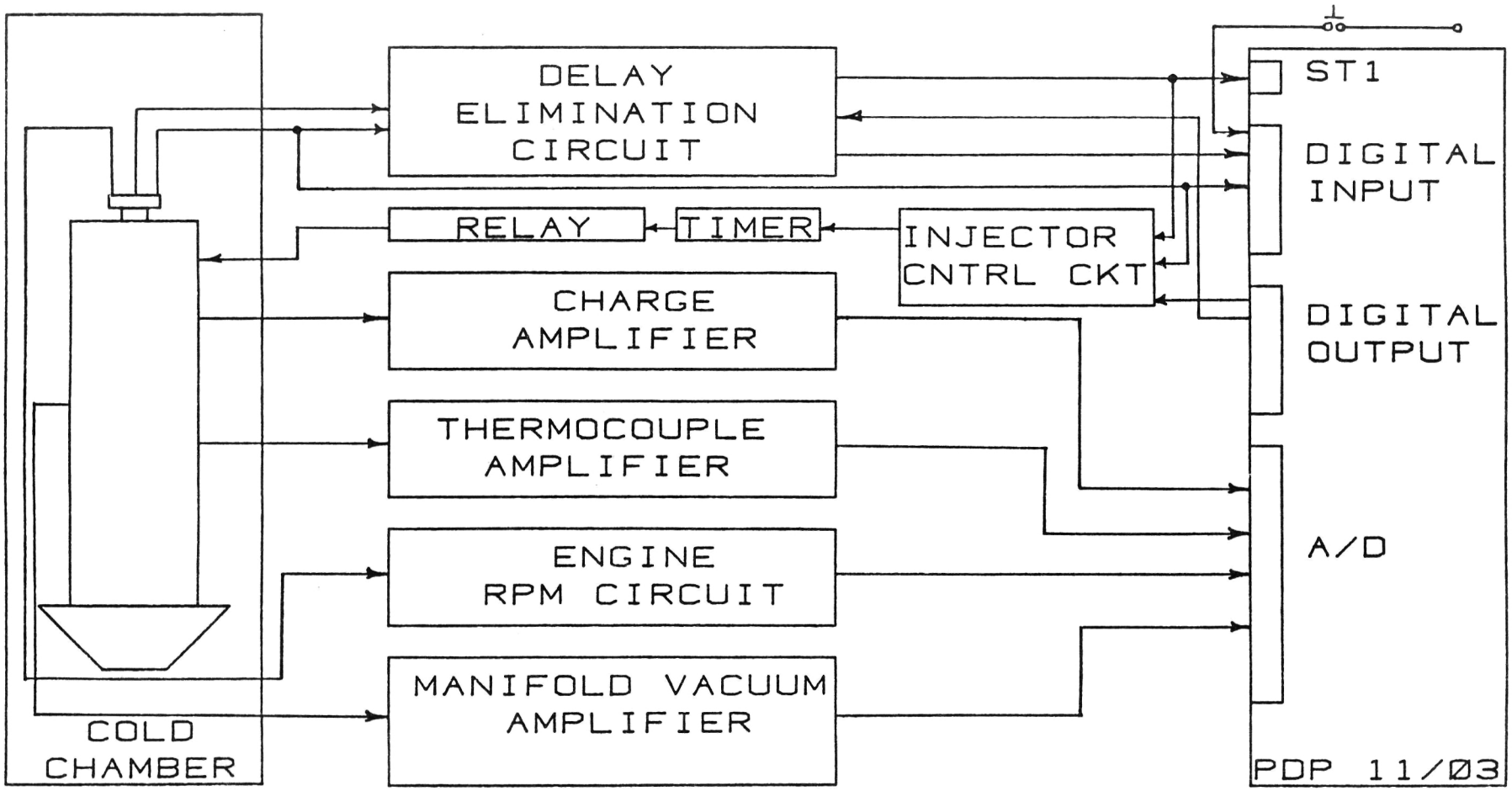

FIGURE III.4 : SCHEMATIC OF EXPERIMENTAL SET-UP

and manifold pressure during the power stroke and to send a control signal to the fuel injector circuit before the start of a pre-selected compression stroke. The control signal from the computer activates the injector circuit which is designed to count a predetermined number of degrees after the engine bottom dead center and activate the injection timing circuit. This timing circuit energizes the injector (from a 12v DC source) and controls the duration of the fuel injection; hence, the quantity of fuel injected during the compression stroke. The counter circuit can count from 0 to a maximum of 60 degrees after bottom dead center. The fuel injection system, an adapted Bosch cold start manifold injector, is operated at 60 psi pressure to ensure good fuel atomization thereby reducing the mass of fuel lost to the cylinder walls (wall wetting). Since the experiment is limited to cranking with no ignition, the injector is mounted in the spark plug hole. The carburetor bowl is dried before the experiment and the solenoid, mounted upstream of the carburetor, prevents any fuel flow into it during the experiment. The shaft encoder is enclosed in an electric blanket to maintain ambient operating conditions during cold temperature tests [III.6,7].

III.4 THE DATA ACQUISITION SOFTWARE

The PDP 11/03 micro computer has 16 A/D ports, 16 digital read-in ports, 16 digital output ports, 2 external clocking ports (called ST1 & ST2) and a real time programmable clock. The computer also has a host of library software written in FORTRAN by the manufacturer for accessing the input/ output ports. The flow chart of the data acquisition program is shown in Fig. III.5. During the execution of the information routine, user defined names for data and text files are created and some textual description of the experiment are accepted interactively from the terminal and written to the text file. When the instrument calibration routine is called, the computer samples the 16 A/D ports continuously and displays the average values, standard deviation and 99% confidence limit of the data on the terminal. The program executes this routine until it receives an external interrupt on one of the digital input ports which causes the program to jump to the main routine. Here, after servicing the external circuits designed to eliminate data acquisition delay, the program invokes the data acquisition routine and, after setting up the necessary protocols for A/D operation, waits in a sampling mode to record the pressure data during cranking. The data sampling routine is programmed to read, digitize

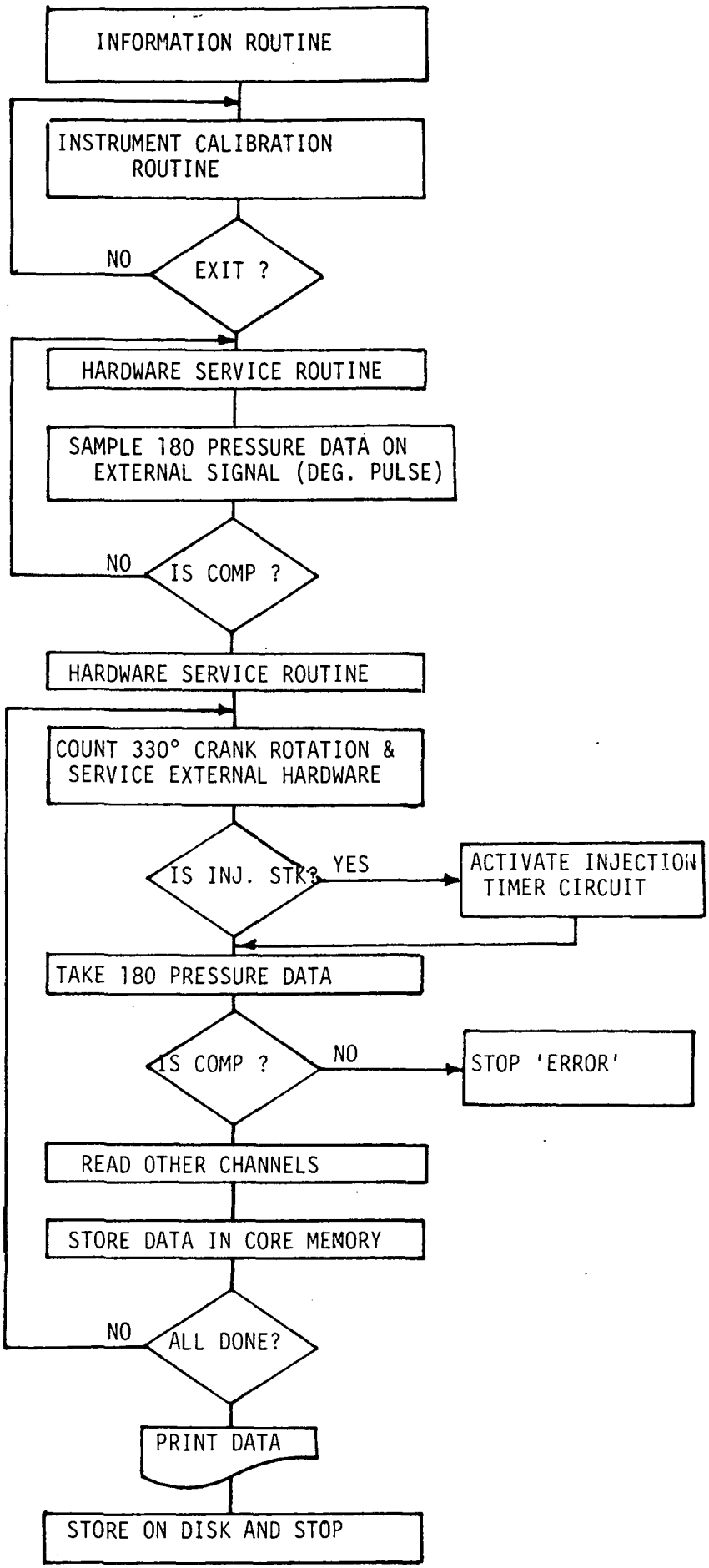

FIGURE III.5 : FLOW CHART FOR THE DATA ACQUISITION SOFTWARE

and store (in computer memory) the pressure at the arrival of each degree pulse in the ST1 port. The transfer of the degree pulse train to the ST1 port is controlled by the delay elimination circuit which implements a sequential logic operation based on the signal status of the bottom dead center pulse and the control pulse from the computer digital output. After digitizing a total of 180 data points, control is transfered to the main routine in which the last three pressure data points are averaged and tested for evidence of high pressure of the compression stroke. This operation enables the computer to synchronize with the engine. Once this is achieved, the cylinder pressure is sampled once every degree during the compression stroke and the temperature, rpm and intake manifold vacuum data are recorded during the following exhaust stroke. Just prior to the preselected compression stroke the injector control circuit is activated by generating a pulse at the digital output port for fuel injection. After a user defined number of compression strokes have been sampled the data is converted from binary representation to equivalent analog quantities and written in the data file [III.6,8,9].

III.5 THE TEST MATRIX AND EXPERIMENTAL RESULTS

Two types of experiments were conducted: The AIR-ONLY tests in which no fuel was injected and the AIR & FUEL tests in which a known quantity of methanol fuel was injected for a selected stroke. These tests were conducted with various ambient air conditions to study its effect on the mass of fuel vaporized. The test matrix appears in Table III.1.

TABLE III.1 Test Matrix

TEST TYPE	TEST TEMPERATURE ^{o}C					FUEL USED	MASS OF FUEL
AIR ONLY	23.0	5.0	0.0	-5.0	-15.0	-	-
AIR & FUEL	23.0	5.0	0.0	-5.0	-15.0	METHANOL	0.07 gr/cycle

Several tests planned for different stiochiometric ratios had to be canceled due to the fuel flow rate limitation of the injector. At a speed of 100 RPM the

injection of 0.07 grams of fuel at 60 psi requires approximately 90 degrees of crank rotatation and the cylinder pressure at the end point is in the range of 30 to 40 psi. At higher speeds or higher fuel amounts the cylinder pressure at the end of injection will exceed fuel pressure, making further fuel injection impossible.

Figure III.6 is a three dimensional plot of the AIR & FUEL test conducted at 23.0 ^{o}C. A stoichiometric amount of fuel was injected on the fifth cycle beginning at bottom dead center. The resulting pressure supression at the end of compression is about 0.85 atm. Note that the subsequent peak pressures are lower than before but are slowly rising. This is thought to be due to vaporization of the fuel sprayed on the wall or increased blow-by due to break down of the oil seal. Figure III.7 shows the pressure suppression at different temperatures for the same mass of fuel sprayed. It must be noted that the A/F ratio is stoichiometric only at 23.0 ^{o}C. At lower temperatures, due to the higher density of the intake air, the A/F is greater than stoichiometric.

III.5a Experimental Determination of Blow-by Area

The leak area is calculated from an experiment in which the crankshaft is locked with the piston of cylinder #1 at top dead center. This cylinder is then charged with pressurized nitrogen. After steady state conditions are attained, the nitrogen supply is cut off and the resulting pressure and temperature histories are recorded by the computer (Fig. III.8). The pressure and temperature decay data is used in a computer model to calculate the leak area.

The equations that adquately describe the engine blow-by are based on the conservation of mass and the conservation of energy principals. The blow-by is treated as compressible flow blow-down of a constant volume reservoir with heat transfer. Since the cylinder boundaries are stationary and there is not much bulk movement of the gas, natural convection heat transfer may be assumed. The combined solution of these equations for an assumed leak area gives the temperature and density of the gas versus time from which the pressure can be computed. The leak area and the convective heat transfer coefficient are modified until the computed pressure and temperature conform to that obtained in the experiment. The leak area was computed to be $4 \times 10^{-3} cm^2$ [III.6].

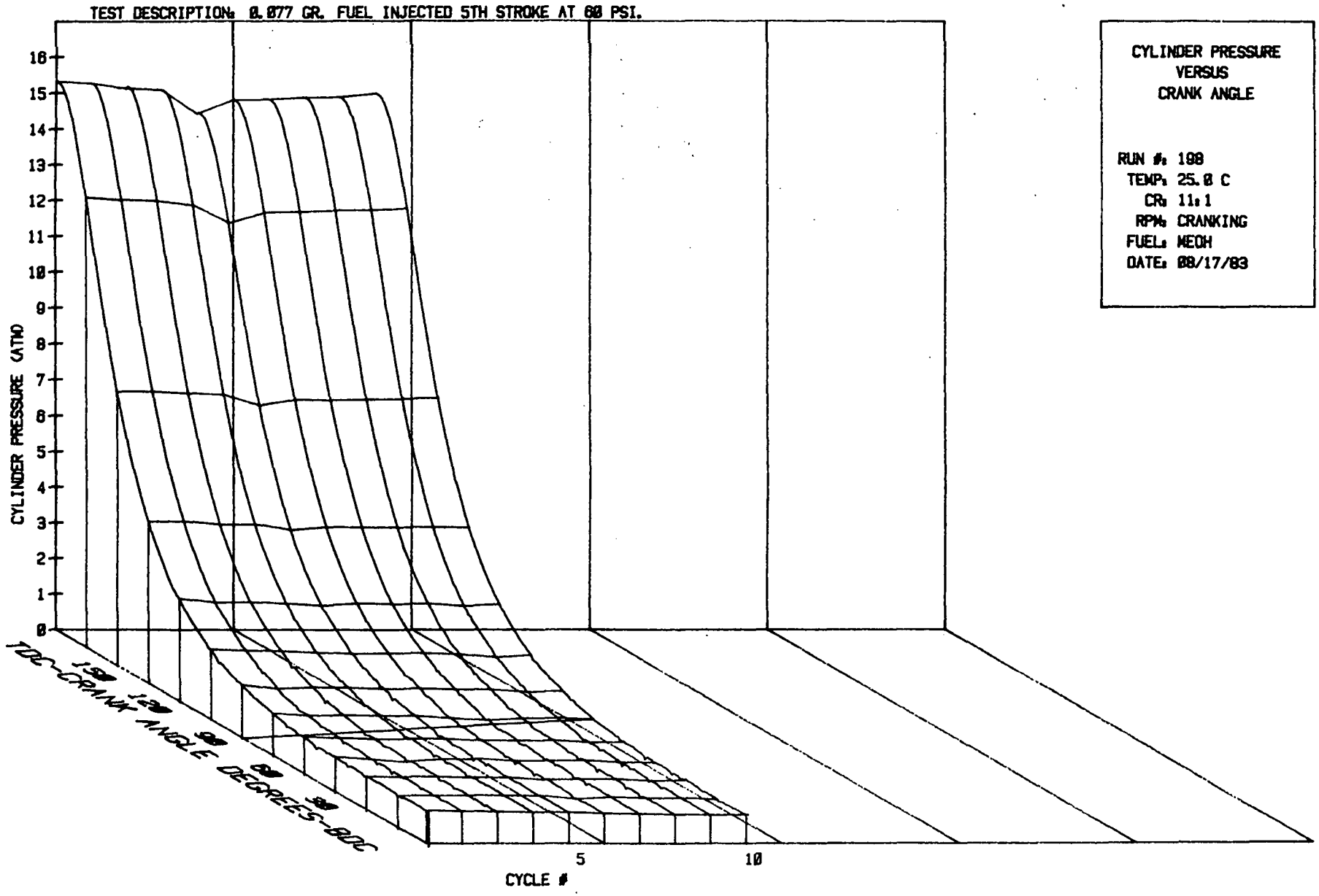

FIGURE III.8 . PRESSURE CRANK ANGLE HISTORY.

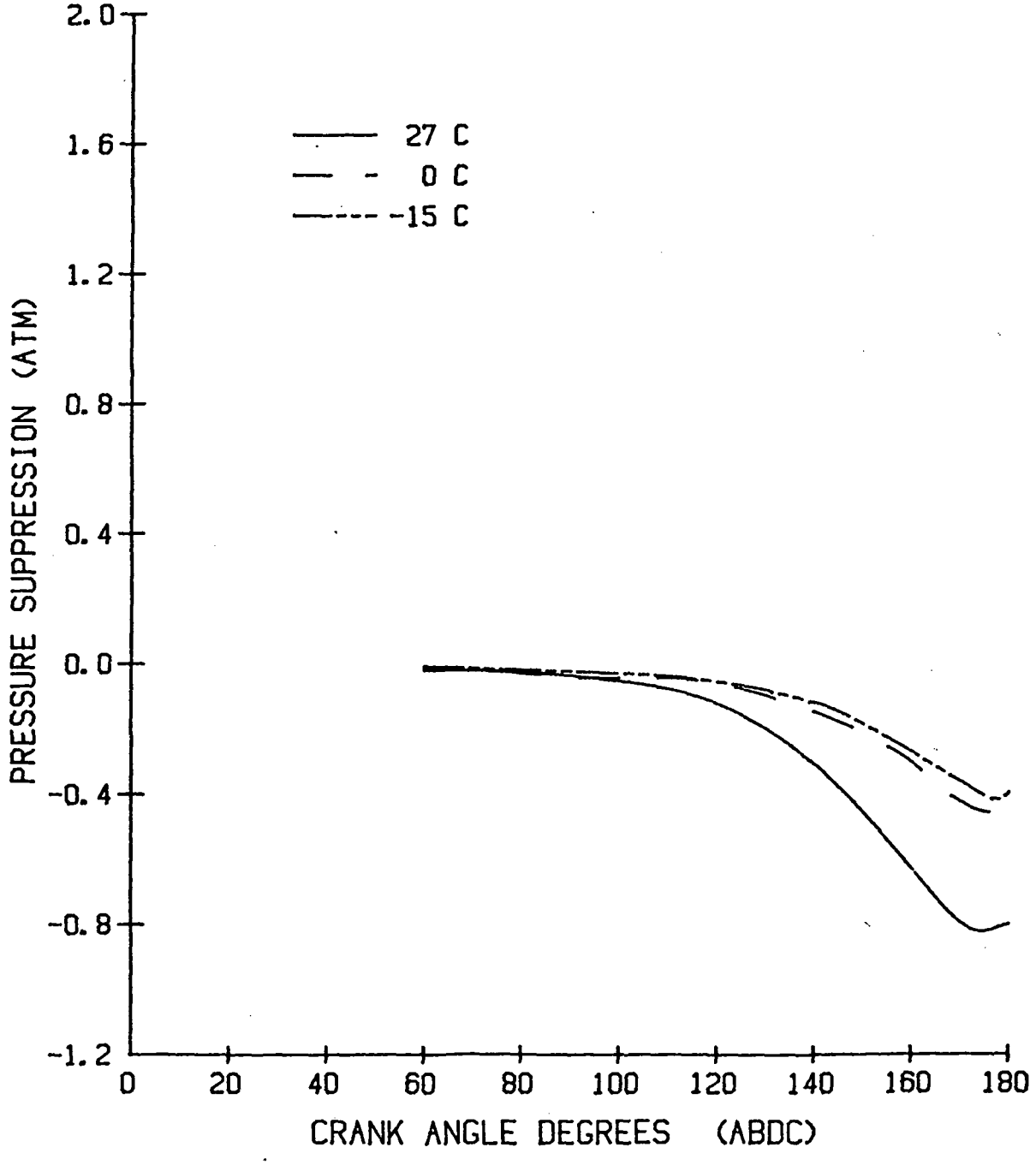

FIGURE III.7 PRESSURE DROP AT DIFFERENT TEMPERATURES

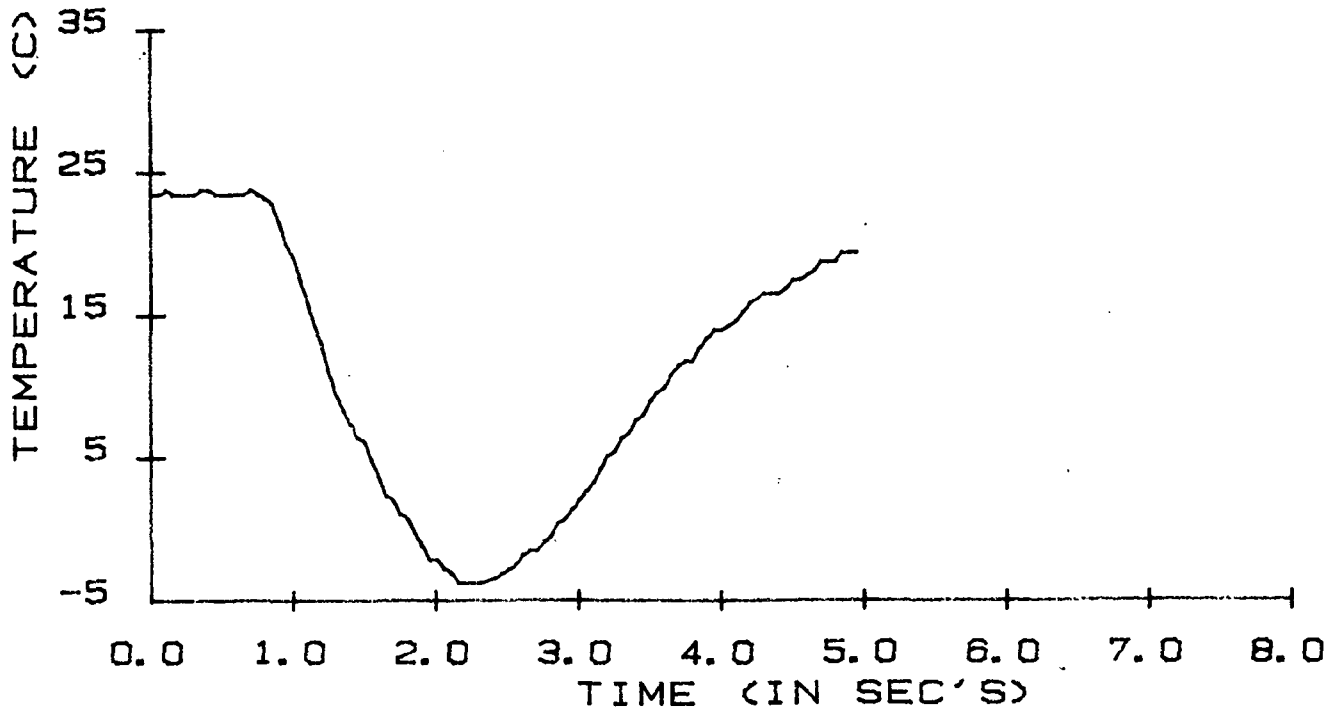

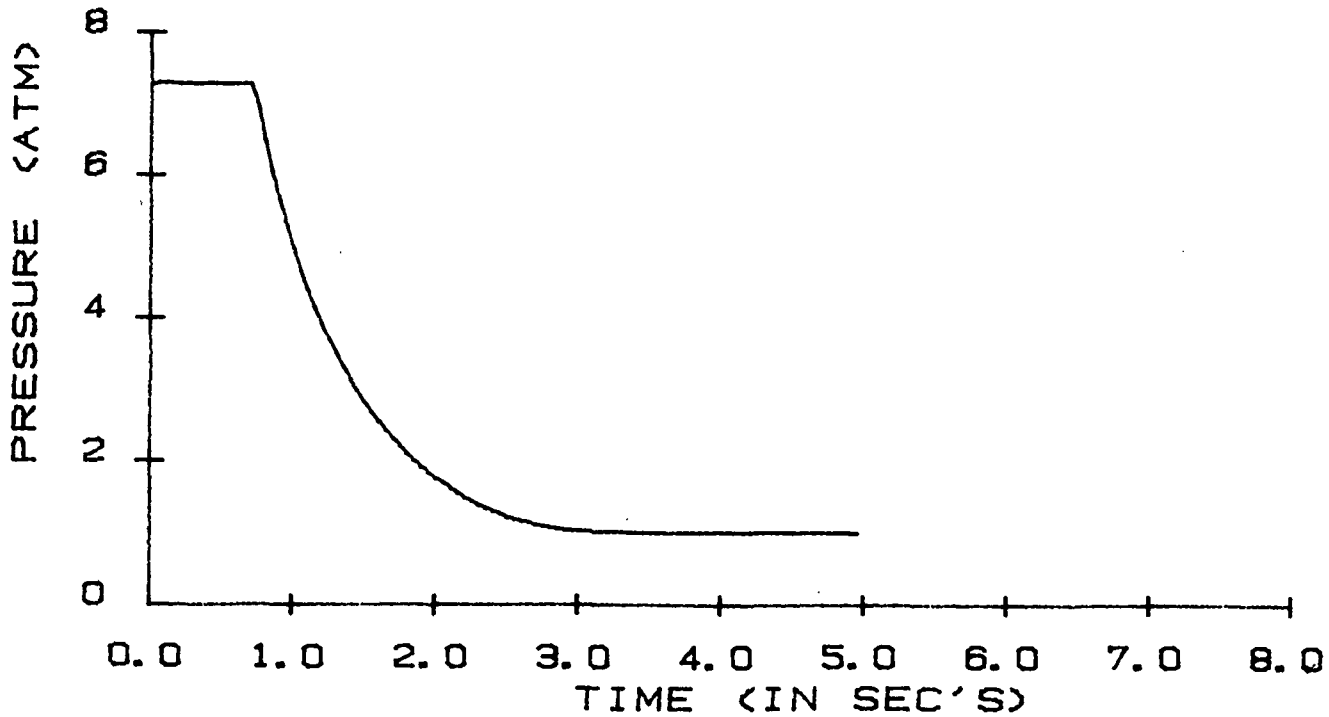

FIGURE III.8 : CYLINDER BLOW-BY.

III. 5b Determination of Valve Discharge Coefficient

When calculations were first carried out, the valve lift was assumed to follow the cam profile and this resulted in very erroneous values for heat flux, especially in the region between 60 and 100 degrees of crank rotation (ABDC) where the intake valve opening changed from 0.5mm to 0.0 mm. The valve lift profile was observed to have a pronounced effect on the heat flux calculations because the duration of the intake valve opening determines the final magnitude of the mass of air trapped in the cylinder. This prompted direct valve lift measurements, which revealed significant departures from the lift derived from the actual cam profile.he valve assembly in the Ford Pinto engine houses a hydraulic lash adjuster which in the absence of any oil pressure, absorbs part of the cam displacement leading thereby to an early closure of the intake valve during compression stroke as shown in Fig. III.9. Since the experimental data is taken during the first few cranks when the oil pressure is almost zero the valve lift profile can be assumed to follow the measured lift which changes from 0.05 mm at 60 degrees (ABDC) to 0.0 at 70 degrees (ABDC).

In order to determine the coefficient of discharge accurately at these low lifts a flow bench was set up. The details of the experiment can be found in Refs. III.2 and III.3 and the results are shown in Fig. III.10 [III.6,8,10].

III.6 DATA REDUCTION AND ANALYSIS

The AIR-ONLY compression stroke is used to deduce the heat transfer. The cylinder pressure of an AIR-ONLY compression stroke as explained earlier, is less than the adiabatic pressure due to heat transfer and leakage. During the initial part of the compression (between 60 to 90 degrees after BDC) the intake valve is partially open and the total leak area is the sum of the constant leak area determined experimentally and the variable leak area of the intake valve. The intake valve area flow is computed from the valve lift and modified by the discharge coefficient determined experimentally as a function of the valve lift. The rate of loss of air from the cylinder to the surroundings or the rate of mass addition from the intake to the cylinder for negative cylinder pressures is computed based on the gas pressure, temperature and the leak area by solving the appropriate gas dynamic equations.

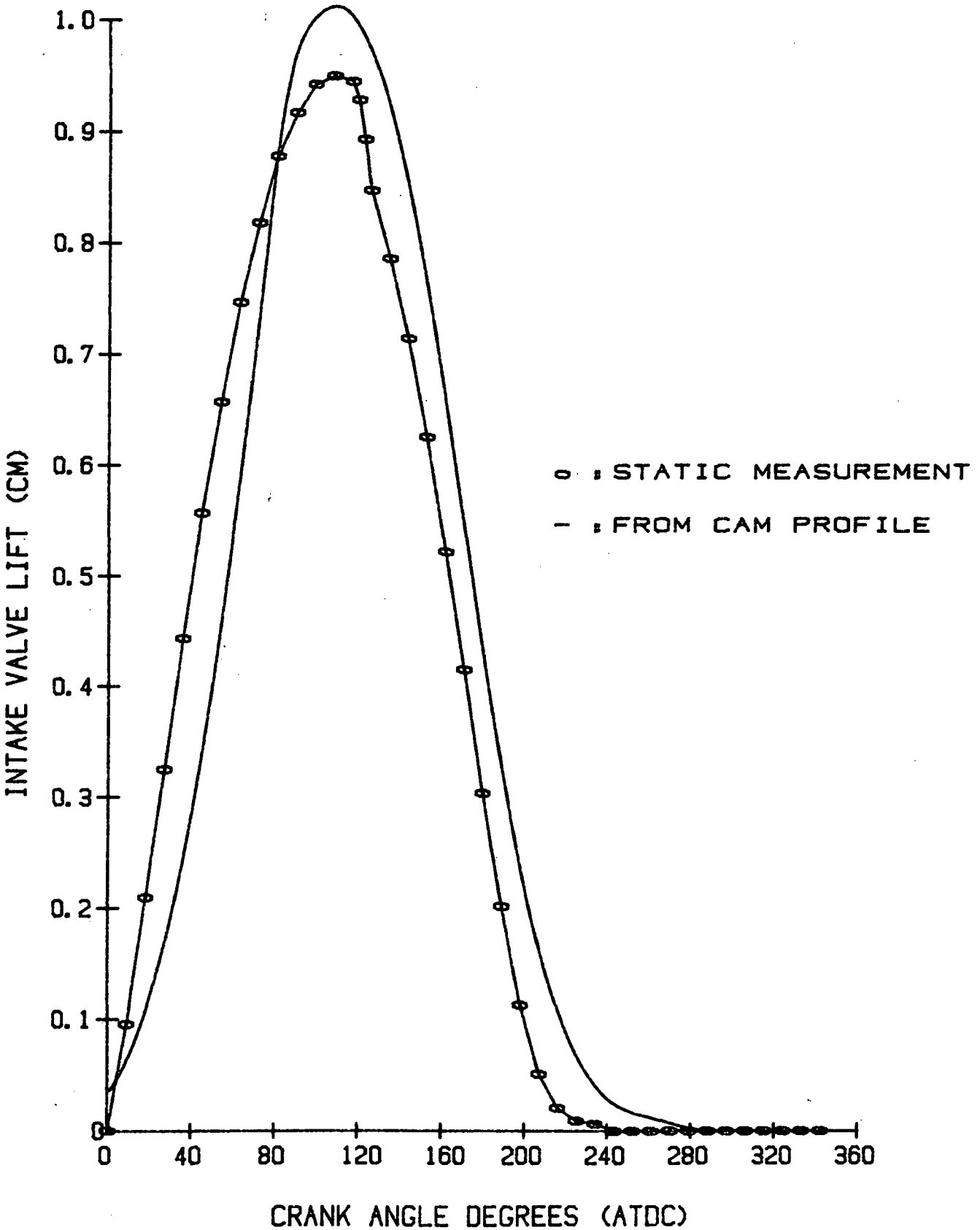

FIGURE III.9: INTAKE VALVE LIFT DURING CRANKING

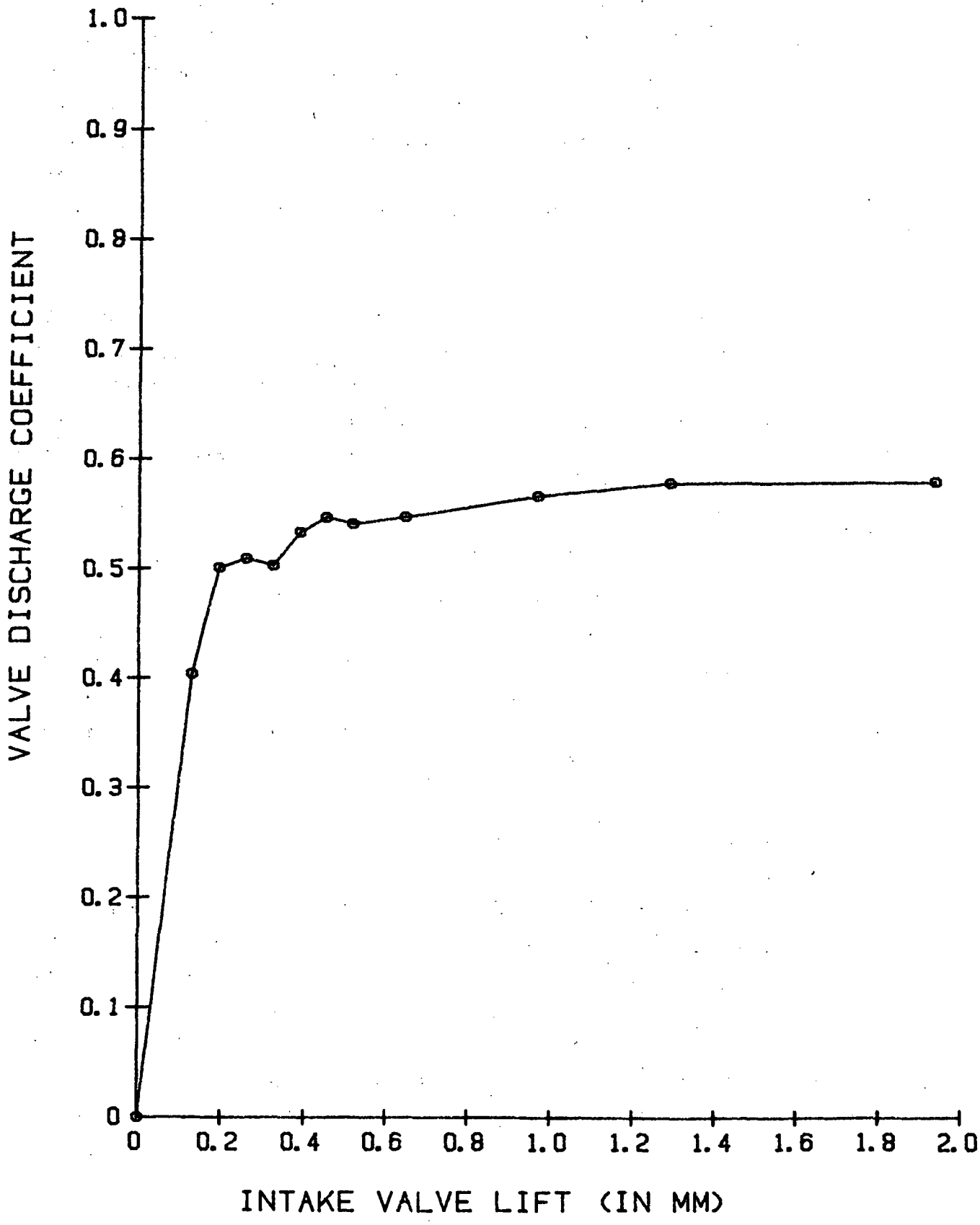

FIGURE III.10. INTAKE VALVE DISCHARGE COEFFICIENT

The general conservation equations applicable to AIR-ONLY tests are solved simultaneously for a certain assumed heat transfer rate by a 6th order RUNGE-KUTTA method to compute the pressure, temperature and density of the gas during compression as functions of crank angle. The heat transfer rate is iterated till the computed pressures and experimental pressures match. The heat transfer computation was found to be extremely sensitive to even low noises in the pressure data and so the data was curve fitted in sections with matching first and second order derivitives at the common points. In the program, the step size chosen was 0.1 degree of crank angle and the heat transfer computed at each interval was stored in a temporary buffer and integrated to obtain the heat transfer rate over a degree.

Figure III.11 shows the heat transfer computed by deduction in comparison with the computer model of Chapter II, wherein the heat transfer is calculated from a convective equation. Figure III.12 shows the computed cylinder gas temperature in comparison with measured data. Figure III.13 shows the corresponding, computed density in comparison with that calculated from the measured pressure and temperature.

With all of the calibrations of the engine, instruments and data acquisition system in place, the stage is now set for the calculation of the mass of fuel vaporized from the pressure data of an AIR & FUEL test. Since the leak area and the heat transfer rate are determined the general conservation equations applicable to an AIR & FUEL test can be iteratively solved for an assumed vaporization rate until both the predicted and the experimental pressures are in good agreement [III.6,10,11,12,13].

III.7 MODEL VALIDATION

One of the goals of the experiment as noted earlier is the verification and fine tuning of the cold start computer model (see chapter II). The computer model was derived from first principles and uses a standard heat transfer correlation. The leak area was based on the same experimental results as used here. The model predicts the cylinder pressure for an AIR-ONLY and AIR & FUEL case with ambient air conditions as a parameter. The mass of fuel vaporized is calculated assuming a certain droplet diameter and size distribution. The validity and

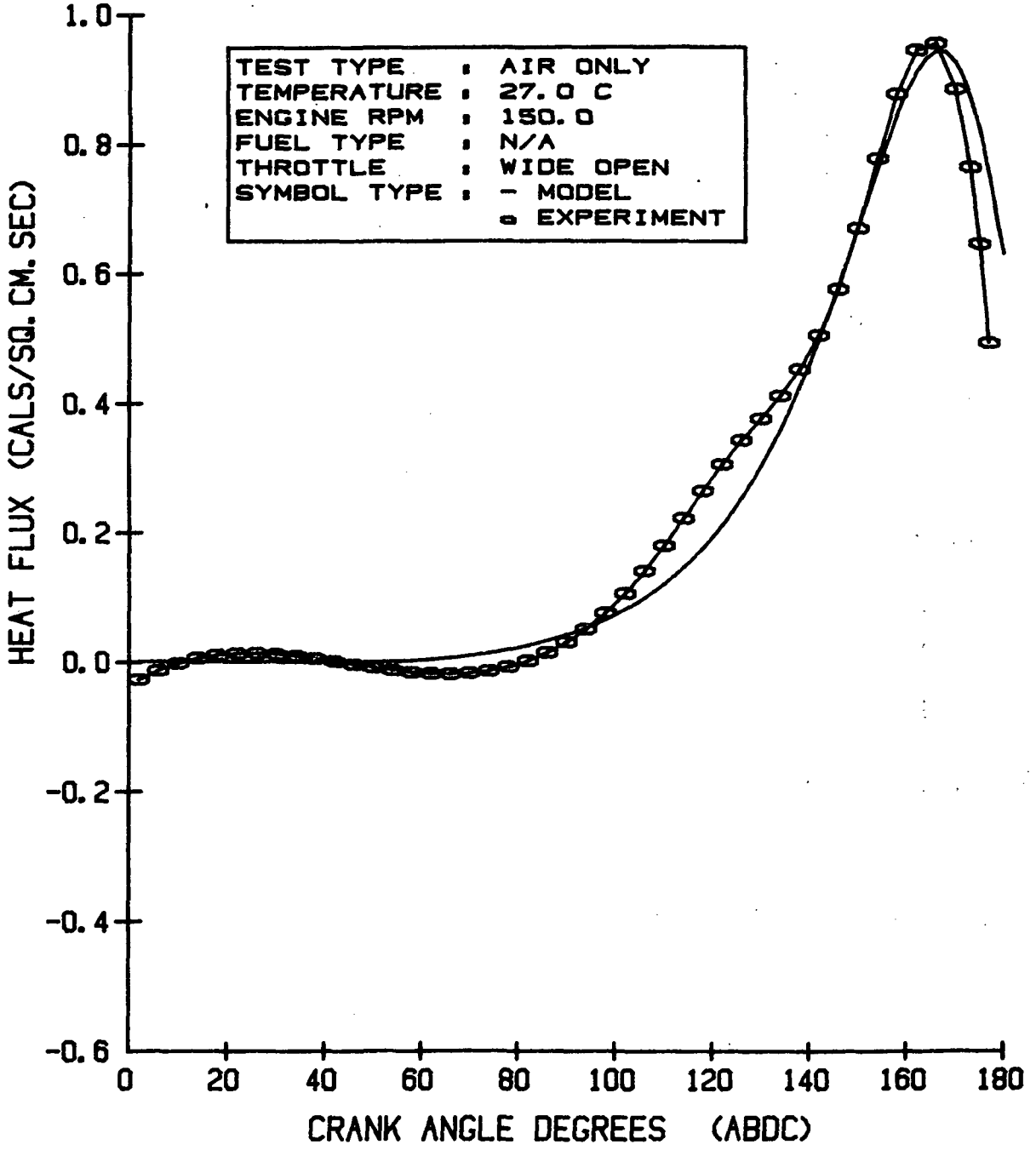

FIGURE III.11: HEAT FLUX MODEL vs EXPERIMENT

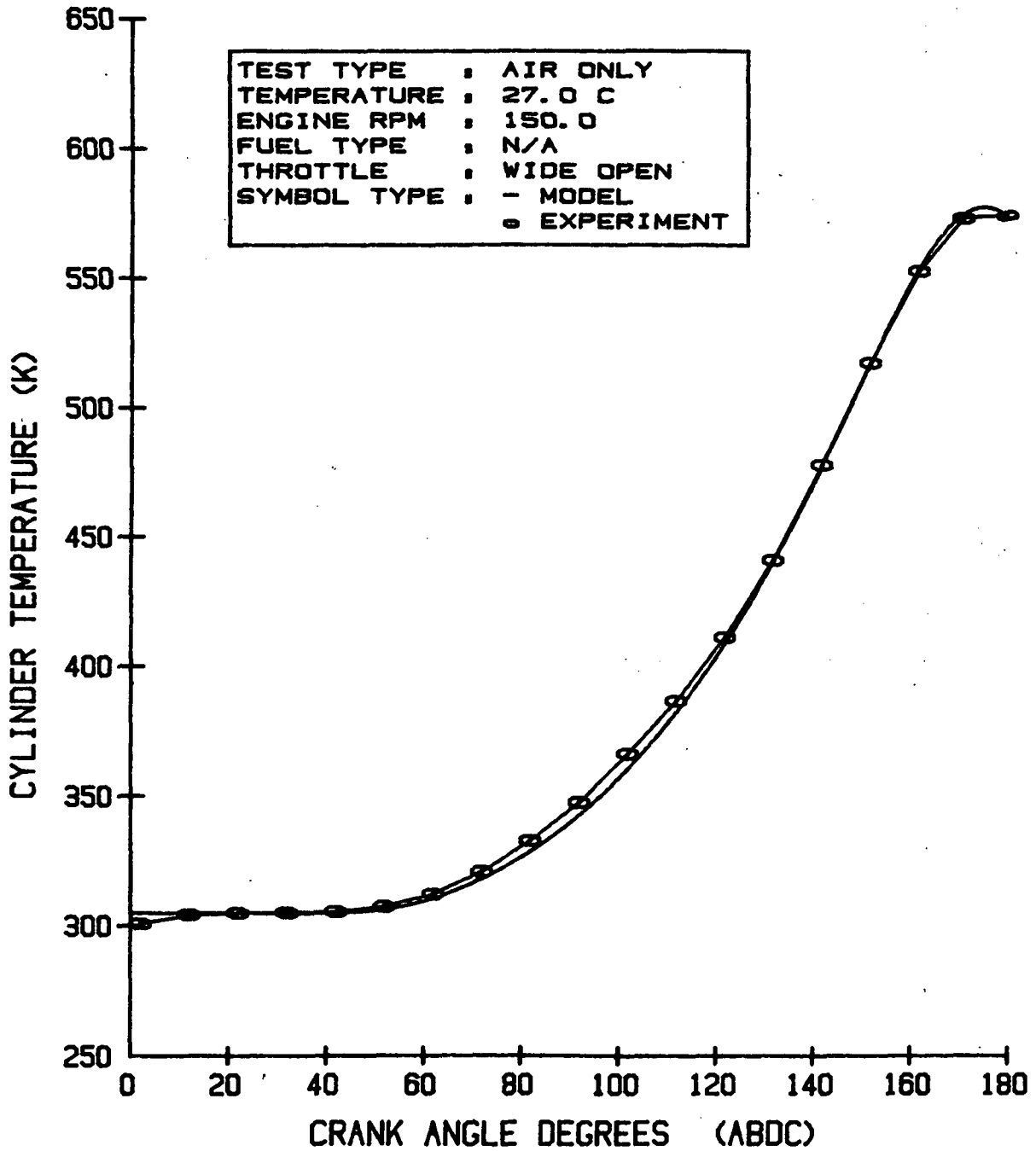

FIGURE III.12 : CYLINDER TEMPERATURE MODEL vs EXPERIMENT

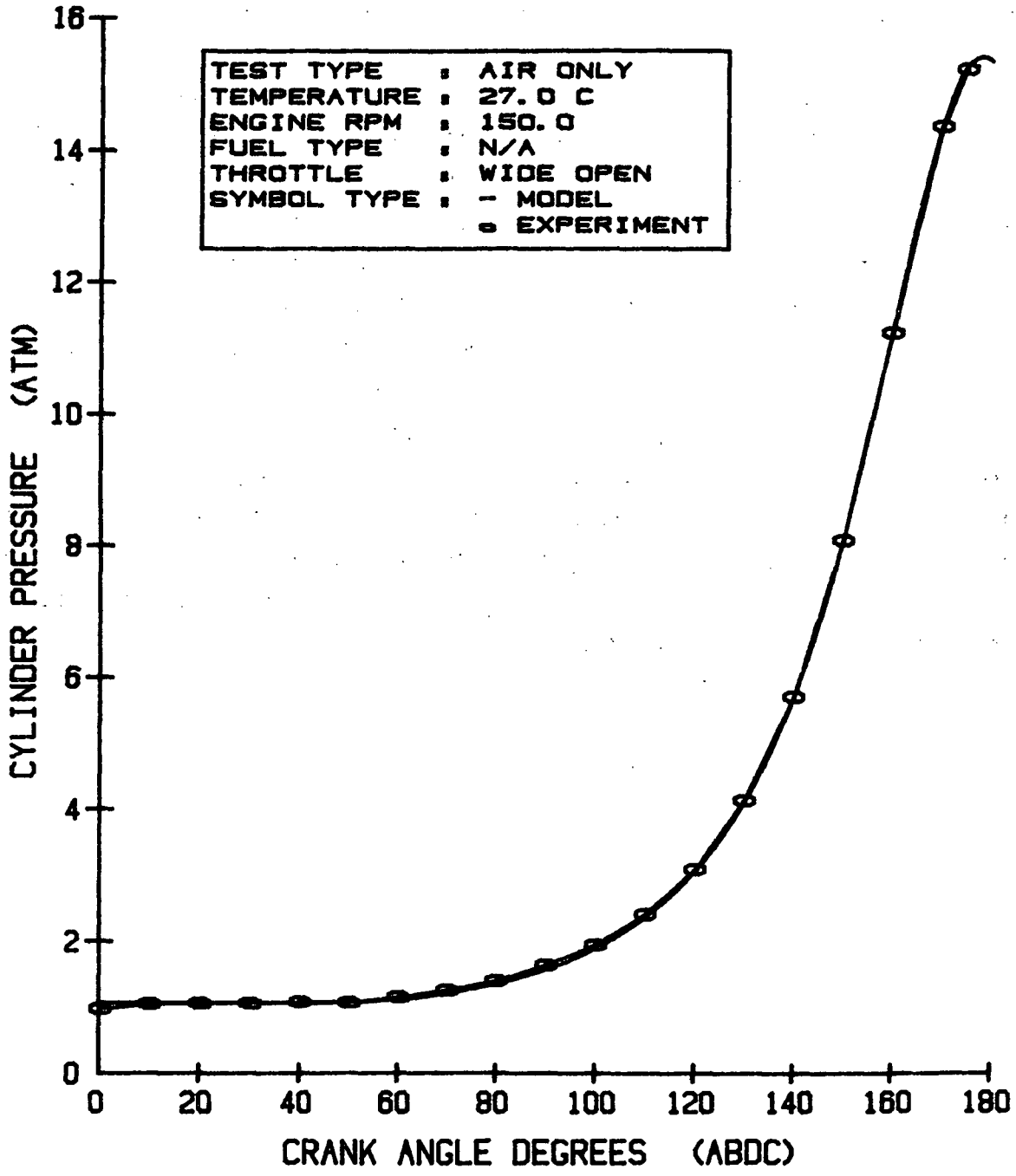

FIGURE III.13 : CYLINDER PRESSURE MODEL vs EXPERIMENT

accuracy of the model can be tested by comparing the experimental pressure data, the computed heat transfer and mass of fuel vaporized with that of the model prediction. Although exact agreement cannot be expected due to the differences in the approaches, a good agreement in the magnitudes of the quantities involved will go a long way in establishing a confidence in the model and improving the accuracy of the parametric studies.

III.8 SUMMARY

To date the model prediction and the experimental results are in close agreement (Figs. III.11, 12, 13) [III.7]. Since the model uses a uniform droplet size of 50 microns the predicted magnitude of the pressure suppression is higher than the experimental value where the droplet sizes are not only much greater than 50 microns but are also distributed over a range of values. This difference points in two directions: one, that current, poor cold starting of alcohol fueled engines is in part due to insufficient nebulization of the fuel and two, that this discrepency must be overcome by using a better fuel injector at higher pressure modifying the computer model to handle the droplet diameter distribution. The droplet distribution can be experimentally calculated from the laser hologram studies and this approach is being currently explored. Although the net heat transfer over the whole cycle is in close agreement (model and experiment) it is felt that a better match can be obtained if the problem of valve lift is overcome by replacing the hydraulic lash adjuster by a solid valve. During the follow-on work these issues will be sorted and the vaporization calculations will be concluded.

III.9. REFERENCES

1. R.K. Pefley, L.H. Browning, et al., "Characterization and Research Investigation of Alcohol Fuels in Automobile Engines," Final Report, DOE Contract No. DE-AC03-78CS, 1981.

2. L.H. Browning, J.E. Nebolon and R.K. Pefley, "Research Investigation of Alcohol Usage in Spark Ignition Engines," ATD/CCM Conference, Oct.1982.

3. J. Nebolon, L.H. Browning, et. al., "Multi-Point Injection of Alcohol Vapor as a Cold Starting Aid for Neat Alcohol Fueled Vehicles" V International Alcohol Fuels Technology Symposium, Vol. 2, 1982.

4. R.J. Nichols and R.J. Wineland, "Technique for Cold-Start of Alcohol Powered Vehicles," V International Alcohol Fuel Technology Symposium," New Zealand Vol 2, 1982.

5. L.H. Browning, "Alcohol Cold Starting--A Theoretical Study," 18 IECEC, Vol 2, Orlando, 1983.

6. G. Raghuraman, "Development of an Experimental Procedure to Calculate the Mass Friction of Fuel Vaporized During the Cranking of an Alcohol Fueled S.I. Engine," M.S. Thesis, University of Santa Clara, 1984.

7. L.H. Browning and G. Raghuraman, "A Detailed Study of Alcohol Cold Starting," VI International Alcohol Fuels Technology Symposium, Ottawa, Canada, 1984.

8. Microcomputer Handbook, Digital Equipment Corporation.

9. DECLab-03 FORTRAN Extensions User's Guide, Digital Equipment Corporation, Maynard, Massachusettes.

10. G.P. Blair and J.M. Mcconnel, "Unsteady Gas Flow Through High-Specific Output 4-Stroke Cycle Engines," SAE Paper 740736.

11. Yasuo Takagi, Yasuo Nakajima, Tsuneaki Saito, Tamotsu Iijima, "Analysis of Fuel Vaporization in S.I. Engine Cylinder During Low Temperature Cranking," SAE Paper 810 , 1981.

12. W.J.D. Annand, "Heat Transfer in the Cylinders of Reciprocating Internal Combustion Engines," Proceedings of the Institute of Mechanical Engineers, Vol. 177, No. 36, 1963.

13. A.C. Alkidas, "Heat Transfer Characteristics of a Spark Ignition Engine," Journal of Heat Transfer, Vol. 102, May 1980.

CHAPTER IV
VEHICLE AND ALLIED ENGINE STUDIES

During this grant there were two major vehicle studies with neat alcohol. In one study, supplementary funds were supplied by the United States Postal Service to develop prototype kits for conversion of Ford Pinto vehicles to methanol or ethanol operation. These kit designs were subsequently accepted and Alcohol Energy Systems, under an independent project, supplied twenty of each to the Postal Service where they were incorporated in the mail delivery fleets at Denver, Colorado and Springfield, Illinois. In the other major study, the Toyota Technical Center continued throughout this grant to make available a Toyota Cressida for evaluation of performance and emissions on methanol gasoline blends.

IV.1. POST OFFICE PROJECT INTRODUCTION

The purpose of this task was to design, for the U.S. Postal Service, modification hardware to convert a small fleet of 40 Ford Pintos with 2.3 liter engines: 20 to methanol and 20 to ethanol, and maintain 49 state exhaust emissions compliance. This was accomplished by engineering the required hardware and creating a conversion manual which fully described the required hardware and the procedures for the conversion [VI.1,2]. The hardware was assembled in the form of kits and delivered to the Postal Service for their mechanics to install in vehicles under an independent project. The manual is a unique and complete description of the conversion of a specific vehicle class to the alcohols. To aid in the development of the conversion specifications, two Postal Service vehicles were loaned to the University. These vehicles are 49 state, 1980 Ford Pintos, equipped with exhaust gas recirculation (EGR) and having CO, UBF two-way (TW) catalyst systems.

IV.1a Vehicle Modification Criteria

Four criteria were used in the development of the conversion specifications. These criteria are: (1) performance and safety of the vehicle, (2) cost of the modification, (3) fuel economy effects, (4) exhaust emission effects. The development of the kit involved computer modeling, hardware development, and

bench and dynomometer tests. The related computer models are described in more detail in Chapter II, while the cold start hardware is described in Ref. IV. . This section is primarily a summary of the actual conversion. The conversion will be summarized under three categories: power and fuel economy, materials compatability, and cold startability and driveability.

IV.1a.1 Power and Fuel Economy

To improve power and fuel economy, the compression ratio was increased from 9:1 to 11:1 by milling the cylinder head as the computer model predicted methanol fuel economy improvements of 5% and 9%, for the postal service and urban driving cycles, respectively (see Sec. II.1). For strength, the OEM head gasket was replaced with the one used in the turbocharged version of the 2.3 liter engine used in the Ford Mustang.

To provide the proper air fuel mixture for methanol or ethanol, eleven jets were modified or changed in the Holley 5200 carburetor. To improve acceleration power, a vacuum delay valve was added to the EGR vacuum signal. This modification reduced the tendency to lean the mixture during acceleration. Thus, some fuel economy was sacrificed for the sake of driveability.

IV.1a.2 Materials Compatability

If not dealt with properly, materials compatability problems can precipitate system failures. The modifications used in this conversion were based on the experience which is documented in the literature. It is common knowledge that methanol will dissolve the terne plate coating of the fuel tank. The terne (90% tin/10% lead) can clog the fuel filter and/or pass through the engine and destroy the catalyst. To eliminate these problems, the terne coat was stripped prior to operation on the alcohols. A woven polypropylene filter providing eight micron absolute filtration was installed to prevent particulate fuel contaminants from affecting the carburetor, engine, or catalyst system. The carburetor was chromate dipped to inhibit corrosion, due the high electrical conductivity of methanol.

IV.1b Cold Startability and Drivability

Cold starting and warm-up driveability are significant challenges in the development of alcohol conversion specifications for climates with temperatures below 0 ^{o}C. The vehicles, to be put in service in Denver, CO and Springfield, IL, required special attention both due to such low temperatures as well as high altitudes at the Denver site when compared with the previous Pinto fleet produced for the Department of energy [IV.1].

Many solutions to the cold start problem were considered. Fuel additives such as iso-pentane and di-methyl ether were investigated. Considerable time and effort were spent on two cold start system prototypes. One system was a multipoint vaporizer. The other was a gasoline injection system. This was developed and then abandoned due to the complex feathering with the alcohol carburetor that is required for multiple speed/load conditions during warm-up. The final choice was the most practical, effective solution available.

An ether injection system, similar to those used in diesel engines, was used for cold starting. Since the ether injection system operates during the cold start only, other modifications were made to improve cold drivability. A barrium titanate electric heater (180 watts) was installed under the carburetor to improve fuel vaporization until heat from the engine was available. Such heaters have temperature sensitive resistances which essentially create an open circuit or switch off at elevated material temperatures. The coolant flow rate past the intake manifold was increased by a factor of thirty, and a copper gasket was used between the head and intake manifold to increase heat transfer to the manifold. The vacuum motor controlling the amount of heated air inducted from the exhaust manifold was connected directly to manifold vacuum. This modification caused heated air to always be inducted, except at high loads, which improved fuel preparation and driveability. Lastly, spark plugs one heat range cooler were installed to prevent hot surface or pre-ignition, which can occur with the alcohols using standard heat range spark plugs under high load conditions.

IV.1c Installation of Kits and Field Experience

The conversion kits were packaged in self-contained units, one per vehicle. Prior to packaging, a Post Office mechanic visited the University of Santa Clara where he studied the instruction sheet, watched the installation of one kit and then performed the installation with a successful drive-away after the contents of another kit were installed. The kits were subsequently shipped to the Postal Service Centers at Springfield, Illinois and Denver, Colorado where they were installed, producing ten ethanol and ten methanol vehicles at each location. The fueling sites at the Service Centers had been prepared with standard metering pumps, fuel vapor recovery systems and filters, all of which were certified alcohol resistent by the fuel system suppliers (see [IV.1]).

IV.1c.1 Field Experience

The field experiences are being extensively documented in Ref. IV.3. Hence, only the highlights are touched upon here.

Although the field adaptation of the Pintos to alcohol went smoothly, in the early phase of vehicle start-ups, several poor operational vehicle behaviors are reported. These were traced to two circumstances: one was a carburetor jet problem and the other was an installation problem.

The carburetor problem arose because the carburetors in the conversion kits were not exact duplicates of those used on the prototype vehicles although the carburetor manufacturer had originally certified them to be duplicates. This required rejetting of the carburetors in the field. The second problem arose because at one installation site the mechanics took their own initiative relative to vacuum line hook-up rather than follow the specified instructions.

Another field problem arose with reports of excessive aldehyde levels around some of the vehicles. This was traced to incorrect idle mixture adjustments, plastic floats that had absorbed alcohol and, hence, enrichened the fuel-air mixture and the type of Postal route driven. The mixture setting and float problems were corrected by field servicing of the vehicles which made aldehyde levels acceptable. However, the park and walk route that some vehicles traveled

would not allow the hydrocarbon exhaust catalyst to reach full operating temperature. As a result, the catalyst served as a very effective aldehyde generator using the unburned fuel as an aldehyde source. This problem, while not serious with a correctly tuned engine, deserves further attention if aldehydes are to be minimized for all types of alcohol fueled vehicle usage.

A puzzling corrosion problem arose with the secondary throttle shaft of the ethanol vehicles, while the methanol vehicles remained free of the problem. This is contrary to expectation that corrosion problems are more severe with methanol and ethanol. To understand the problem it is important to note that exhaust gas recirculation (EGR) was required by the ethanol vehicles while it was not required by the methanol vehicles to bring them into compliance with EPA's 49-state emission standards. It has been observed (see Chapter V) that the condensate of the exhaust gases for alcohol fueled engines has a higher dew point and may be more acidic than for gasoline vehicles. This combined with the increased cooling of the carburetor from the high heat of vaporization of the ethanol and the low power required for the postal driving route keeps the secondary throttle shaft bathed in acidic condensate and corrosion results. The absence of this condensate due to the absence of EGR in the methanol fueled vehicles excluded the problem.

Engine corrosion and wear have been reported for the Pintos primarily relating to the methanol fueled vehicles. The corrosion evidence is presented in Ref. [IV.4]. Chapter V of this report gives a detailed explanation of the mechanism as it is now understood.

IV.1d Summary

The Post Office methanol and ethanol fleet posed some unique challenges: very cold tempertures, very low loads--primarily starting, driving short distances and stopping.

The fleet was operated essentially complaint free as it relates to cold starting. However, cold starting with a secondary fuel and fast idling to warm engine state before driving are not considered to be fully satisfactory cold weather protocol by the authors. The aldehyde problem and engine corrosion and

wear evidence also deserve careful study in the interest of generating fully successful field vehicles for the Postal Service.

IV.2 EGR STUDY

An engine dynomometer experiment was employed to study the effect of EGR on emissions and fuel economy [IV.5]. There were two motivating factors for this experiment. One, since EGR is used to decrease NOx emissions and noting that these emissions are already lower for methanol than gasoline, could high EGR rates reduce NOx emissions, possibly enabling the elimination of the two-way catalyst (TWC). Two, since the aldehyde emissions are of major concern, could the effect of high EGR rates be an effective way to reduce them.

A Ford 2.3 liter engine was used for this study, which was equipped with a turbocharger, a feedback controlled carburetor, and a three-way catalyst system. The EGR system was modified to provide manual control of the EGR rate. The spark setting was also manually controlled and all data points were taken at MBT settings. The emissions reported are NOx, UBF, and HCHO, measured by NDIR, FID, and MBTH methods, respectively.

The EGR rate was varied over a matrix of test points: a fixed speed of 2000 RPM at 1/3, 2/3 and full throttle, and a fixed load of 36 psi bmep at 1300, 2000, and 3000 RPM. This load represented approximately 40, 35, and 20% of full load, respectively. All test points were taken at stoichiometric air-fuel ratio and MBT spark setting.

IV.2a EGR Limits

The limiting factor of allowable EGR is the lean misfire limit, which is indicated by rough engine operation and high UBF emissions. This limit was found to be approximately 25% EGR. A more practical limit is indicated to be 18% EGR, at which the UBF emissions sharply increase.

IV.2b Variable Load Tests at Constant Speed

As can be expected, NOx emissions increased with increasing load, due to higher

combustion temperatures. At high loads the NOx emissions could be reduced by a factor of two, from 9.0 to 4.5 gm/kwh, with high EGR rates. At the low load point, EGR reduced the NOx by an order of magnitude, from 8.0 to approximately 0.8 gm/kwh. Lower NOx rates with EGR are due to decreased temperatures from the addition of the inert recircled exhaust gas. Unburned fuel emissions increased with decreasing load and increasing EGR rate. Formaldehyde emissions followed the same trends as the unburned fuel emissions, but were not as strongly influenced by load or EGR rate as UBF. Brake specific fuel consumption improved with increasing EGR due to two factors: decreased pumping losses as the throttle is opened to compensate for the combustion mixture dilution and improved mixture preparation due to the higher charge temperature.

IV.2c Variable Speed Tests at Constant Load

The NOx emissions increased with the increasing speed at constant brake man effective pressure. High EGR reduced the NOx as much as 95% for these light load points. Unburned fuel emissions increased with decreasing speed and, again set a practical limit for EGR at about 18%. The HCHO emissions also increased with decreasing speed, but were not strongly a function of EGR until 18% or higher. As in the previous matrix, the BSFC improved slightly (about 5% average) with higher EGR rates, until the misfire limit was reached.

IV.2d Conclusions

As in the case of gasoline fueled engines and consistent with the modeling evidence in chap. II, EGR in the range of 0 to 18% is found to be effective in reducing the NOx levels in alcohol fueled vehicles. The suppression can exceed 50% at high loads which suggests that lean burn engines which have high thermal efficiencies may be successfully equipped with two-way instead of the three-way catalyst systems currently being used on gasoline vehicles. Also, a gain in fuel economy is possible by this technique. However, driveability may deteriorate. Evaluations of these contrasting strategies need to be continued. Aldehyde evaluations need also to be continued but the EGR effect on them appears to be of secondary importance.

IV.3 UNBURNED FUEL EMISSIONS CHARACTERIZATIONS

Unburned fuel emissions characterizations are important in the assessment of the photochemical smog and direct exposure health effects of alternative fuels. For the alcohols in particular, high hydrocarbon emissions may influence their implementation. The high evaporative loss from gasoline blended with small percentages (<10%) of methanol is a significant environmental factor retarding the marketing of this fuel today. In the near future, utilization of neat or near neat alcohol fuels may be retarded due to concern over aldehyde emissions. The objective of the study conducted at the University is to aid in assessing the impact of these fuels, and also aid the designer of alcohol systems to design acceptable solutions.

Several segmental tests have been conducted for various reasons during this contract period. The purpose of this article is to summarize the results of these experiments(some, not previously published or reported) , and present them in a meaningful way. Tables IV.1 and IV.2 are summaries of the exhaust and evaporative emissions, respectively. This data is reported in the usual manner: gm/mi for the FTP exhaust emissions, and gm/test for the FTP diurnal heat build and hot soak evaporative emissions tests. Unfortunately, each test varied in the kind of analysis performed. Therefore, if no detailed analysis was made, the measurement is entered solely as UBF. If various components were identified, these are listed, and their sum(except for aldehydes) is entered as UBF. These data include the oxygen mass of the alcohol. The standard for exhaust emissions is .41 gm/mi, while the evaporative emission standard is based on the sum of the diurnal heat build and hot soak test, and is 2 gm. It should be noted that emissions testing of alcohol and blend fueled vehicles can produce a variety of answers depending upon the protocol (see [IV.6] and Sec. IV.4).

Figures IV.1 and IV.2 are summaries of the same data as in the tables, but in a different format. To combine the results of the exhaust and evaporative tests, the following assumptions made by the EPA were used [IV.7]. The gm/mi value for the urban driving cycle is multiplied by 29.4, the total vehicle miles per day. To this value is added the diurnal heat build value plus 3.3 (the average number of trips per day) times the hot soak value. This results in a total of grams of unburned fuel emissions per day. The detailed emissions data is summarized in

Table IV.1 Detailed UBF Exhaust Emissions Summary [1]

VEHICLE	FUEL	UBF	CH3OH	C2H5OH	CH4	NMHC	C5M12	HCHO	C2H3OH
P.O. Pinto [2]	M100	8.20	-	-	-	-	-	.341	-
P.O. Pinto [3]	M100	6.72	-	-	-	-	-	.097	-
P.O. Pinto [4]	M100	.67	-	-	-	-	-	.073	-
Flt I Pinto	M100*	.31	.23	-	.05	.03	<.01	.052	-
Flt I Pinto	MEOH*	.65	.47	-	.12	.06	.05	-	-
Flt II Rabbit	M100*	.66	.63	-	.03	<.01	<.01	-	-
Flt II Rabbit	MEOH*	.71	.62	-	.02	.07	.05	.076	-
Flt II Rabbit	CDA-20	.47	-	-	-	-	-	-	.273
1982 Cressida	M80	.51	-	-	-	-	-	.110	-
1982 Cressida	M90	.48	-	-	-	-	-	.068	-
1982 Cressida	M100	.56	-	-	-	-	-	.075	-
1980 Cressida	Gas	.29	<.01	<.01	.04	.25	-	.005	.001
1980 Cressida	M30	.29	.05	-	.04	.20	-	.004	.002
1980 Cressida	M70	.44	.26	-	.03	.15	-	.041	.001
1980 Cressida	M100	1.19	1.16	-	.01	.02	-	.090	<.001
1980 Cressida	E30	.22	<.01	.03	.04	.15	-	-	-
1980 Cressida	E70	.30	<.01	.05	.04	.20	-	.005	.021
1980 Cressida	E100	.80	<.01	.65	.06	.09	-	.001	.066
Cavalier	Gas	.15	-	-	-	-	-	.011	-
Cavalier	M8.5	.15	-	-	-	-	-	.122	-
Celebrity	Gas	.13	-	-	-	-	-	-	-
Celebrity	M8.5	.27	-	-	-	-	-	-	-

---

* 5.5% Isopentane added

1 All emissions are expressed in gm/mi
2 Vehicle tested as received
3 Vehicle tested with carburetor float replaced
4 Vehicle tested with new float and jets replaced

Table IV.2 Detailed UBF Evaporative Emissions Summary[1]

VEHICLE	FUEL	UBF	CH3OH	HC	C6H6CxHy	C5H12	UBF	CH3OH	HC	C6H6CxHy	C5H12
P.O. Pinto	M100	-	-	-	-	-	-	-	-	-	-
Flt I Pinto	M100*	4.65	4.65	.00	-	.00	1.06	1.06	.00	-	.00
Flt I Pinto	MEOH*	4.07	3.27	.80	-	.80	1.04	.94	.10	-	.10
Flt II Rabbit	M100*	1.26	1.26	.00	-	.00	.55	.55	-	-	-
Flt II Rabbit	MEOH*	1.90	1.23	.67	-	.67	.52	.44	.08	-	.08
Flt II Rabbit	CDA-20	3.28	-	-	-	-	1.04	-	-	-	-
1982 Cressida	M90	1.42	-	-	-	-	.39	-	-	-	-
1980 Cressida	Gas	1.06	-	-	-	-	.62	-	-	-	-
1980 Cressida	M30	2.76	-	-	-	-	-	-	-	-	-
1980 Cressida	M70	4.51	-	-	-	-	-	-	-	-	-
1980 Cressida	M100	-	-	-	-	-	-	-	-	-	-
1980 Cressida	E30	2.27	-	-	-	-	.70	-	-	-	-
1980 Cressida	E70	2.34	-	-	-	-	-	-	-	-	-
1980 Cressida	E100	1.32	-	-	-	-	-	-	-	-	-
Cavalier	Gas	.44	.00	.44	.21	-	.54	-	.54	.12	-
Cavalier	M8.5	.44	.11	.33	.19	-	.55	.08	.46	.15	-
Celebrity	Gas	.66	-	-	-	-	.90	-	-	-	-
Celebrity	M8.5	3.29	-	-	-	-	1.35	-	-	-	-

[1] All emissions are expressed in gm/mi

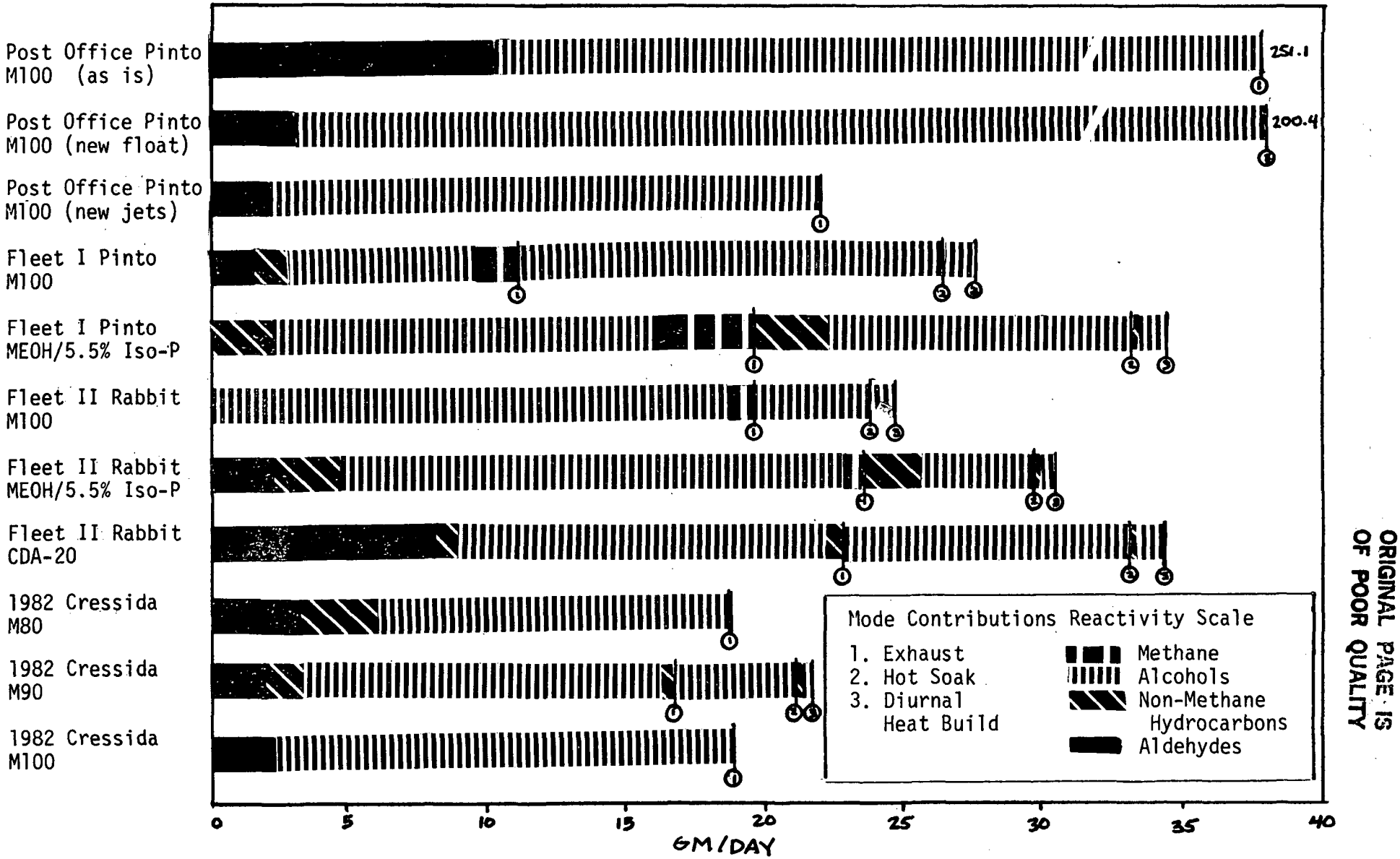

FIGURE IV. 1 UNBURNED FUEL EMISSIONS FROM NEAT OR NEAR NEAT ALCOHOL FUELED VEHICLES

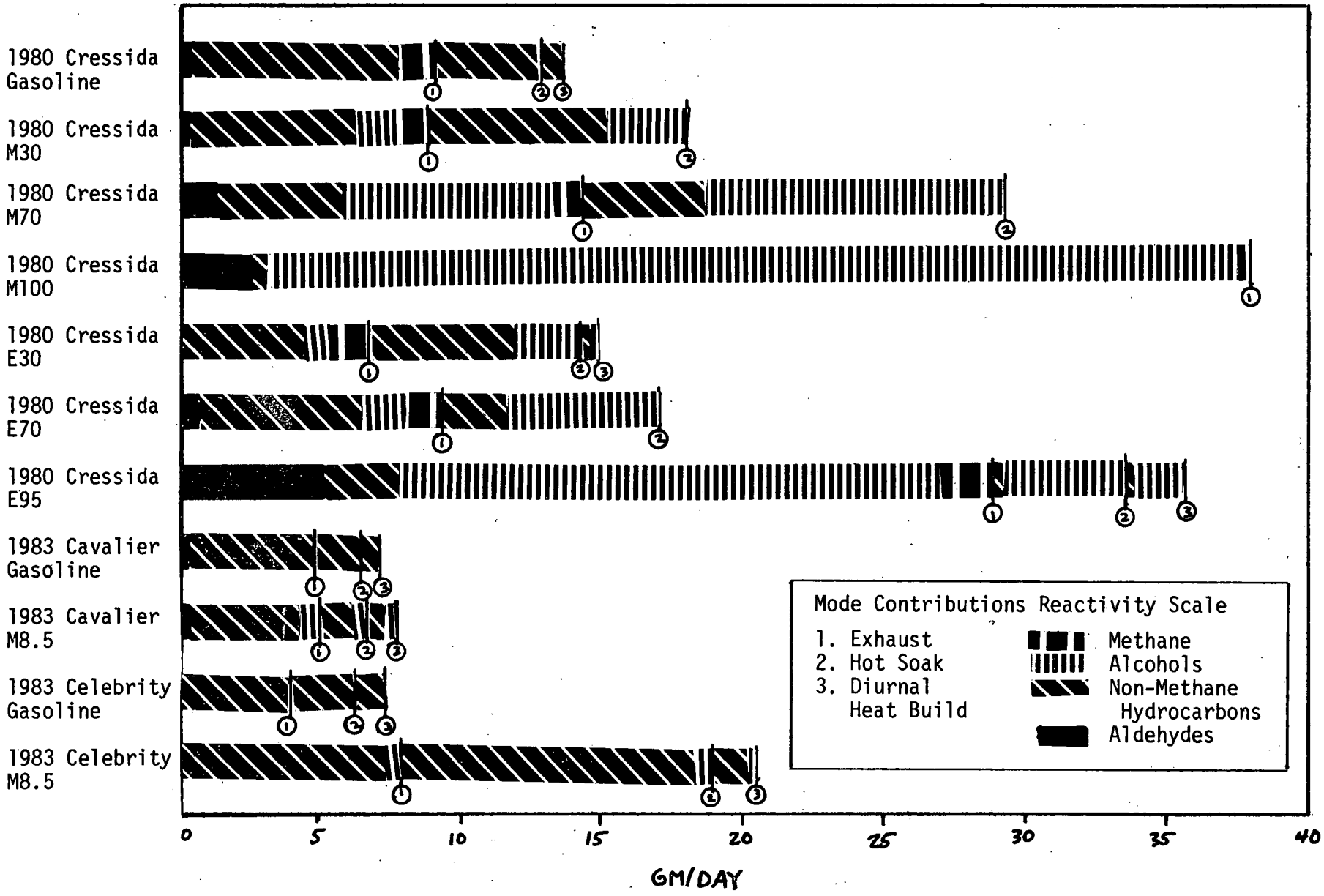

FIGURE IV.2 UNBURNED FUEL EMISSIONS FROM ALCOHOL/GASOLINE BLEND FUELED VEHICLES

four basic groups of photochemical reactivity: aldehydes, non-methane hydrocarbons, alcohols, and methane. If no detailed analysis was performed, the emission was assumed to be of the same composition as the original fuel. The emissions contribution from the exhaust, hot soak, and diurnal heat build are indicated by a "1","2", and "3", respectively.

IV.3a Description and Results of The Blend Tests

Two major studies and several experiments were conducted with blend fuels. One study was the chacterization of the 1980 Toyota Cressida, which was conducted at the Bartlesville Energy Technology Center [IV.8]. This was an exhaust emission study measuring as many as 69 individual compounds. The fuels for the vehicle were a gasoline baseline, M30*, M70, and M100, E30, E70, and E100. In addition, several SHED tests with these fuels were conducted at the University; however, no gas chromatograph analysis was performed.

The values obtained from these tests can be found in the tables; the trends will be discussed here. With the oxygen mass included, total UBF emissions were comparable to the gasoline baseline for the M30, E30, and E70 tests, and the .41 standard was met for all these fuels. This statement could also be made for the M70 tests, with the oxygen excluded. Only on pure methanol and ethanol were the UBF emission rates significantly higher. The aldehyde rates were significantly more than the baseline for the 70 and 100% runs, and were consistently about 8% of the UBF emissions. Interestingly, the evaporative emissions contribution is as much or more than that of the exhaust emissions for some of these blend fuels. None of the blend fuels tested could meet the evaporative standard, even with the oxygen mass excluded. Note that this was basically a gasoline vehicle, and was not optimized to run on neat alcohol, nor high blend percentages.

Another study was conducted at the University with two 1983 vehicles. The fuels tested were gasoline and a post refinery blend of 90% unleaded gasoline, 8.6% methanol and 1.4% iso-butanol as a cosolvent. Two GM vehicles were used: a Cavalier, which was fuel injected, and a Celebrity, which was carbureted. The

* 30% methanol by volume added by post refinery mixing to the gasoline.

interest was primarily in the evaporative emissions effects. The methanol and aromatic components of the hot soak and diurnal heat build emissions were measured; no such analysis was made of the exhaust UBF measurements.

Surprisingly, the fuel injected vehicle showed no increase in evaporative emissions, even with the oxygen mass included, and met the standard on both fuels. Exhaust emissions decreased by 3% with the blend. The carbureted vehicle showed a three-fold increase in evaporative emissions on the blend, and failed to meet the standard. The exhaust UBF emissions doubled, but remained within the .41 gm/mi standard.

To summarize the results of this study, the short term evaporative emission changes with a 10% oxygenate blend were excessive for a carbureted vehicle, and negligible for a fuel injected vehicle.

IV.3b Description and Results of the Neat Fuel Studies

One major study and many experiments were conducted involving the measurement of UBF and aldehydes as well as a detailed analysis of the UBF emissions with neat or near neat alcohol fuels.

A series of tests was conducted on an in-service Post Office vehicle operating on methanol. As reported in the previous section, the Post Office vehicles on occasion were operating extremely rich, and this series of tests was meant to investigate the causes and resulting exhaust emissions effects of the rich operation. Based on CO measurements, a test vehicle was found to have an equivalence ratio at idle of approximately 1.3. The vehicle was tested as it was received. The CO emissions were extremely high (100 gm/mi) and the UBF emissions were 8.20 gm/mi. Aldehyde emissions were also extremely high (0.341 gm/mi). It was first thought that the rich operation was due to the carburetor float sinking from absorbing methanol. This cause was first tested by replacing the float and retesting the vehicle. The UBF emissions dropped to 6.72 gm/mi and the aldehyde rate dropped to 0.097 gm/mi. Then, the fuel and air jets were replaced with their proper sizes, and the emissions were markedly decreased further: UBF, 0.67 gm/mi; and aldehydes, 0.073 gm/mi. The conclusion of this study as described in Sec. IV.1b was that a miscalibrated alcohol car can be a

major aldehyde emitter, and , as expected, a heavy carburetor float can produce a measureable difference in emissions.

The major characterization with neat alcohol fuels was of the California Energy Commission Fleet I and II vehicles: 1980 Ford Pintos and 1981 Volkswagon Rabbits, respectively [IV.9,10]. The fuels used were neat methanol, and a 5.5% mass iso-pentane/methanol blend. The vehicles were tested for UBF emissions of methanol and C_1 to C_5 hydrocarbons. The aldehydes reported here were taken from another series of tests which have been presented in a previous progress report and elsewhere [IV.9,10]. A Fleet II Rabbit on denatured ethanol was also tested (without GC analysis), and the results are reported here [VI.10].

The UBF emissions were less for both Fleet I and II vehicles on methanol when compared with the isopentane blend. The Pinto vehicle met the 0.41 gm/mi standard with the oxygen mass included; all other cases met the standard with the oxygen excluded. The Pinto UBF exhaust emissions averaged 17% by mass methane, compared to 3.3% for the Rabbit. The evaporative emissions were quite high for the Pinto, due to that fact that it is carbureted, and that the cannister was probably heavily loaded with methanol after 13,000 miles of operation. The Rabbit met the 2 gm evaporative standard on methanol with the oxygen included, and on the isopentane/methanol blend with the oxygen excluded. Aldehyde emissions were measured for both cars only on their "standard" fuels (neat methanol for the Pinto and the methanol/isopentane blend for the Rabbit). Formaldehyde rates were 16% of the UBF rates for the Pinto and 11% of the UBF rates for the Rabbit.

With the oxygen mass excluded, the Rabbit on denatured ethanol* met the exhaust standard, but failed the evaporative standard. The aldehydes level, using the MBTH technique, and calculated as acetaldehyde, was .273 gm/mi, which was 58% of the UBF emission.

A 1983 Toyota Cressida (see Section IV.4) was also tested for aldehydes and evaporative emissions. The vehicle was tested on M80, M90, and M100 and various spark settings (0^o, 2^o and 4^o BTDC) were also used. The UBF results were very

* CDA-20 denatured with 10% of gasoline type hydrocarbons.

similar for all three fuels. The average aldehyde rate for the three fuels was 0.084 gm/mi, about 15% of the UBF emissions were measured for the M90 blend and were quite low: 1.81 gm total with the oxygen included.

IV.3c Concluding Observations

Several observations can be drawn as a summary of these studies:

1. Short term evaporative emission effects can be excessive with post refinery blend fuels, particularly with carbureted vehicles.
2. Long term effects of evaporative emissions on neat fuels should be investigated further, due to the lowered purging efficiencies of the cannister.
3. A properly tuned vehicle optimized for alcohol will produce acceptable UBF and aldehyde emission rates, and may even be superior to gasoline.
4. Fuel injection systms may be superior to carburetion systems in adapting to small fuel composition shifts; hence, in controlling exhaust and evaporative emissions.

IV.4 TECHNIQUES FOR EVALUATION OF EMISSIONS OF TESTING ALCOHOL FUELED VEHICLES

The Federal Test Procedure for light duty vehicles defines the method for determining emission rates and fuel economy for comparison with the regulated standards. This test procedure is based on gasoline or diesel, and to maintain data integrity, must be modified for alcohol. Many of the modifications were described elsewhere [IV.7,11] and are summarized here. The primary areas of concern are unburned fuel emissions, fuel economy, and exhaust condensation.

IV.4a Unburned Fuel Emissions

For gasoline and diesel, a H/C ratio of the emissions is assumed for the exhaust emissions, hot soak, and diurnal heat build tests. A similar assumption is required whenever an alternative fuel, such as alcohol, is used. The accuracy of the assumption will limit the accuracy of the mass emission measurement. Based on the tests of the 1980 Cressida and the Fleet I and II vehicles previously described, the assumption that the UBF emissions are of the same composition as the original fuel was checked. This simple assumption resulted in errors of 2 to

26%, primarily due to a decrease in the oxygenate fraction in the emission relative to the fuel.

It is important to reach a common agreement as to how the UBF emission is to be defined,i.e. whether or not the oxygen mass is included as it often determines whether or not the vehicle meets the standard. From photochemical considerations (see Chapter VI and [IV.11]), which are the basis for controlling UBF emissions, it is reasonable to define the emission without the oxygen mass associated with the alcohol molecule. Excluding the oxygen mass results in a secondary benefit: the accuracy of the UBF emissions measurement improves. Based on the same tests, but now excluding the oxygen, the assumption that the emission is of the same composition as the fuel results in errors of only 0 to 2.4%.

The measurement of unburned fuel emissions is further complicated because the response of the flame ionization detector (FID) to alcohol is reduced by 10 to 30% compared to propane, the standard calibration gas. This response factor varies with the instrument model, burner configuration and operating conditions. A technique was developed at the University to determine the response factors of its instruments [IV.7]. Further experiments showed that the response factor is a linear function of the components of a blend sample. Thus the best solution at this point is to determine the response factor for a particular FID for methanol and ethanol, and calculate the response factor for any blend fuel tested. The assumption of a response factor of unity for the hydrocarbons would be consistent with current FTP protocol.

IV.4b Fuel Economy Calculations

The calculation of fuel economy for alcohol fuels is incorrect using the carbon density of gasoline. The errors for methanol and ethanol are of the order of 116 and 56% high for the neat fuels, respectively. Using the correct carbon density of the fuel will result in a correct volumetric fuel economy. However, a volumetric based fuel economy is not the best way to compare fuels of different energy densities. An energy based fuel economy, such as $mi/10^6$ Btu is more appropriate.

IV.4c Water Condensation

Stoichiometric air/fuel mixtures produce a methanol exhaust which contains 23 molar percent water, an ethanol exhaust which contains 18 molar percent water, compared to 12 percent for gasoline. If corrective action is not taken, condensation will occur in most exhaust dilution tunnels used in CVS testing when evaluating these alternate fuels. Condensation will cause UBF and NO_x emissions to be artificially low. Calculations have been performed that determine what temperature is needed to avoid condensing the exhaust mixture for a given vehicle and blower flowrate. For the system at the University, condensation is prevented by heating the dilution air to 120 F, which has proven adequate. Condensation has not been observed in the sample bags. This may occur but can be avoided by recognizing the difference between the exhaust condensate of gasoline and alcohol fuels.

IV.4d Conclusion

The aforementioned areas of concern should always be addressed whenever one is testing an alcohol fueled vehicle. The issues raised should be the subject of discussion among testing groups, leading to the establishment of a defined test fuel, a formaldehyde emission standard, and a test procedure. This achievement is seen by the authors as a necessary step to the development and commercialization of alcohol fuels.

IV.5 TOYOTA CRESSIDA--A UNIQUE TEST VEHICLE

IV.5a Introduction

Having recognized the alcohol fuels as extenders and replacers of petroleum based fuels in the transportation industry, in the near term it is possible to accommodate the use of 5% anhydrous methanol or 10% ethanol as gasoline extenders for current production vehicles as is evident by Environmental Protection Agency waivers for such fuels and earlier work [IV.13]. Although current alcohol production may be used in blends, it is presently nowhere near the level required to provide fuel for a significant number of pure alcohol-fueled vehicles. Conversely, manufacturers are reluctant to produce vehicles

capable of operating on alcohol until an abundant supply of fuel becomes available. One solution to this circular impediment to utilization lies in the development of an inexpensive modification to an existing vehicular engine control system to permit operation on any blend of gasoline and alcohol. If a large number of such vehicles were available, implementation of alcohol fuels could be carried out in a more flexible and expeditious manner.

Multipoint Electronic Fuel Injection systems (EFI) with feedback control are currently appearing in new cars and have excellent potential for meeting the above requirements as well as maintaining fuel economy and emissions levels. The feedback systems provide precise air-fuel (A/F) ratio control and thus offer automatic compensation for the shift in stoichiometry required by the alcohol fuels thereby retaining performance, emissions, fuel economy, and driveability. They are also attractive for use with alcohol fuels if properly compensated for fuel stoichiometry shifts since they inherently provide better acceleration transient response, warm-up driveability, and essentially no maldistribution of the air-fuel mixture among the cylinders; characteristics which have been persistent problem areas for carburetted vehicles and are exacerbated by the alcohols [IV.14]. When EFI is used in conjunction with a three-way catalytic exhaust system, very low levels of exhaust emissions can be obtained. Correct combustion stoichiometry required for optimum control of exhaust emissions in such three-way-catalyst (TWC) systems requires some type of feedback logic. This feature can automatically maintain stoichiometry for alcohol/gasoline blends to some blend level depending upon the compensation range of the EFI system. The Toyota system has been shown to have a wide inherent compensation range [IV.15].

IV.5b The Toyota Closed Loop Feedback Controlled Fuel Injection System

The Toyota EFI system represents the "state-of-the-art" in current EFI systems. It has been adapted from the Bosch L-Jetronic system. A schematic diagram of the fuel system components is presented in Fig. IV.3.

An air flow meter provides the major input to the electronic control unit (ECU). The exhaust oxygen sensor "feeds back" information about combustion product composition so that the ECU can fine tune its fuel injection duration commands.

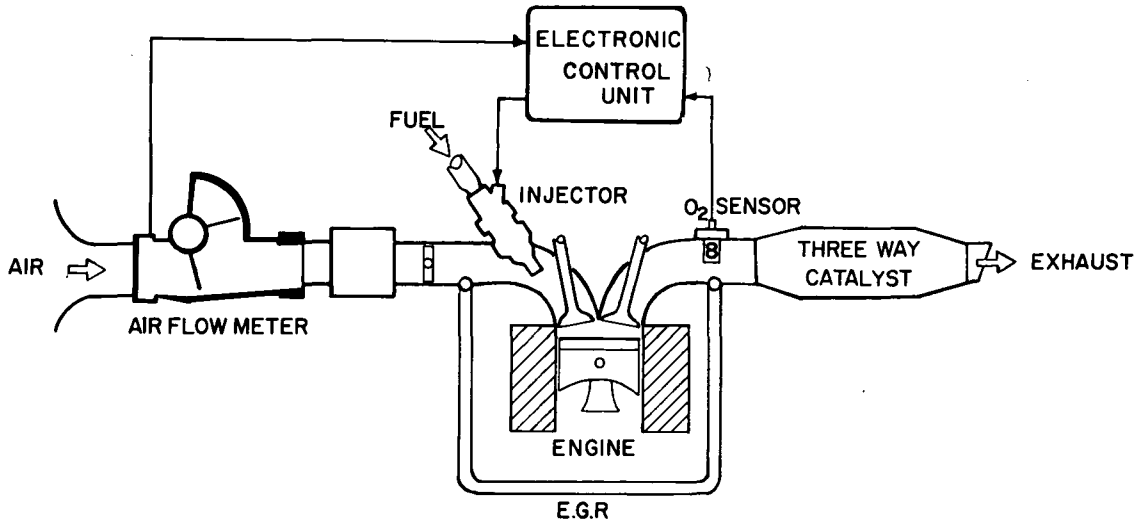

FIGURE IV.3 TOYOTA EFI CLOSED LOOP CONTROL SYSTEM

All injectors are connected electrically in parallel and simultaneously inject one-half of the required fuel to each cylinder once each revolution of the crankshaft. The resulting air-fuel ratio alternates rapidly about the stoichiometric mixture within a narrow range. The TWC system requires such a precisely controlled mixture in order to optimally reduce nitric oxide (NO_x) while simultaneously oxidizing carbon monoxide (CO) and unburned fuel (UBF) emissions.

Reference IV.15 presents evidence that an unmodified Toyota EFI system with feedback control can accommodate a post refinery blend of 50% ethanol/gasoline (by volume) or 30% methanol/gasoline before the leaning effects cannot be fully compensated and the leaning effect on emissions limits further increase in alcohol percentage. These blends represent a stoichiometric compensation of 18% relative to gasoline. The ECU of a 1980 Cressida was subsequently modified in a minimal fashion so that the impulse time generated by the control multivibrator could be selected manually in ten steps ranging from 1.0 to 2.0 times the original injection duration. The oxygen sensor coupled with the feedback logic was relied upon to maintain stoichiometric conditions for all fuel blends tested. Pre-test checks were made to assure that the system was within the authority range of the feedback control system for each blend. A supplemental 10 micron polypropylene fuel filter was also installed downstream of the original filter to keep the EFI system free of any particulates loosened by the presence of the alcohols blended into the gasoline.

These changes allowed the exploration of the concept of a "smart car", i.e., a vehicle capable of handling any combination of alcohol and gasoline.

IV.5c Test Results and Discussion--1980 Cressida

Using the 1975 Federal Test Procedure (FTP), the vehicle was evaluated over the entire spectrum of gasoline/alcohol blends for the purpose of evaluating driveability, fuel economy, and emissions. Dilute exhaust emissions were measured using conventional instrumentation and FID response factors were applied for the methanol and ethanol fractions of the exhaust [IV.10]. Evaporative emissions were quantified as functions of blend percentage. Detailed unburned fuel characterizations were conducted for the purpose of having an inventory useful in photochemical reactivity studies. Aldehyde emissions were also studied.

Carbon monoxide emissions, meeting for all blends the 1980 California emission standard of 9.0 gm/mile, were generally unchanged during the alcohol blend test series and the fuel economy on an energy basis remained constant regardless of the blend used [IV.15]. Good driveability was maintained for blends ranging from pure gasoline to 90% ethanol and methanol.* This suggests that the injection duration modifications incorporated with the electronic control logic maintained near-stoichiometric operation with alcohol blends in all driving modes, otherwise a substantial change of CO emissions and mileage, and/or serious driveability problems would have been observed.

Hydrocarbon emissions calculated as UBF, show very consistent emission levels for light and moderate blends of both alcohols. For higher percentage blends, the UBF nearly doubled when compared to gasoline. Part of this increase can be attributed to the oxygen mass contribution of the alcohol. On a carbon basis, the unburned fuel remained constant or decreased for methanol blends of 50% or greater, and all ethanol blends. For the lower blend percentages of methanol, carbon-based unburned fuel emissions increased by 24 to 55% over the Indolene baseline. In all instances, the blend HC emissions were below the 1980 California standards of 0.41 gm/mile [IV.15].

The post catalyst NO_x emissions were higher for the blend fuels and generally increased with alcohol percentage. Lower engine exhaust NO_x emissions for neat alcohol fuels relative to gasoline are repeatedly reported and it is true here. The implication is decreased TWC efficiency. There is other evidence of this rising NO_x with other TWC fuel injected vehicles operating on blends suggesting a generic problem [IV.10].

IV.5d Rise of NO_x Emissions From Alcohol Blends

To investigate the NO_x increase with increasing alcohol blend, attention was focused on the oxygen sensor [IV.16,18]. Dummy catalyst (no catalytic materials) tests confirmed engine-out NO_x emissions were lower for the alcohols than with Indolene, supporting

---

* The 90% ethanol fuel contained 10% hydrocarbons as a denaturant and the 90% methanol contained 10% gasoline for cold startability.

prior research. Therefore catalyst performance must be affected by the addition of alcohol and/or transient operation factors. A lean bias of the O_2 sensor associated with exhaust temperature increase during acceleration for alcohol fuels was predicted using a form of the Nernst equation. A lean mixture can result in decreased NO_x conversion efficiency for a TWC. Therefore, if during a vehicle acceleration when most of the NO_x is formed and exhaust temperatures increase, the mixture shifts lean and the oxygen-rich exhaust lowers NO_x catalyst efficiency, the result could be a relative increase of post-catalyst NO_x emissions in comparison with Indolene.

To evaluate this possible lean bias, several modifications were made. First, the O_2 sensor reference voltage in the feedback loop was raised from 0.45 to 0.75 volts in 0.05 increments and the integrator output which divides the cycle into rich and lean periods was changed to a non-symmetric profile. Second, an oxygen sensor composed of a thinner zirconia ceramic was installed, resulting in a 20% faster air-fuel ratio modulation. The Cressida was then tested using various combinations of these modifications.

The effect of the feedback control modifications was a significantly richer air-fuel mixture. Tailpipe CO and UBF emissions increased with slight reductions in NO_x for all fuels. However, NO_x emission levels for alcohol were still above those for the baseline Indolene. Addition of the fast response oxygen sensor produced a slight leaning effect which was evident from decreasing CO and UBF and increasing NO_x. This was opposite to the intended effect.

In conclusion, the overall effect of the modifications showed that improvement in engine-out emissions was possible through improved stoichiometry management, but the TWC efficiency would still need improvement if the addition of alcohol fuels is to result in an NO_x reduction relative to gasoline as expected.

IV.5e Operating Experience

The Cressida was extensively operated on all blends of alcohol and gasoline for 45,000 miles. Several material compatibility problems arose. The terne plate coating of the fuel tank was removed by the methanol. Due to some vapor lock problems the fuel filter had been removed and the terne plate particles plugged

the fuel injection system. The coating was subsequently removed chemically and the injectors replaced. The original fuel immersed electric fuel pump failed due to galvanic corrosion. It was replaced with a corrosion resistant pump which had its electric drive isolated from the fuel.

Vapor lock was experienced on a 10% methanol blend at high altitude and warm weather. It was caused by improper placement of the additional fuel filter. After relocation of the filter, no additional problems occurred.

At approximately 43,600 miles, abnormal engine noise became apparent. Upon disassembly it was found that three out of the six connecting rod bearings had spun around the crankshaft throw. Visual inspection showed evidence of chemical attack. This was another piece in the body of growing concern for corrosion and wear caused by the alcohol fuels. (See Chapter V, Corrosion and Wear Mechanisms). The engine was subsequently rebuilt and limited testing performed.

IV.5f Test Results and Discussion--1982 Cressida

A 1982 Cressida was provided by the Toyota Corporation to continue the study of the NO_x issue. It subsequently was equipped with a high compression ratio engine and tested on various methanol/gasoline blends. It was supplied as a gasoline blend vehicle, i.e., the fuel system parts were alcohol compatible, the distributor modified as well as the ECU. The high compression ratio engine has a CR of 12.5:1. This engine is restricted to operate on high alcohol blends because of its high octane requirement.

Emission results from the 1982 Cressida show the same blend-leaning effect as the original Cressida. Studies are underway with the intent of defining modifications that will enhance catalyst efficiency on high percentages of alcohol.

The high-compression Cressida offers a significant increase in power and performance as well as an increase in energy economy of about 10% over that of the low-compression Cressida, based on the Federal Test Procedures. However, the high compression Cressida suffers from blend-leaning effects from increased alcohol blends to a much greater degree than the low-compression engine. This

can be seen in Figs. IV.4, IV.5, IV.6. Figure IV.4 presents the CO emissions versus the methanol blend percentage with the spark held constant at 4 degrees before top dead center (BTDC). The dotted lines represent the testing performed with the high-compression engine and the solid lines represent the previous tests performed with the low-compression engine. The lean shift is apparent in the decreasing CO emissions as the percentage of methanol is increased. Note the more pronounced effect in the high-compression engine for the cold and hot transient segments of the FTP driving cycle. However, the stabilized CO emissions remained very low for both engines.

The UBF emissions shown in Fig. IV.5 also decrease with increasing methanol percentage, again consistent with a leaning of the air/fuel ratio. This effect is also more pronounced in the high-compression engine.

Figure IV.6 reflects this lean shift in terms of the NO_x emissions for each phase of the FTP. The spark was held at 4^o BTDC. The amount in grams per mile of NO_x emissions increases as the percentage of methanol in the fuel increases. This effect is much more pronounced in the high-compression engine than the low-compression engine. Also, for each driving phase, the NO_x level in the exhaust was higher for the high-compression engine at equivalent methanol blends, consistent with other evidence on high-compression ratio engines.

Figure IV.7 shows the effect of retarding the spark on the FTP combined cycle NO_x emissions. Consistent with literature expectation, see Chapter II, the high-compression engine shows a definite decrease in NO_x as the spark is retarded from 4^o BTDC. This effect was also noticeable although to a lesser degree in the low-compression Cressida. Spark retard had little or no consistent effect on the UBF or CO emissions nor the fuel economy and drive-ability.

IV.5g Operating Experience

The 1982 Cressida has now been operated on methanol/gasoline blends for approximately 10,000 miles. One fuel injector has failed. The cylinder head had to be replaced due to a damaged spark plug. No other problems have surfaced. Driveability and performance are excellent with all methanol blends when powered by

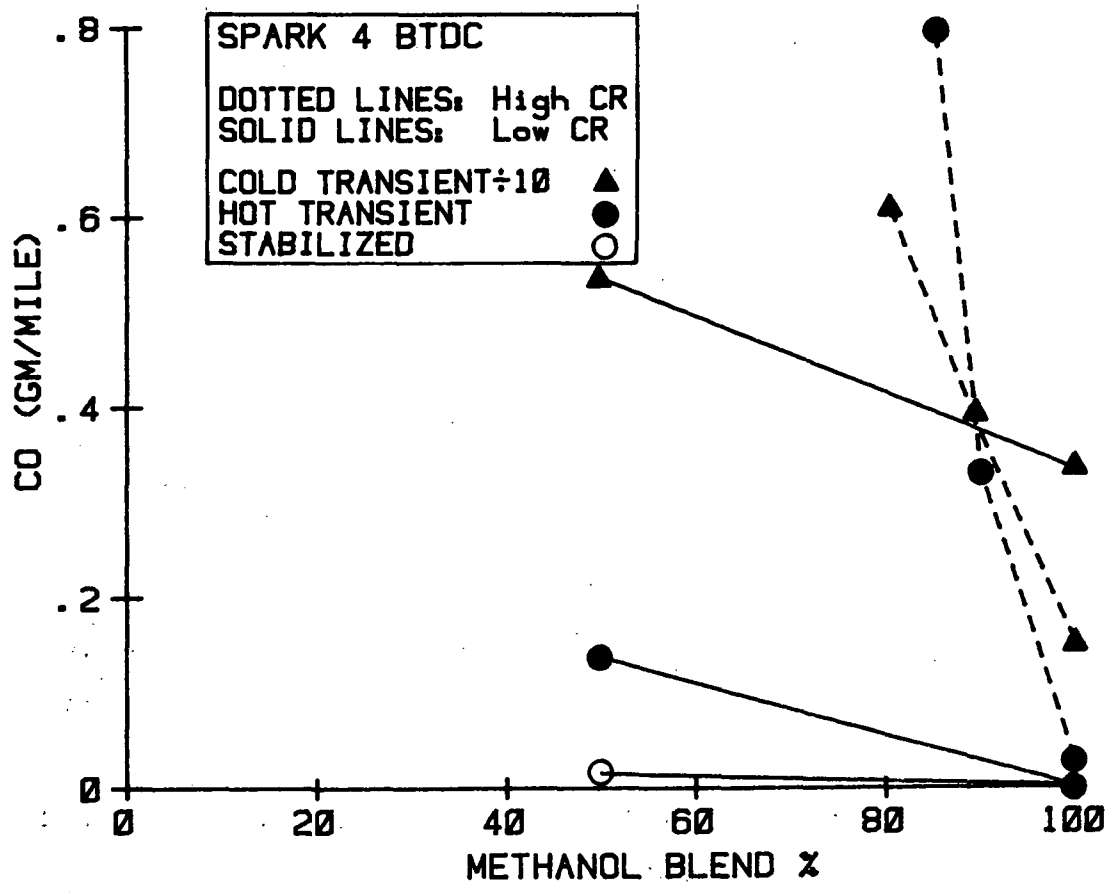

FIGURE IV.4 FTP CO EMISSIONS vs. METHANOL BLEND

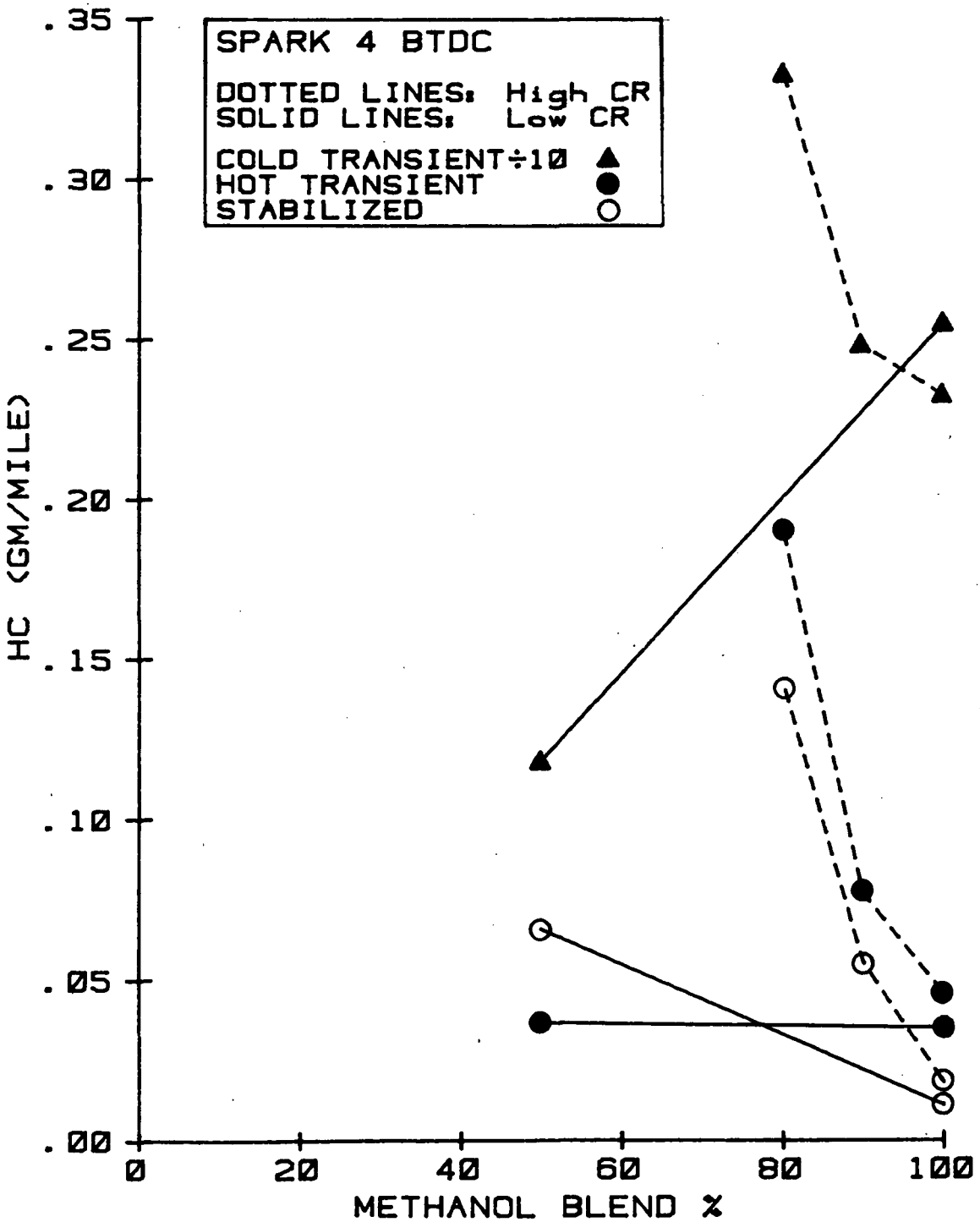

C-2

FIGURE IV.5 FTP HC EMISSIONS vs. METHANOL BLEND

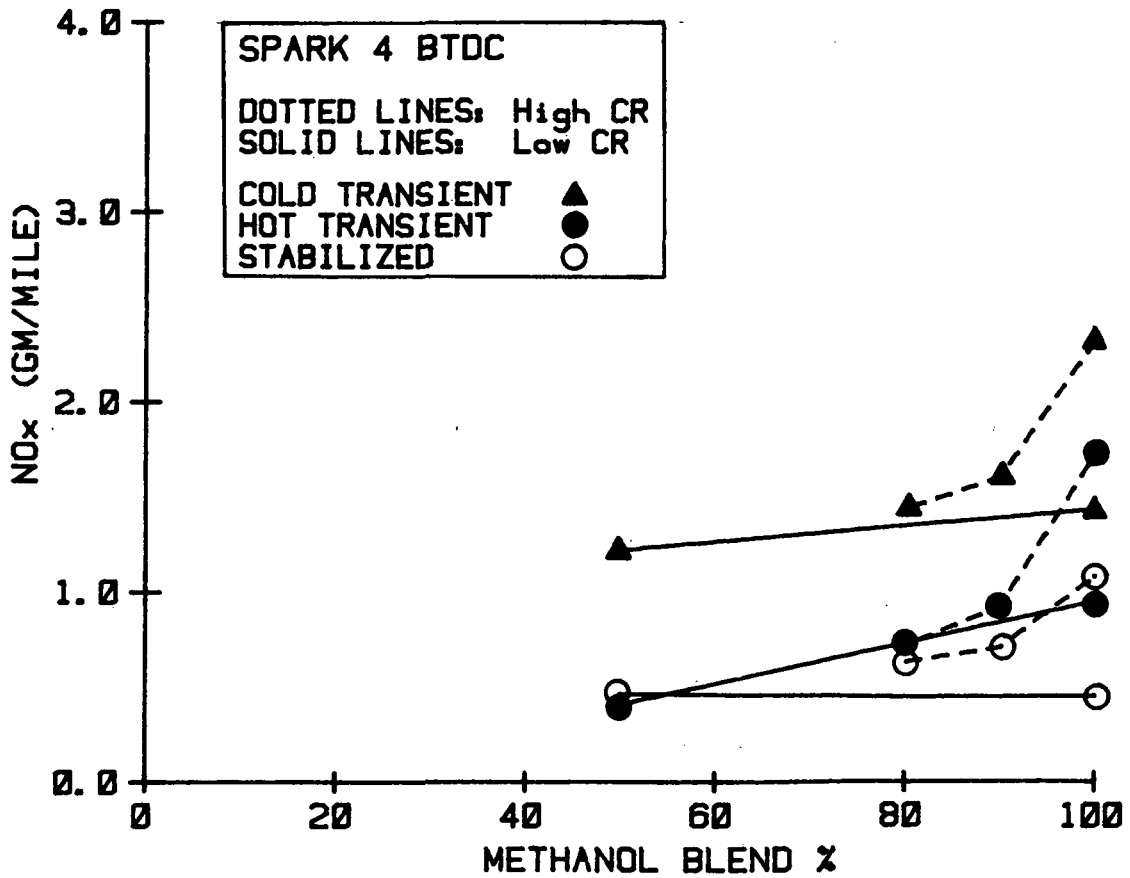

FIGURE IV.6 FTP NOx EMISSIONS vs. METHANOL BLEND

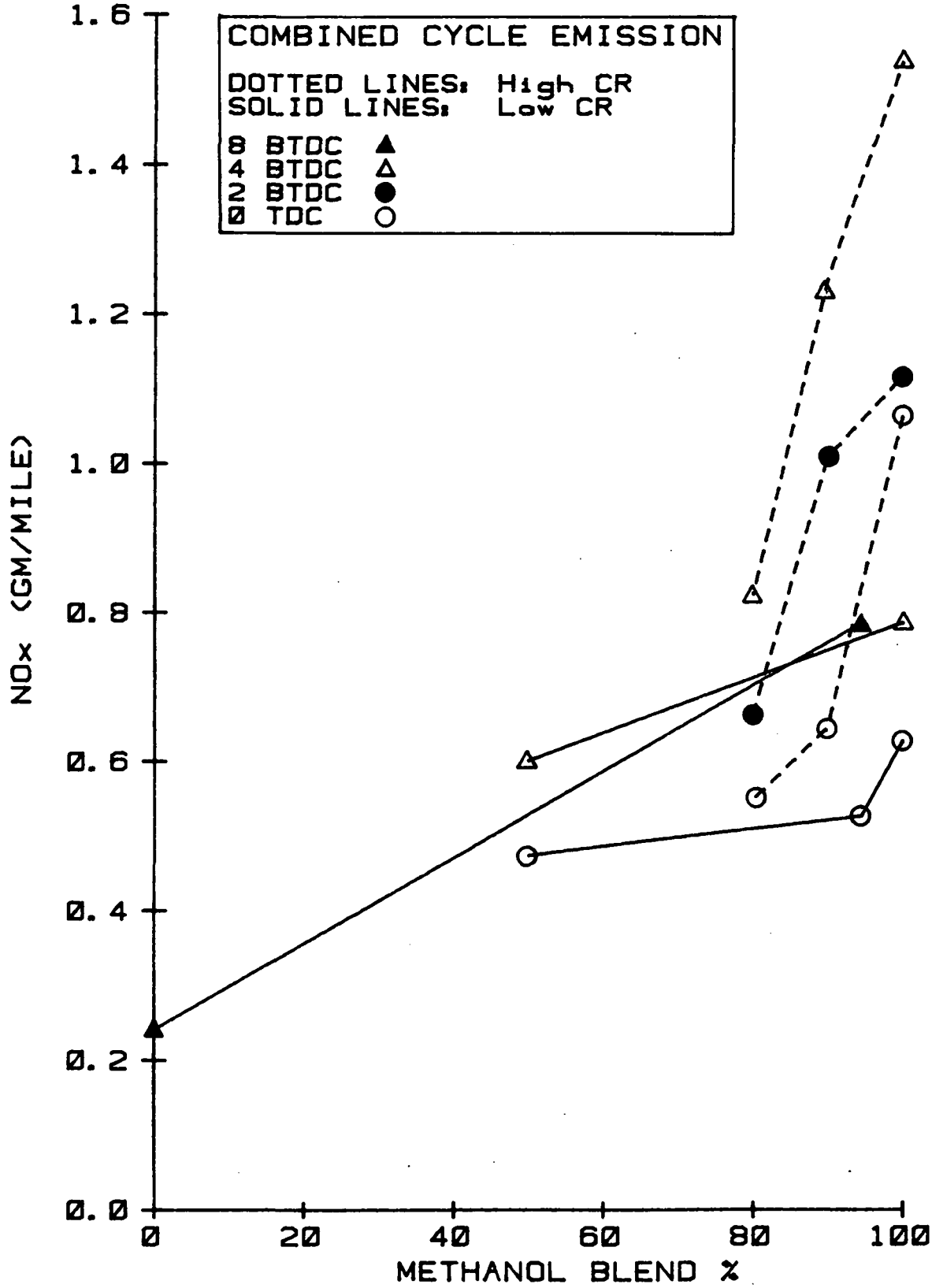

FIGURE IV.7 FTP NOx EMISSIONS vs. METHANOL BLEND WITH SPARK RETARD

the standard compression ratio engine and are outstanding for the limited blend range suitable for the high compression engine.

IV.5h Conclusions

The evidence accumulated with the 1979 and 1982 Cressidas clearly shows that a current, state-of-the-art system is available that will allow a broad range usage in a vehicle without significant adjustments, while maintaining fuel efficiency, driveability and emissions standards. Admittedly a vehicle will have somewhat improved performance when set up for a single blend. However, in times of fuel uncertainty, this project has clearly demonstrated the broad range blend versatility of the EFI feed-back controlled system and it is recommended that automotive manufactures note the evidence and incorporate it in their planning to maximize the worth of their new products to the consumer.

IV.6 REFERENCES

IV.1 J.F. Nebolon, R. O'Meara, R.K. Pefley, "Pinto Fuel System Conversion To Pure Methanol And Denatured Ethanol", Final Report, NASA/Grant No. NAG 3-143, February 1982.

IV.2 J.F. Nebolon, R. O'Meara, R.K. Pefley, R. DiVacky, "The Develoment and Application Of Kits To Convert A Fleet To Neat Alcohol", V International Alcohol Fuels Symposium, Aukland, NZ, May 1982.

IV.3 Post Office Alcohol Fueled Vehicles--Final Report in preparation by the Post Office Department.

IV.4 W.H. Baisley and C.F. Edwards, "Emission and Wear Characteristics of an Alcohol Fueled Fleet Using Feedback Carburetion and Three-Way Catalyst System", IV International Alcohol Fuels Symposium, Guaruja, BR, October 1980.

IV.5 B. Busenthur, "Effects of Exhaust Gas Recirculation on the Specific Fuel Consumption and the Emissions of NO, HC, CO, and Aldehyde from a Methanol

Fueled, Turbocharged Spark Ignition Engine", Santa Clara University Mechanical Engineering Research Report, June 1981.

IV.6 S.A. Espinola, A.T. Tamura, J.F. Nebolon, R.K. Pefley, "The Effects of Fuel Additives on Alcohol Exhaust and Evaporative Emissions", 75th Annual Meeting of the Air Pollution Control Association, New Orlean, LA, June 1982.

IV.7 U.S. Environmental Protection Agency, "Compilation of Air Pollution Emission Factors", Supplement No. 5, Appendix D. AP-42,Research Triangle Park, NC, December 1975.

IV.8 T. Suga, S. Espinola, R. Pefley, F. Cox, J. Allsup, "Performance and Detailed Emissions of an Electronic Fuel Injection System Which Operates on any Alcohol/Gasoline Blend", V International Alcohol Fuels Symposium, Auckland, NZ, May 1982.

IV.9 Alcohol Fleet I Test Program Final Report, California Energy Commission, August 1982.

IV.10 California Alcohol Fleet II Test Program Final Report, California Energy Commission, Unpublished Report.

IV.11. S.A. Espinola, R.K. Pefley, "Alternate Fuel Influences on Emissions Test Procedures," Symposium on Oxygenates in Fuels, American Chemical Society, Kansas City, MO, September 1982.

IV.12. R. Bechtold, J.B. Pullman, "Driving Cycle Economy, Emissions, and Photochemical Reactivity Using Alcohol Fuels and Gasoline", SAE Paper No. 800260.

IV.13 R.K. Pefley, H.A. Adelman and T.P. Suga, "Methanol/Ethanol/ Gasoline Blend Fuels Demonstration with Stratified Charge Engine Vehicles," California Energy Commission, Contract No. 500-115, Final Report, March 1980.

IV.14 W. Baisley and C.F. Edwards, "Emission and Wear Characteristics of an Alcohol Fueled Fleet Using Feedback Carburetion and Three-Way Catalyst," presented at the Fourth International Symposium on Alcohol Fuels Technology, Guaruja, Brazil, October 1980.

IV.15 R.K. Pefley, J.B. Pullman, T.P. Suga and S. Espinola, "A Feedback Controlled Fuel Injection System Can Accommodate Any Alcohol-Gasoline Blend," presented at the Fourth International Symposium on Alcohol Fuels Technology, Guaruja, Brazil, October 1980.

IV.16 R.K. Pefley, et al., "Research and Development of Neat Alcohol Fuel Usage in Automobiles," Six-Month Progress Report, NASA-Lewis Contract NAG 3-143, July 1982.

IV.17 T.P. Suga, "Thesis," Master of Science degree in Mechanical Engineering, University of Santa Clara, to be published.

IV.18 Alcohol Energy Systems, "California Alcohol Fleet Two Test Program," Final Report, California Energy Commission Contract No.500-80-054, 1983.

IV.19 R.K. Pefley, T.P. Suga, S.A. Espinola, "Performance and Detailed Emissions of an Electronic Fuel Injection System which Operates on any Alcohol/Gasoline Blend," Fifth International Symposium on Alcohol Fuels Technology, New Zealand, 1982.

CHAPTER V
CORROSION AND WEAR MECHANISMS

Based on our earlier work, it was thought that wear would not be a problem with alcohol fuels using typical gasoline matched lubrication oils. A 1972 Plymouth Valiant (225 CID), and a 1970 AMC Gremlin, had both been driven 50,000 miles on neat methanol in typical to severe driving conditions. Oil change intervals were 4000 miles for both vehicles. In 1979, after 50,000 miles, both engines were disassembled, and neither engine showed signs of abnormal wear [V.1].

The first evidence of wear problems related to the Santa Clara/DOE program began with a fleet of five 1979 Ford Pintos operating on neat alcohols. After 10,000 miles, crankcase blowby and oil consumption dramatically increased for three of these vehicles on neat methanol. Teardown of all three engines revealed extremely high upper cylinder wear [V.2]. A fleet of 1980 Ford Pintos on alcohol (known as Fleet I and operated by the state of California) also suffered from significant upper cylinder wear. The low compression engines were more inclined to failure than the high compression engines, and those fueled on methanol showed greater wear rates than those on ethanol. Again, some engines failed at approximately 10,000 miles [V.3].

Wear studies with dynamometer mounted engines reported in 1977 by Southwest Research Institute (SwRI) also resulted in high cylinder bore and ring wear when using methanol [V.4]. Further studies showed that wear rates with methanol were equivalent to gasoline if the oil sump temperature was above a temperature of approximately 70 ^{o}C. Below 70 ^{o}C, the wear rate with methanol, based on PPM iron in the oil, greatly increased. Wear rates with an oil sump temperature of 46 ^{o}C were approximately 10 times the wear rates on gasoline, under equivalent test conditions [V.5]. Furthermore, the addition of 11% water to the methanol aggravated the wear rate by 3 times compared to anhydrous methanol [V.6].

The development of oil additives specifically for methanol have reduced the wear rate to "only" twice that of gasoline, based on the standard V-D test [V.7]. This appears to be an improvement, but to effectively deal with the wear problem, an understanding of the mechanisms which are causing the increased wear is necessary. Several well-designed experiments at SwRI showed that the wear

was not caused by oil degradation or excessive oil dilution with water [V.6,8].

As acids are known products of combustion, it was hypothesized that the increased wear is caused by acid corrosion of the cylinder by the combustion condensate [V.9]. The pH of the condensate would provide a clue, and early evidence agreed with others [V.10]. A subcontract was signed with Pinnacle Research Institute, specialists in electrochemistry, to provide analysis and conduct experiments to investigate the hypothesis [V.11]. Samples of condensed pre-catalyst exhaust were obtained from a Pinto on methanol, ethanol and gasoline. Samples were also obtained from a 1981 Volkswagon Rabbit and a 1981 Ford Escort on methanol with 5.5% iso-pentane, and a 1982 Toyota Cressida on neat methanol. The pH of the Pinto exhaust condensate on methanol was very low: 1.79 to 1.99. Furthermore, the pH increased with ethanol use and was still higher for gasoline. Comparison of the Pinto on methanol with the other three vehicles was also interesting: the pH was higher for the Rabbit, Escort and Cressida. These pH trends conform to the wear patterns observed with these vehicles--lower pH values (more acidic) corresponding to higher wear rates. The condensate was further characterized by titration. The results of these tests, given in Table V.1,

TABLE V1: pH AND ACID-BASE TITRATIONS OF PRE-CATALYST EXHAUST CONDENSATE

Vehicle	Fuel	pH[1]	a_{H^+}(N)[2]	Total Acid[3] Content	[HCOOH](N)	No of tests
Pinto	MeOH	1.92	.012	.018	.0048[4]	5
Pinto	EtOH	2.24	.0058	.0088	--	1
Pinto	Gas.	2.78	.0017	.0063	--	2
Rabbit	MeOH/iso-P	2.96	.0012	.0023	.0011[4]	3
Rabbit	EtOH	3.44	.00041	--	--	2
Escort	Meoh/iso-P	3.07	--	--	--	2
Cressida	MeOH	3.47	--	--	--	1

[1] Measured by pH probe

[2] Calculated from pH value

[3] By titration

[4] Assumes HNO_3 and HCOOH are the only acids present

show that the activity of hydronium ions, based on the pH reading, is quite high. The total acid number, from the titrations, indicates the presence of strong acid(s), as well as weak acid(s). It was hypothesized that the strong acid is nitric (HNO_3), and an increased wear mechanism theory was proposed, based on the following:

1. Methanol produces twice as much water when combusted compared to gasoline. This causes a higher dewpoint temperature within the cylinder when operating on methanol.

2. Methanol has seven times the evaporative cooling effect of gasoline, which increases the time for the cylinder temperatures to rise above the dew-point after cold starting.

3. Unburned methanol will enter the condensate, while unburned gasoline will enter the oil. The methanol in the condensate will decrease the surface tension of the condensate.

4. The condensate may be more acidic compared to gasoline.

Research conducted by Pinnacle Research Institute consisted of four major areas:

1. Definition of the chemical mechanisms which are implied by this wear theory, and measurement of the following parameters,
2. The corrosion potential of the condensate,
3. The corrosion rate of the condensate,
4. The diffusion rate of the condensate through the lube oil.

V.1 A PROPOSED WEAR MECHANISM

The mechanism of wear in methanol fueled engines is based on corrosion due primarily to hydronium ions (H_3O^+) attacking the cylinder wall. These ions will be present regardless of the type of acids that exist in the condensate. The most widely accepted mechanism of dissolution of iron in acidic solutions was proposed by Huesler [V.12], i.e.:

$$Fe + OH^- \leftrightarrow Fe(OH)_{ads} + e^- \quad (V.1)$$

$$Fe(OH)_{ads} + Fe \leftrightarrow Fe(FeOH)_{ads} \quad (V.2)$$

$$Fe(FeOH)_{ads} + OH^- \leftrightarrow Fe(OH)_{ads} + FeOH^+ + 2e^- \quad (V.3)$$

$$FeOH^+ + H^+ \leftrightarrow Fe^{2+} + H_2O \quad (V.4)$$

In this mechanism, reactions 1,2 and 4 are rapid, while 3 is quite slow and is considered the rate determining reaction. $Fe(OH)_{ads}$ accelerates the dissolution of iron, and is assumed to be an absorbed surface species. Reaction 4 is strongly pH dependent; if there are high concentrations of hydronium ions H_3O^+, or simply H^+, the reaction is fast. However, when the H^+ is depleted at the metal/condensate interface, pH increases and reaction 4 may change course to any of the following:

$$FeOH^+ + H_2O \leftrightarrow Fe(OH)_2 + H^+ \quad (V.5)$$

$$FeOH^+ + OH^- \leftrightarrow FeO + H_2O \quad (V.6)$$

$$FeOH^+ + OH^- \leftrightarrow Fe(OH)_2 \quad (V.7)$$

The formation of ferrous oxide or ferrous hydroxide would shield the iron from further attack. However, these products of corrosion, whether FeO, $Fe(OH)_2$, Fe_3O_4, or some other compound, are less dense than iron, and would be scraped away by the piston rings. What is important here is this: if the pH of the condensate is low ($\leq$4.00), corrosion will occur.

Since methanol is a pure compound, and it or its products of combustion do not readily react to form any strong acids, some other source of strong acid must be suspected. The most likely source is NO_2, which can be converted to nitric acid by dissolving in water and the following reaction taking place:

$$3NO_2 + H_2O \rightarrow 2HNO_3 + NO \quad (V.8)$$

When the oil sump, and therefore cylinder wall, is cold and below the dewpoint temperature, water will condense on the oil film. The condensate is a site for the nitric acid to be formed. There will be two periods when condensation will occur: when the vehicle is started cold until the lube oil warms up, and after the vehicle has stopped and the gases trapped in the cylinder cool and condense.

To summarize, nitric acid was proposed as the main source of hydronium ions for the following reasons:

1. The pH measurements and titrations definitely indicate the presence of a strong acid, which can not be attributed to a methanol derived acid. Formic acid would have to be in concentrations approximately 1000 times that of nitric acid to produce the same pH value.
2. Methanol exhaust has a higher NO_2/NO ratio and more water than gasoline exhaust.
3. NO_2 concentrations are higher in the quench zone, where condensation and acid formation will occur.
4. Engine wear was observed to be worse at low temperatures, was aggravated by the presence of water in the fuel, and appeared to be caused by corrosion [V.8,10,13].

V.2 MEASUREMENT OF THE CORROSION POTENTIAL AND CORROSION RATE

The condensate was characterized by determining its corrosion potential and corrosion rate using standard experimental techniques. These experiments require approximately 500 ml of condensate, which would have been impractical to obtain using the exhaust sampling technique. Therefore, the electrolytic solutions used in these experiments were surrogates of the exhaust condensate. These solutions were formulated to have the same pH value as the measured values of the condensate, and it was assumed that the acids in the condensate were primarily nitric and formic (HCOOH). The composition of the electrolytic solutions is given in Table V.2.

TABLE V.2: COMPOSITION OF THE ELECTROLYTIC SOLUTIONS

Electrolyte Number[1]	$[HNO_3]$(N)	[HCOOH](N)	pH
1	0.0200	0.000	1.70
2	0.0180	0.002	1.74
3	0.0160	0.004	1.78
4	0.0140	0.006	1.83
5[2]	0.0160	0.004	1.77
6[3]	0.0160	0.004	1.75
7[4]	0.0160	0.004	1.73
8	0.0027	0.000	2.53
9	0.0020	0.0007	2.68
10	0.0013	0.0014	2.80
11	0.0006	0.0021	2.95
12[2]	0.0013	0.0014	2.78
13[3]	0.0013	0.0014	2.74
14[4]	0.0013	0.0014	2.73

1 Electrolytes 1-7 were tested with electrode of Pinto block material. Electrolytes 8-14 were tested with electrode of Rabbit block material.

2 Contains three volume percent methanol

3 Contains six volume percent methanol

4 Contains ten volume percent methanol

A standard three-electrode electrochemical cell was used for the experiments. The working electrode was a cast iron rod 0.2" in diameter. The rods were machined from the engine blocks of a Ford Pinto and VW Rabbit, and were encased in an epoxy sheath so that only one end was exposed to the electrolyte. The other end of the rod was attached to a rotating disc electrode(rde) shaft. A silver/silver chloride (Ag/AgCl) half-cell was used as the reference electrode.

A platinum gauze of 6.2 in_2 exposed surface area was used as the counter electrode. The electrochemical cell is illustrated in Fig. 1 [V.11].

The corrosion potential or rest potential, E_c, was determined as the voltage produced at the electrode(engine block)/electrolyte interface. It is a measure of the tendency of the metal to corrode and was found to be a linear function of the pH of the electrolyte over the range of pH tested. The results from the experiments are shown in Fig. V.2. The change in E_c with respect to pH is a constant, and can be expressed as:

$$\frac{dE_c}{dpH} = -60 \text{ mv/decade}$$

In later experiments, a potential was applied across the cell and the current was measured. The total potential equals the rest potential, E_c, plus the applied, or over potential, . ,The anodic polarization curves are plots of the logarithm of current versus overpotential. Figure V.3 is a typical plot, which is based on the tests with electrolyte 1.

The linear portion of the curves are dominated by the kinetics of the metal dissolution and are often referred to as Tafel lines. The Tafel lines can be expressed as:

$$i = i_c[\exp(2.3\eta/b)]$$

where: i_c = corrosion current density obtained by linearly extrapolating to intercept $E_c(\eta = 0)$

and b = Tafel slope $= \frac{d\eta}{d\log i}$

The Tafel slope and pH dependence of the corrosion potential are consistent with studies of the corrosion of iron in acid media [V.14,15].

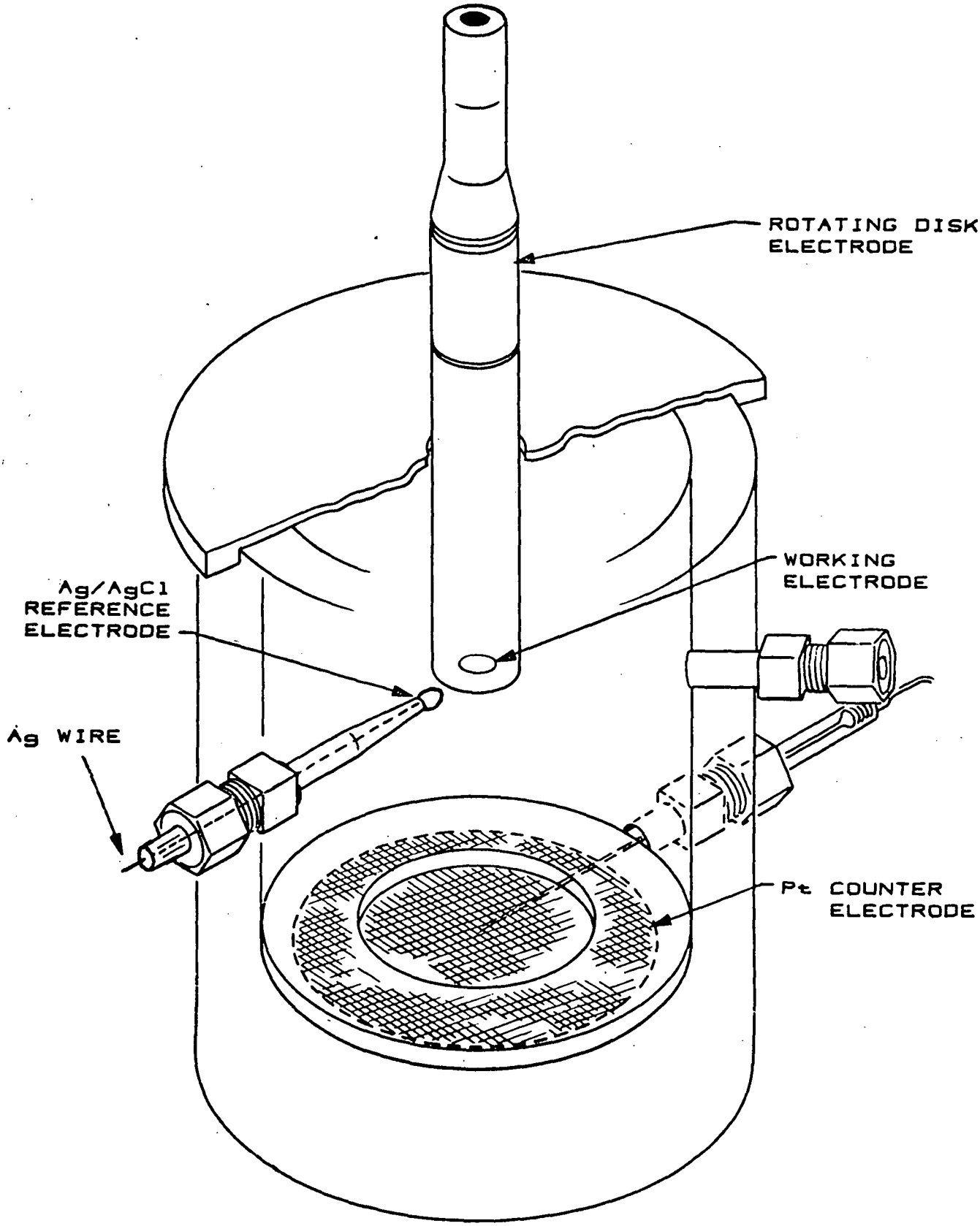

FIGURE V.1: THE ELECTROCHEMICAL CELL

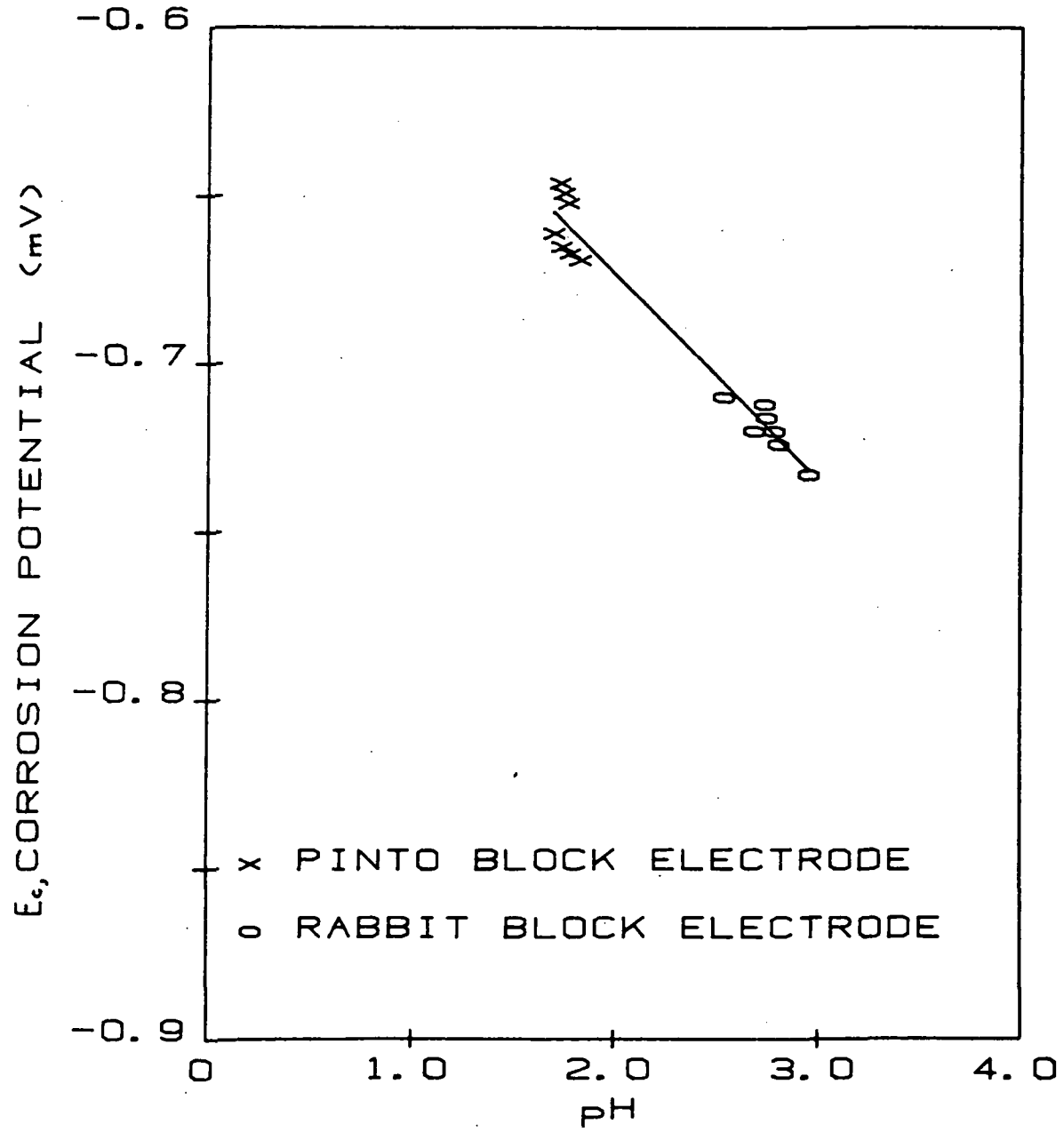

FIGUREV.2 : CORROSION POTENTIAL vs. pH

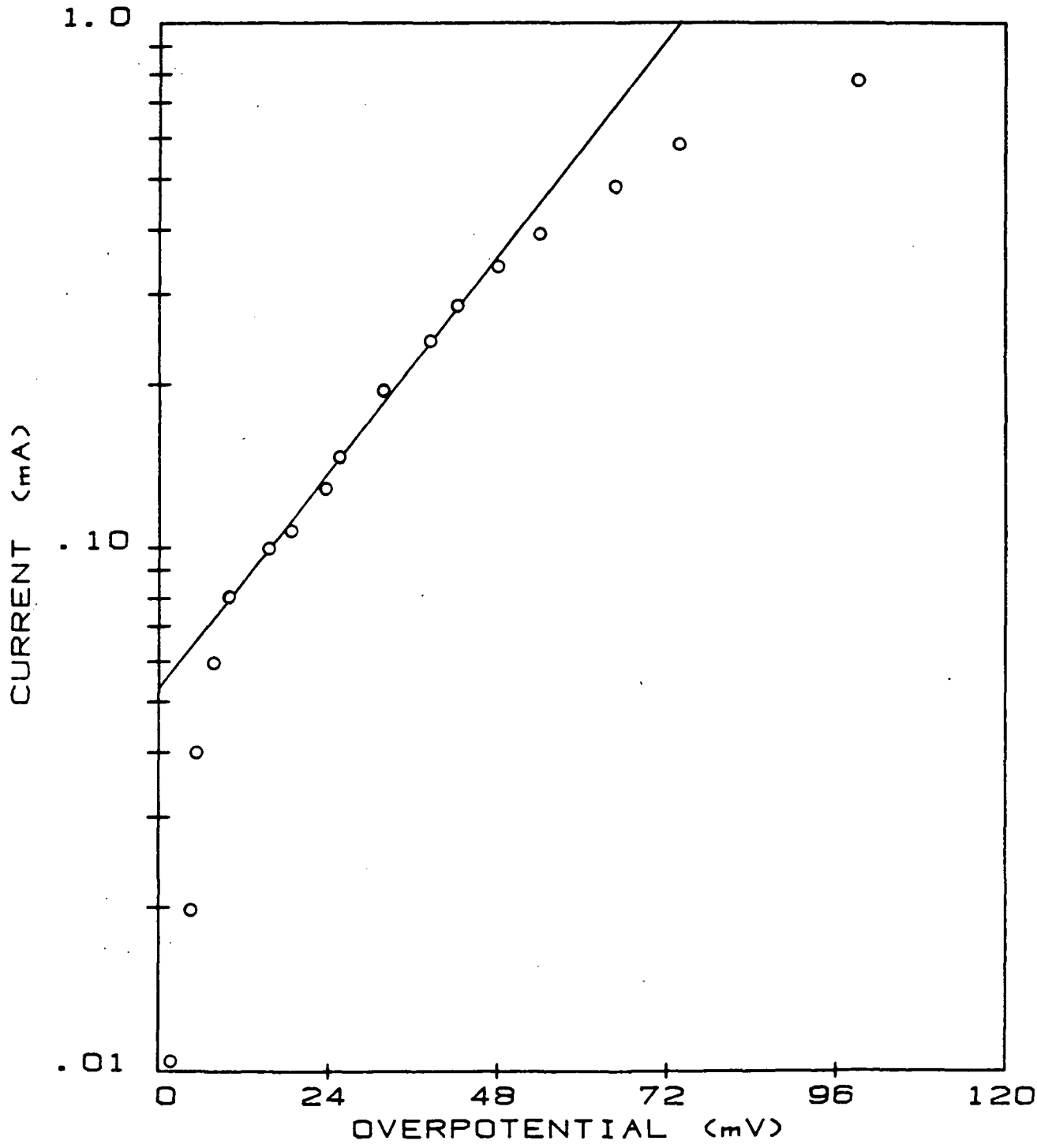

FIGUREV.3: TYPICAL ANODIC POLARIZATION CURVE

The corrosion rate based on i_c can be calculated using the following equation:

$$ipy = \frac{i_c \; t \; MW}{n \; F \; \rho} \quad (1) \quad (2.54)$$

where: ipy = inches penetration per year (in/yr)

i_c = corrosion current density (A/cm_2)

t = number of seconds per year ($3.1536 \times 10_7$ sec/yr)

MW = molecular weight of the corroding metal (55.847 gm/mole for iron)

n = number of charges transferred, or the oxidation state of the respective corrosion products (n = 3 for iron)

F = Faraday constant (96,500 A sec/equiv)

ρ = density of the metal (7.89 gm/cm_3 for iron)

The corrosion rates based on these tests were calculated to range from 0.009 to 0.059 ipy. Of course, these rates are an overestimate, because in actual conditions the condensate exposed to the cylinder wall is much less, and the acid would be depleted as corrosion proceeds. Nevertheless, these calculations are useful in comparisons among different condensate compositions.

V.3 MEASUREMENT OF THE CONDENSATE DIFFUSION RATE

The condensate diffusion rate was measured by immersing an oil coated carbon steel electrode into an electrolytic solution. When the condensate penetrated the oil film and reached the electrode, the open circuit voltage across the electrode became the rest potential. The elapsed time from the immersion of the electrode into the condensate until the detection of E_c is called the transition time, measured in seconds.

The oil film thickness was varied by dipping the electrode into an oil (20W-40 weight SF-CC oil, by Conoco), and rotating the electrode at a given speed for at least 30 minutes. The thickness was determined by measuring the weight increase of the electrode. A plot of the data indicates that oil film thickness is inversely proportional to rotating speed (Fig. V.4).

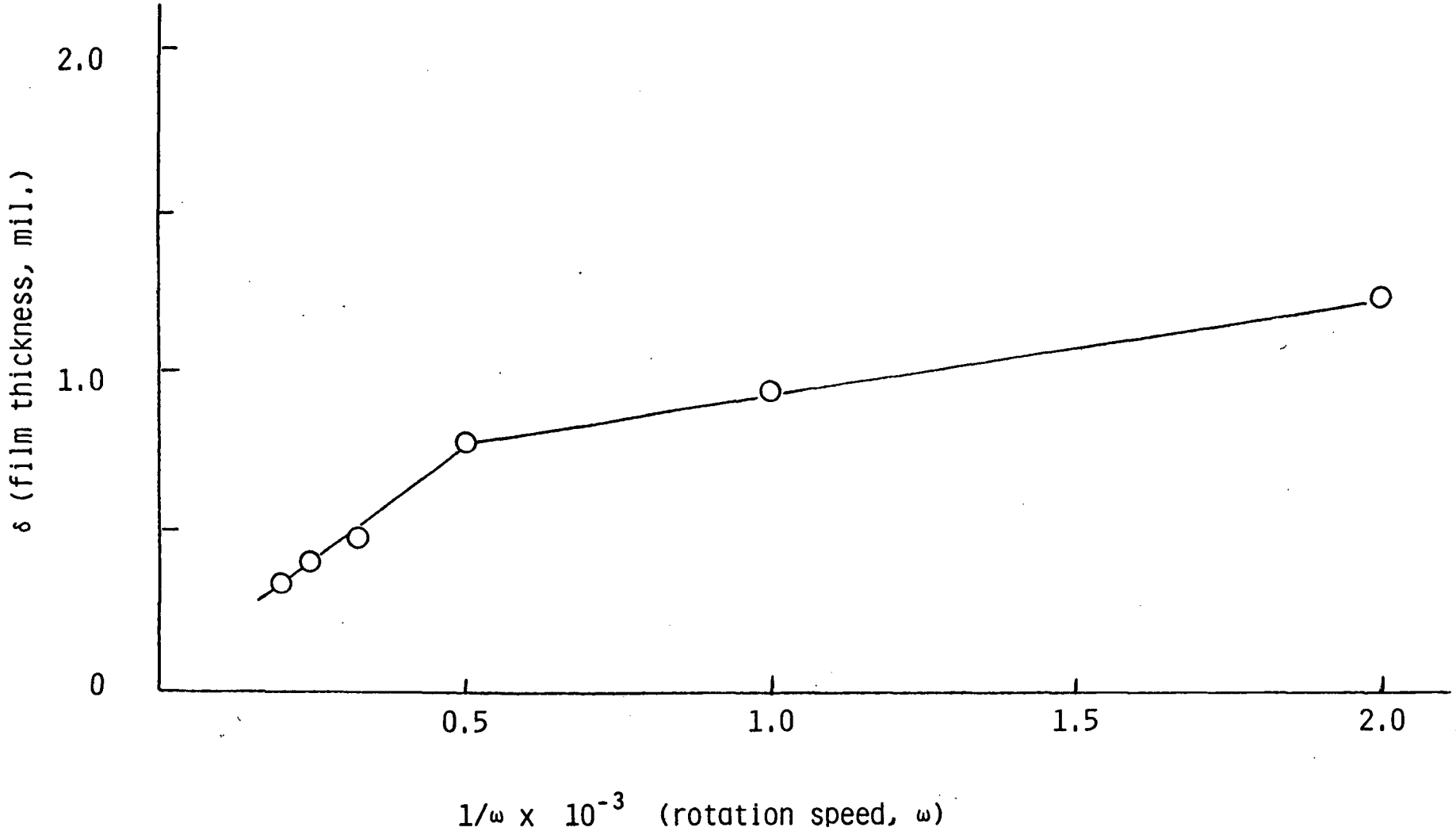

Figure V.4: Correlation of Oil Coating Film Thickness with Rotation Speed

The electrolyte was composed of 0.016 M HNO_3 and 0.004 M HCOOH which was modified to produce four test electrolytes by adding 0, 3, 6, and 10 volume percent methanol. The results of these tests, transition time for four different solutions and three different oil film thicknesses, are given in Fig. V.5.

These results are truly significant. Methanol in the condensate can greatly increase the ability of the condensate to penetrate the oil film on the cylinder wall and initiate corrosion. Of course, unlike the experimental conditions the oil film in the cylinder is not static; the film is wiped and replenished with each passing of the piston rings. However, with the engine running more methanol laced condensate will reach the cylinder, continuing the corrosion until the cylinder wall rises above the dewpoint temperature.

V.4 FURTHER ANALYSIS OF THE CONDENSATE

In parallel with the corrosion tests, more exhaust condensate samples were obtained and analyzed for pH. Ten different vehicle/fuel combinations were tested: Ford Pintos, on methanol, ethanol (CDA-20), and gasoline, VW Rabbits, on ethanol and 94.5% methanol/5.5% iso-pentane, a Ford Escort, on the same methanol/iso-pentane blend, and a Toyota Cressida on M80, M90, and M100 (M100 with a high and low CR engine). These samples were obtained from pre- and post-catalyst exhaust and blow-by gases directly from the crankcase, all while the vehicle engines were idling. This data was taken from in-use vehicles over a period of a year, and all the variables were not well controlled. However, several trends can be observed in Fig. V.6.

Post catalyst exhaust was generally at least one pH number higher compared to pre-catalyst exhaust. Blow-by exhaust condensate from the Escort had the same pH as the pre-catalyst sample, while the Pinto blow-by showed a definite increase of about 1.3 above the pre-catalyst exhaust. All the vehicle/fuel combinations except for two showed a consistent value of pH. Note that methanol condensate pH values were on both sides of the gasoline data. What besides fuel affects pH values is not completely understood at this point. However, one possible answer was revealed in recent work.

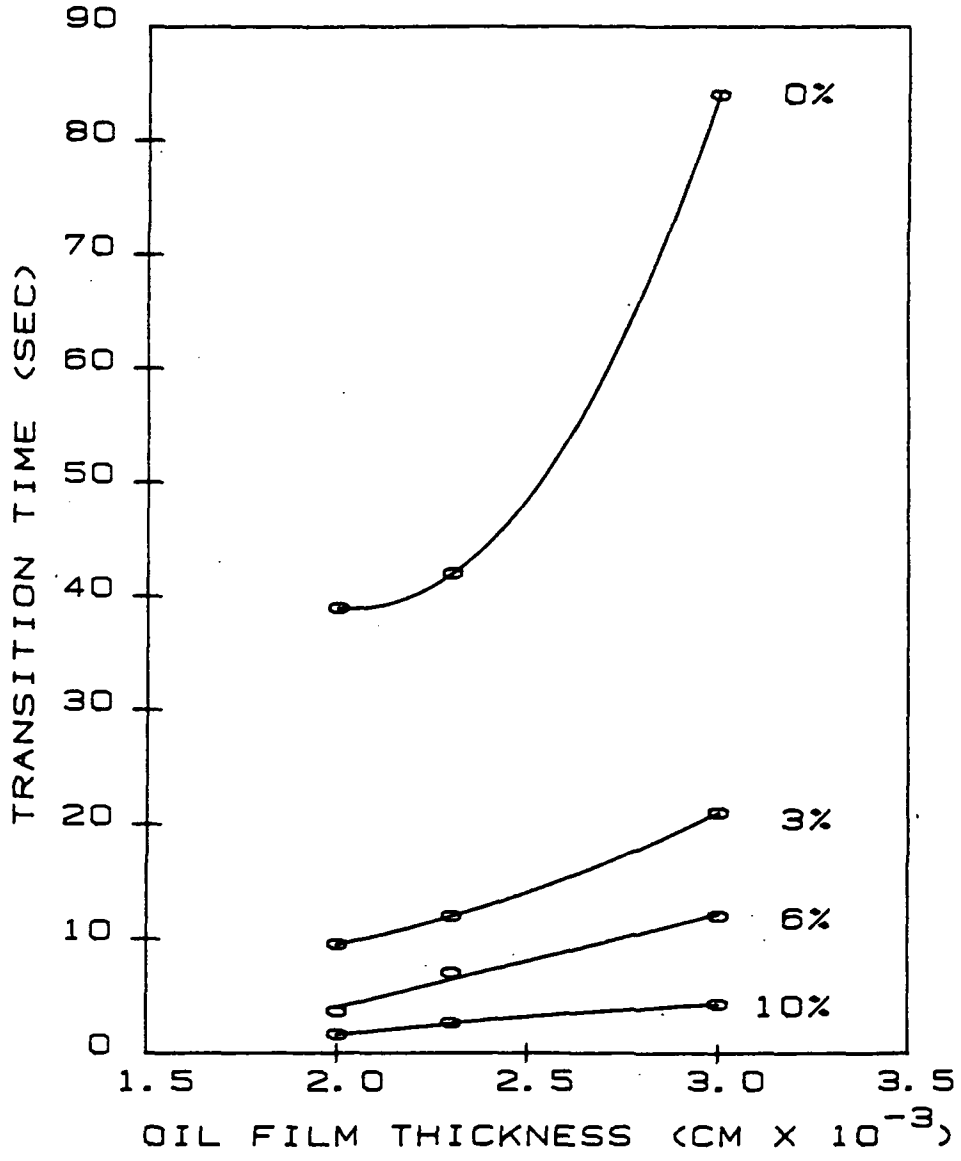

FIGURE V.5 TRANSITION TIME VS. OIL FILM THICKNESS FOR CONDENSATE WITH VARIOUS METHANOL PERCENTAGES

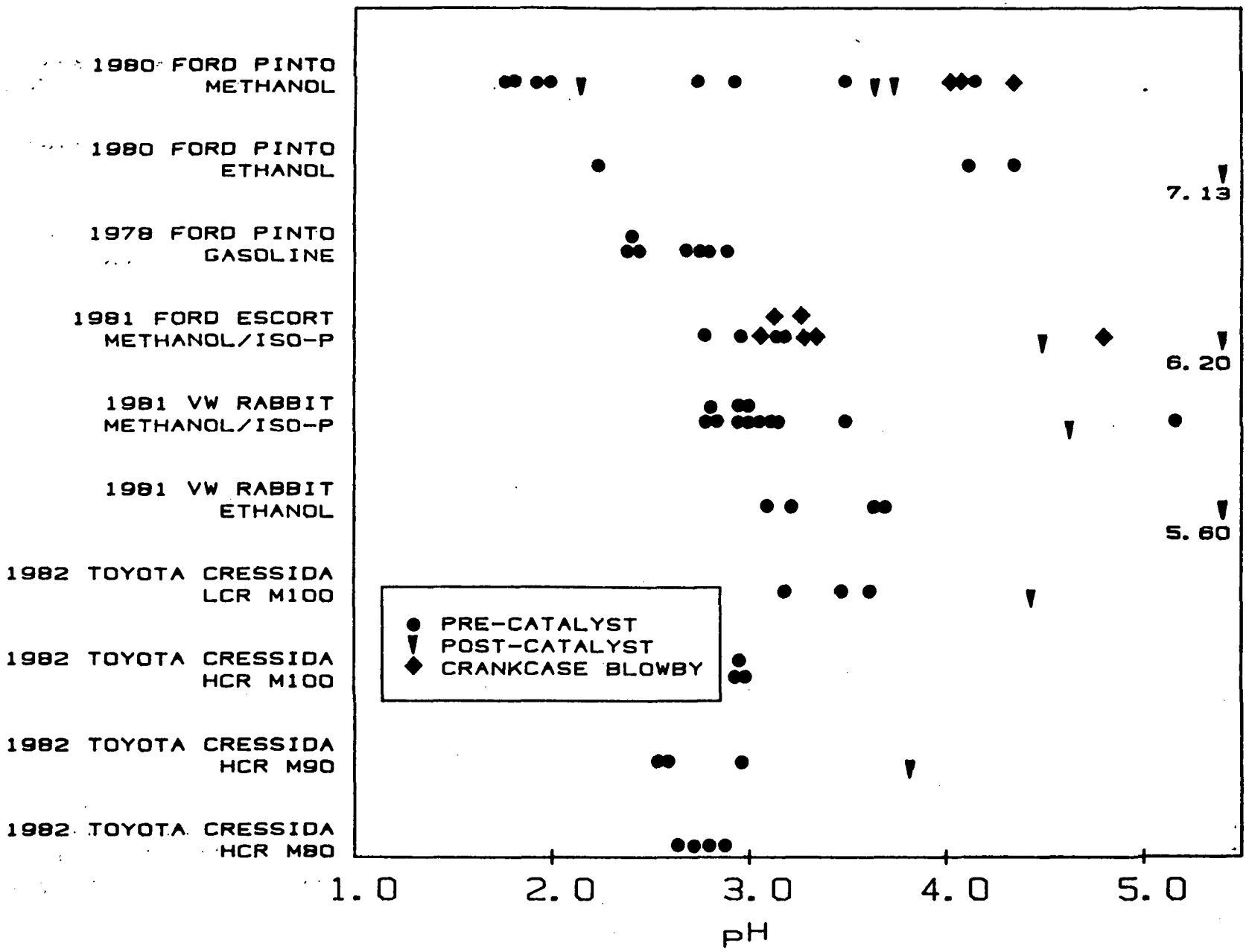

FIGURE V.6: EXHAUST CONDENSATE pH VALUES FOR VARIOUS VEHICLE/FUEL CONFIGURATIONS

Pre-catalyst samples were obtained and analyzed for pH and the presence of ions by ion chromatography. The ions which were detected were nitrate, nitrite, formate, sulfate, and chloride, which were assumed to exist as nitric, nitrous, formic, sulfuric, and hydrochloric acid, respectively. The concentrations of these ions are given in Table V.3.

TABLE V3: ION CONCENTRATIONS(mg/L) AND pH VALUES
OF PRE-CATALYST EXHAUST CONDENSATE

Vehicle: 1980 Ford Pinto(49 state)

Fuel:	Methanol		Ethanol(CDA-20)	
	Sample 1	Sample 2	Sample 1	Sample 2
Formate	21.	1.2	62.	41.
Nitrate(as N)	15.	6.6	9.4	11.
Nitrite(as N)	0.56	0.23	0.66	3.1
Sulfate	8.6	24.	9.3	15.
Chloride	9.4	6.5	9.9	3.7
pH	3.49	4.15	4.12	4.35

Nitrate was a major part of the ions detected; however, there were equally large amounts of sulfate and chloride ions. This data indicates fuel contaminants, specifically sulfur and chlorine compounds, as a source of corrosive agents, at least in these tests. Other groups have reported instances of fuel contaminants which could affect wear rates [V.7,10,16]. Unfortunately, analysis of the fuel was not a part of this study, but one conclusion has been reached: analysis of the fuel prior to use is necessary to maintain quality control and to allow accurate interpretation of wear data.

V.5 CONCLUSIONS AND FUTURE WORK

Follow-on studies will focus on three aspects of the alcohol fueled engine corrosion and wear problem.

1. Future exhaust condensate experiments will concentrate on improving the procedure for sampling and analyzing the combustion condensate toward better correlation of pH and ion evidence with vehicle operating conditions. Fuel quality will be part of the data and the in-cylinder condensate will be compared with exhaust and blowby condensate.

2. Existing computer combustion reaction kinetics modeling will be used to interpret the condensate evidence and provide clues to suppression of the acidic nature of the condensate.

3. The accelerated corrosion measurement procedures will be modified as necessary based on the new condensate evidence and restudied to obtain clues as to how best block the corrosion attack if the corrosive elements cannot be suppressed.

The dominant mechanism proposed for corrosion and wear of methanol fueled engines is based on the hydronium ion, which is provided by acids in general and involves the following features of alcohol combustion:

1. There is more water formed by combustion and more time for it to condense relative to gasoline because of the high dew point temperature of the exhaust gases and high heats of vaporization of the alcohols.

2. With pH values of less than four having been measured for blowby and pre-catalyst exhaust condensate, electrochemical experiments show that corrosion of cast iron will occur when exposed to these solutions.

3. The diffusion of the condensate through the oil film is much faster when small percentages of methanol are present in the condensate in comparison with condensate from gasoline engines.

4. Based on all the evidence to date, an acidic corrosion wear mechanism involving the hydronium ion is most likely, particularly when considering the conditions for highest wear rates. Whether the dominant acid is nitric or other remains to be proven but some of the most severe corrosion cases are clearly linked to strong acids by the condensate evidence.

V.6 REFERENCES

1. R. K. Pefley; 1981; "Characterization and Research Investigation of Alcohol Fuels in Automobile Engines;" DOE Contract No. DE-AC03-78CS; Final Report; pp 121-124.

2. W.H. Baisley, C.F. Edwards; " Wear Characteristics of Fleet Vehicles Operating on Methyl Alcohol;" SAE Paper No. 811202.

3. R. Ernst, R.K. Pefley, F.J. Weins; 1983; "Methanol Engine Durability;" SAE Paper No. 831704.

4. E. C. Owens; 1977; "Methanol-Fuel Effects on Spark Ignition Engine Lubrication and Wear; " II International Symposium on Alcohol Fuel Technology Methanol and Ethanol; 2-6.

5. E.C. Owens, H. Marbach, Jr., E. Frame and T. Ryan; 1980; "Lubrication Requirements for Alcohol-Fueled Spark Ignition Engines;" IV International Symposium on Alcohol Fuel Technology; Vol. 2 (B-66); pg 691-700.

6. E.C. Owens, D.W. Naegeli, H.W. Marbach, T.W. Ryan III and E.A. Frame; 1983;"Approaches to Controlling Wear in Alcohol Fueled Engines;" V International Alcohol Technology Symposium; Vol. 2 (C3-5);pg 443-450.

7. H.W. Marbach,Jr., E.C. Owens and E.A. Frame; 1983; "Technical Report for Resolving Wear Problems in Alcohol-Fueled Engines;" Technical Report No. SwRI-7152/1; pp 20.

8. T.W. Ryan III, D. Naegeli, E.C.Owens, J. Barbee; 1981; "The Mechanisms Leading to Increased Cylinder Bore and Ring Wear in Methanol-Fueled SI Engines;" SAE Paper No. 811200.

9. R.K. Pefley; "Alcohol Fuel Corrosion and Wear Effects;" 1982; presented at the United Nations Industrial Development Conference; Dehra Dun, India.

10. H.C. Wolff, D. Smith, P. Fry; 1982; "Motor Oil Development for Methanol Engines;" V International Alcohol Fuels Technology Symposium; Vol 2(C3-8); pg 467-474.

11. Pinnacle Research Institute,Inc.; 1983; "The Corrosion of Metals in Methanol-Fueled SI Engines;" Final Report, in preparation.

12. K.E. Huesler; 1958; "Z. Electrochem;" Vol 2(12); pg 1371.

13. D.H.T. Milliard, B.J. Howlett, S. Chaibongsai; 1982; "Crankcase Oil Development for Alcohol Fueled Engines; "V International Symposium Alcohol Fuel Technology; Vol 2(C3-4);pg 435-442.

14. G.M. Florianovich, L. Sokolova, Y.M. Kolotyrkin; 1967; "Electrokhemya;" Vol 3(9); pg 1027.

15. T.D. Zytner, A.L. Rotinyan; 1966; "Electrokhemya;" Vol 2(12); pg 1371.

16. H.W. Marbach, Jr., E.A. Frame, E.C. Owens, D.W. Naegeli; B.D. Wielgos; 1983; "The Effects of Lubricant Composition on SI Engine Wear With Alcohol Fuels;" SAE Paper No. 831702.

CHAPTER VI.
PHOTOCHEMICAL SMOG CHAMBER STUDIES

The 100 cubic foot photochemical smog chamber was transferred to the University of Santa Clara from Bartlesville Energy Technology Center (BETC) in January 1977. During the first year it was installed and supporting equipment and instrumentation were acquired. Continuous measurement techniques were developed for total hydrocarbons, oxides of nitrogen, ozone and formaldehyde. The original aluminum- and Pyrex- walled chamber used 84 blacklights and 18 sunlamps for solar simulation.

The smog chamber and its supporting equipment were unused from 1980 through mid-1982 when renewed interest in methanol's photochemistry emerged and an improved program and experimental plan were devised. The rationale for conducting additional photochemical smog chamber studies of urban hydrocarbon and methanol exhaust surrogates is to provide validation for their chemical kinetic mechanism. The chemical kinetic mechanism is subsequently modeled along with the sunlight, temperature, physical transport, emissions mixing and dilution processes which occur in a vertical column of air as it traverses an urban path. This Empirical Kinetic Modeling Approach (EKMA) is endorsed by the U.S. Environmental Protection Agency for use in the formulation of 1982 and subsequent air quality State Implementation Plans. Therefore, the methodology seemed most appropriate for an assessment of methanol fuel's impact in the Los Angeles Air Basin. However, because this work is independently funded by a multiclient group and is still underway, the present report concerns the restoration efforts, characterization studies and experimental progress achieved with the photochemical smog chamber apart from the EKMA modeling study.

VI.1 FACILITY UPGRADE

The restoration of the photochemical smog chamber facilities required several months of effort. The chamber was first relocated adjacent to the laboratory's electrical power bus. Electrical power connections and circuit breakers were needed to supply the 1.5 kilowatts consumed by the 84 blacklights and 18 sunlamps. Additional power for the rack-mounted instrumentation package was

also supplied. The electric furnace which contains a catalytic combustor for air purification also required an independent power supply.

The clean air supply for calibration zeroes and chamber dilution purposes was redesigned incorporating a new blower. An ozone generating ultraviolet lamp was purchased and installed downstream from the blower. This was intended to oxidize any nitric oxide into nitrogen dioxide. The ozonated air supply was next routed to a dust filter and then into a potassium permangenate (Purofil) adsorbent canister. The removal of the majority of inorganic material was thus accomplished. The clean air supply was next routed to the catalytic combustor for removal of organic contaminants. The furnace temperature and air flowrate parameters were adjusted to produce a clean air supply of about ten liters per minute. A portion of that supply was pumped into a combination instrument calibrator and chamber dilution rate controller. The remaining supply of clean air can be vented into the laboratory; or it can be diverted into the chamber for rapid dilution and flushing of old experiments.

VI.2 INSTRUMENTATION

The instrumentation set which was previously acquired with DOE support, was removed from storage and rack mounted. The instruments consist of:

(1) Monitor Labs Model 8500 calibration controller
(2) Beckman Model 400 Total Hydrocarbon (THC) Analyzer
(3) Dasibi Model 1003 AH ozone monitor
(4) Monitor Labs Model 8440 Nitrogen Oxides (NOx) Analyzer

A dual pen chart recorder and two data multiplexers were also installed to record the raw data from the experiments. Separately located was a CEA 555 automated wet chemistry formaldehyde analyzer and its companion calibration standard. A formaldehyde permeation device was located within a glass U-tube which was immersed in a 100^{o}C temperature controlled silicone oil bath.

A Hewlett-Packard Model 5721 gas chromatograph was located adjacent to the smog chamber. Air samples were pumped from the smog chamber and into a glass-wool-filled sample trap. The 1/8 inch stainless steel trap was submerged in a liquid

argon bath in order to adsorb and collect an increased concentration of hydrocarbons for measurement. A six port valve was used to switch the sample loop into the nitrogen carrier gas stream. The cryogenic trap was immediately plunged into a boiling water bath to rapidly desorb the collected sample. A Hewlett-Packard model 3380 integrator was used to assist in quantifying the measured gas concentrations. The lower detectable limit for propene was measured at 2 to 3 parts per billion carbon using the trapping technique described. The linearity of the propene measurements was checked by a series of analyses after repeated addition of a fixed volume of propene to the chamber. Good linearity was found for the sample trapping, desorbtion and gas chromatography procedures used.

VI.3 CHAMBER GAS SAMPLING

The sampling system originally obtained continuous gas samples from several locations around the chamber. Stainless steel, glass and Teflon were the only materials in contact with the samples. Some of the instruments chemically altered the samples so that they had to be discarded after use. However, the unaltered total hydrocarbon analyzer and the ozone analyzer samples were recirculated back into the chamber in order to minimize sample loss dilution effects.

The preceding is a description of the experimental facilities when the first series of characterization studies and the multi-client supported methanol photochemistry study commenced in late 1982 and during the first six months of 1983. The characterization studies and initial methanol photochemistry validation studies were found to be subject to chamber wall contamination and aging effects about one month or less after the aluminum and Pyrex surfaces were cleaned. The magnitude of the contaminant effects was substantial enough to strongly interfere with the reaction rates of the hydrocarbons and NOx under study. The severity of the problem was not fully assessed until mid-June of 1983. It was then decided to upgrade the smog chamber walls with the addition of an inner flouro-ethylene-polymer (FEP) Teflon film bag. In that way the hydrocarbon and NOx surrogate mixtures would only be in contact with their FEP film enclosure. The FEP film was purchased and a 100 ft^3 bag was constructed to conform with the aluminum and glass walls of the original chamber. The FEP film

bag was supported with detachable Velcro strips along its two upper sides. The effective volume of the chamber was reduced to 70 ft^3 since the two ends were unsupported and partially collapsed.

The clean air supply was also upgraded with the addition of a high efficiency particulate air (HEPA) filter located just after the catalytic combustor. A fraction of the clean filtered air was permanently routed into the buffer-zone air surrounding the FEP film bag, but within the aluminum and glass chamber walls. This was a further precaution against the diffusion of hydrocarbon and NOx contaminants from the external laboratory air into the FEP film bag.

The sampling system was also modified at that time. One inlet and one exit bulkhead union were fitted through the aluminum chamber walls. A large Teflon plug was drilled and tapped and located so that the FEP film wall was sandwiched between the Teflon plug and the aluminum chamber wall for sealing purposes.

The four sample lines were routed to their respective instruments outside of the chamber. The recirculated sample (ozone and THC) was returned via the bulkhead union on the opposite end of the chamber. An external one half inch Teflon tube and mixing pump were also added to help homogenize the contents of the bag when concentrated hydrocarbon and NOx reagents are added. This completed the modifications to upgrade the clean air and sampling systems and reduce chamber wall effects.

VI.4 CALIBRATION STUDY

A repeat series of chamber characterization studies was performed next. These experiments were modeled by a subcontractor (Systems Applications, Inc. (SAI) of San Rafael, California) in order to confirm the performance of the chamber against their knowledge of other chambers and the known chemistry of particular experiments. The most fundamental chamber characteristic to model is simple dilution of a hydrocarbon with a measured flowrate of clean air. Given the chamber volume and the dilution flowrate one can readily calculate the theoretical decrease in concentration C(t) as a function of time:

$$C(t) = C(init) * \exp(-b)t \qquad (VI.1)$$

$$\text{where } b = \frac{\text{dilution flowrate}}{\text{chamber volume}}$$

t = time elapsed since initial concentration: C(init)

Figure VI.1 shows the agreement between the calculated and measured chamber dilution rates.

A second fundamental chamber characterization involved the increase in chamber temperature after turning on the lights. Interpreting and modeling of the experimental results is enhanced by a knowledge of the temperature profile. A typical temperature profile over time is presented in Fig. VI.2. The curve maxima are due to the evening cooling effect of the surrounding laboratory air. Some of the chemical kinetic rates are sensitive to temperature effects although these are generally small in magnitude.

A series of special experiments were designed with guidance from SAI to measure the reactivity contribution of the chamber's walls. These experiments involved the use of NOx, CO, and acetaldehyde. The acetaldehyde experiments used only acetaldehyde near the ppm level to determine the rate of NOx off-gassing from the chamber walls. Such off-gassing could be important to experiments limited by NOx concentrations. For example, the ozone peak under high hydrocarbon to NOx ratio conditions is usually determined by the point when NOx approaches zero. If nothing is purposely added to a chamber and NOx measurements are made, very little if any NOx is seen because there is usually some radical concentration available to convert any residual NOx to NO_2 and then any hydroxyl radicals (OH) would rapidly convert the NO_2 to nitric acid. Hence the NOx measurements would show only a trace steady-state sum of NO and NO_2 (i.e. NOx) even though NOx might be off-gassing at a significant rate. Acetaldehyde provides some radicals by photolysis and OH radicals produce peroxyacetyl radicals from acetaldehyde. Hence, any NOx off-gassing leads to peroxyacetyl nitrate (PAN) formation. Most chemiluminescent NO_2 measurements include interference by PAN. Hence any off-gassing of NOx in the presence of acetaldehyde and ultraviolet

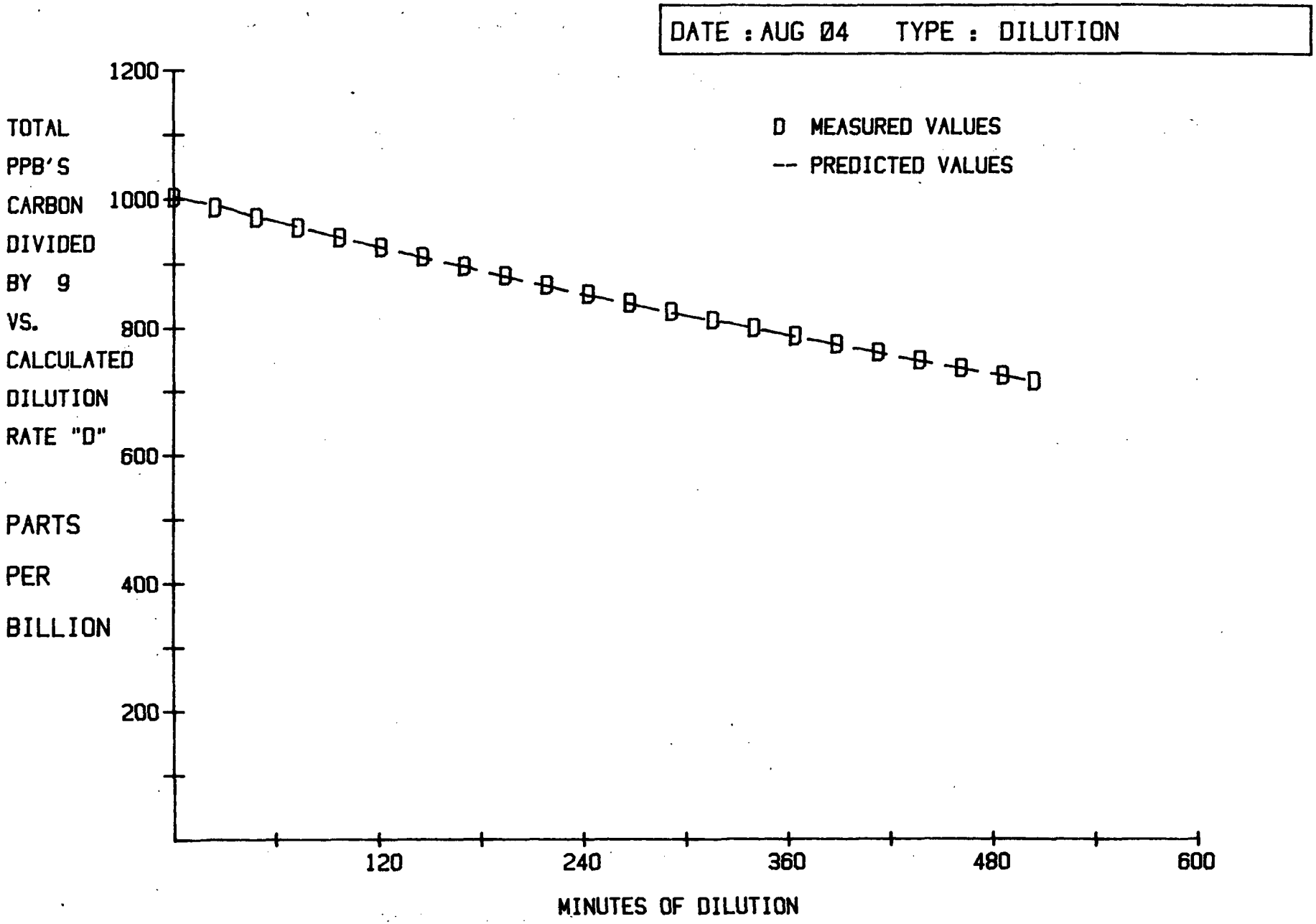

FIGURE VI.1 : EXPERIMENTAL VS. CALCULATED SMOG CHAMBER DILUTION COMPARISON

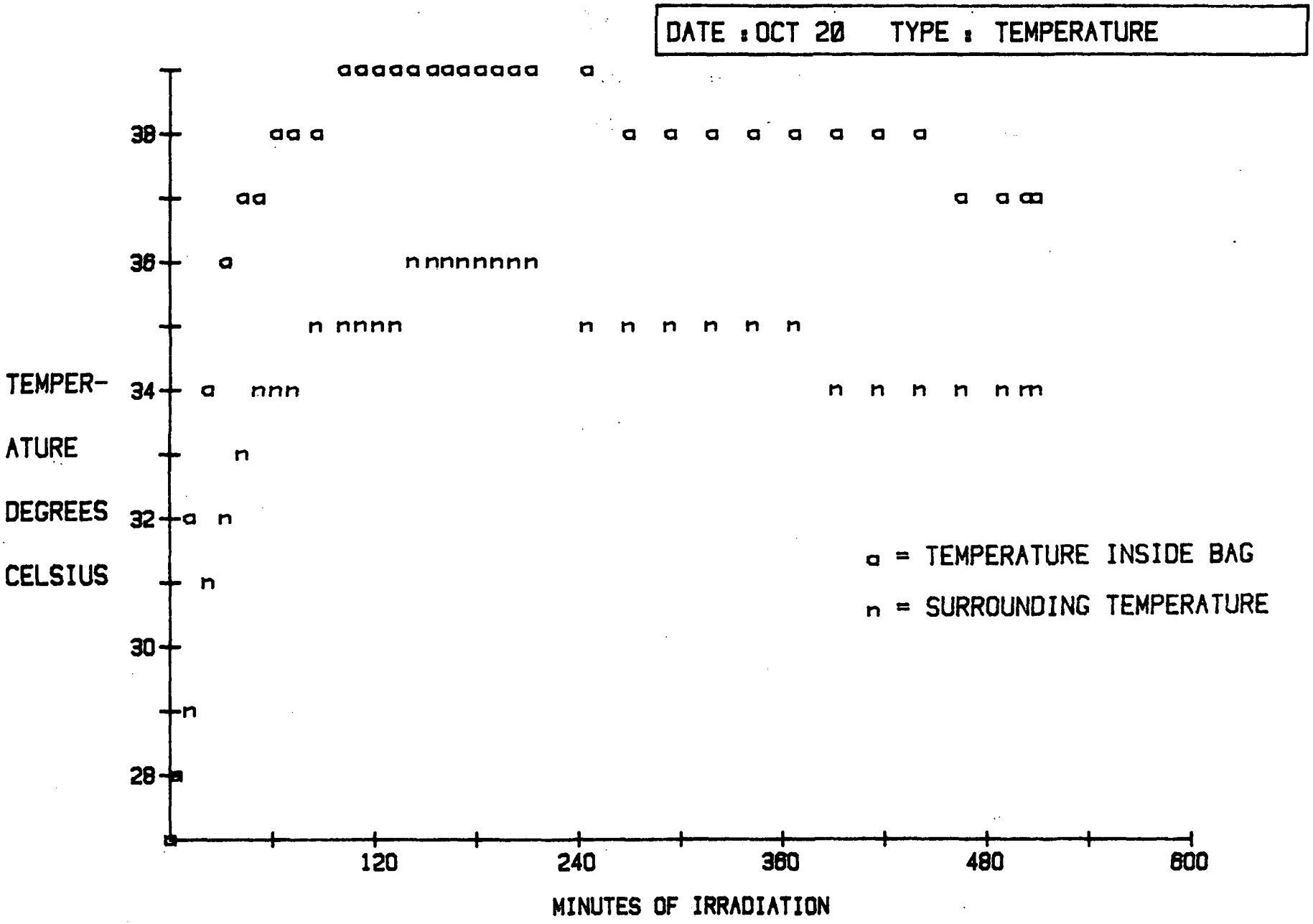

FIGURE VI.2 : TYPICAL TEMPERATURE PROFILE DURING SMOG CHAMBER EXPERIMENT

light would show a buildup of PAN and could be measured with a normal NO_2 detector. Figure VI.3 shows the acetaldehyde experiments performed recently which were modeled with acetaldehyde chemistry and a NOx off-gassing rate of only 0.04 ppb per minute. The modeled rate of NOx off-gassing is a low enough value to not seriously affect the results of this study and its value is consistent with other smog chambers.

Two types of experiments have been used to determine the organic and radical reactivity of the smog chamber. In the first experiment about 0.5 ppm of NO is the only precursor added to the chamber. Any observed conversion of NO to NO_2 would be caused by trace organics reacting in the presence of some source of radicals. The second experiment is the same except 50-100 ppm carbon monoxide (CO) is added. The CO supersedes any trace organic reactivity because CO reacts with OH to generate CO_2 and the hydroperoxy radical (HO_2) which in turn reacts with NO to give NO_2 and return the OH. Unlike most organics CO does not produce any products which can photolyze and provide radicals to sustain the smog chemistry associated with conversion of NO to NO_2. Hence the NO to NO_2 conversion in the CO experiment amplifies the source of radicals in the chamber. The experiment without the added CO shows the result of both the chamber radicals and the organic reactivity.

Figures VI.4 and VI.5 show the NOx and NOx plus CO experiments which were fitted using an assumed initial background level of formaldehyde of 0.04 ppm plus a trace of formaldehyde coming off the walls at a rate of 0.0002 ppm per minute, plus a conversion of NO_2 to nitrous acid (HONO) with a rate constant of 0.00024 per ppm per minute. This last value corresponds to a recently determined heterogeneous pathway studied by Sakamaki et al. [VI.1]. Such a reaction provides radicals from the subsequent fast photolysis of HONO to OH and NO. The use of assumed trace levels of formaldehyde is based on the work of Whitten, Killus, and Hogo [VI.2]. Such low levels of organic and radical species required to fit the chamber characterizations correspond to one of the lowest seen in smog chambers. Some recent data from a similar chamber at the University of California at Riverside required similarly low levels to simulate such experiments. The radical source strength corresponding to the formaldehyde off-gassing and heterogeneous NO_2 to HONO conversions is about 0.05 ppb per minute,

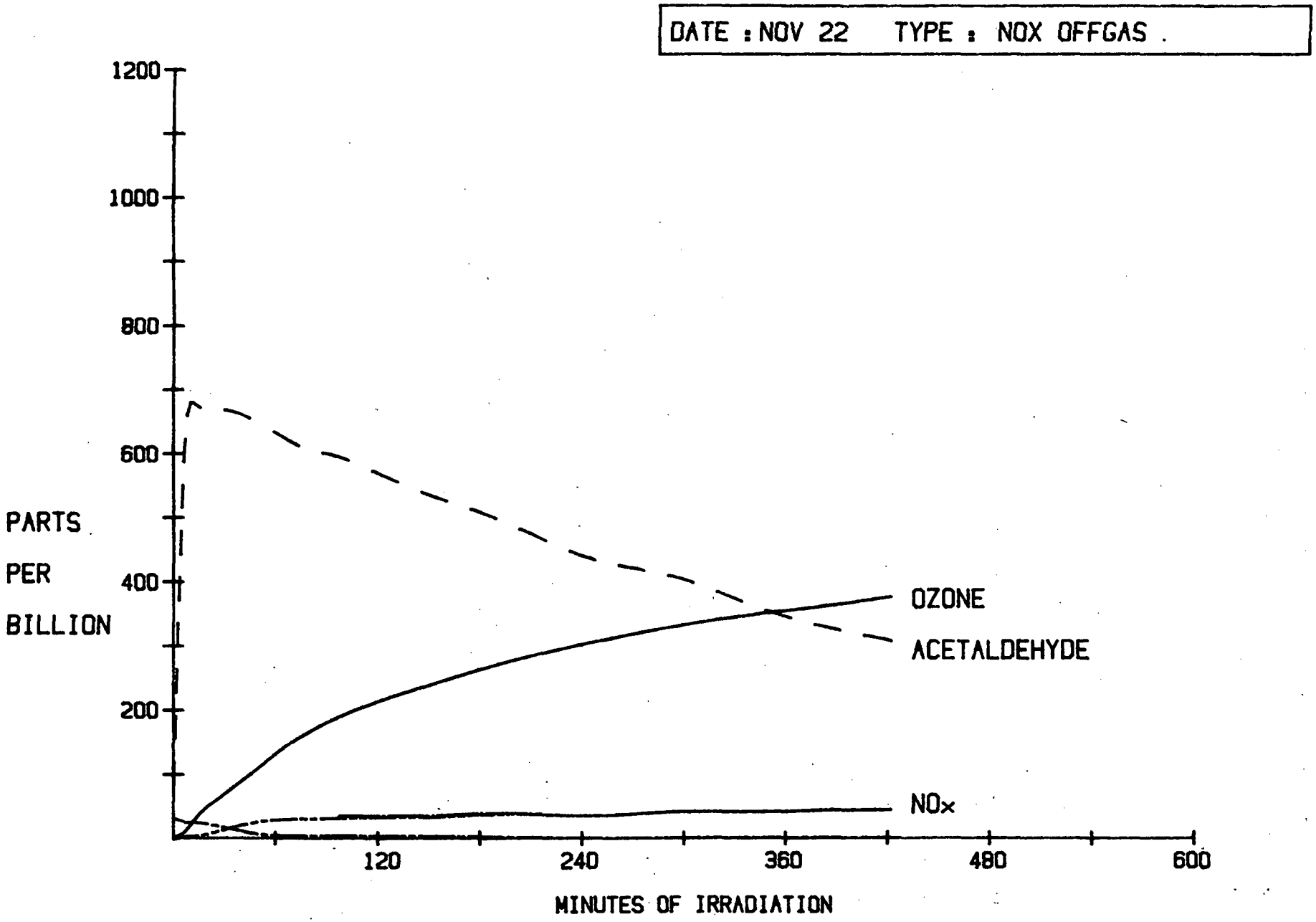

FIGURE VI.3 : ACETALDEHYDE CHARACTERIZATION TO MEASURE NOx OFFGASSING RATE

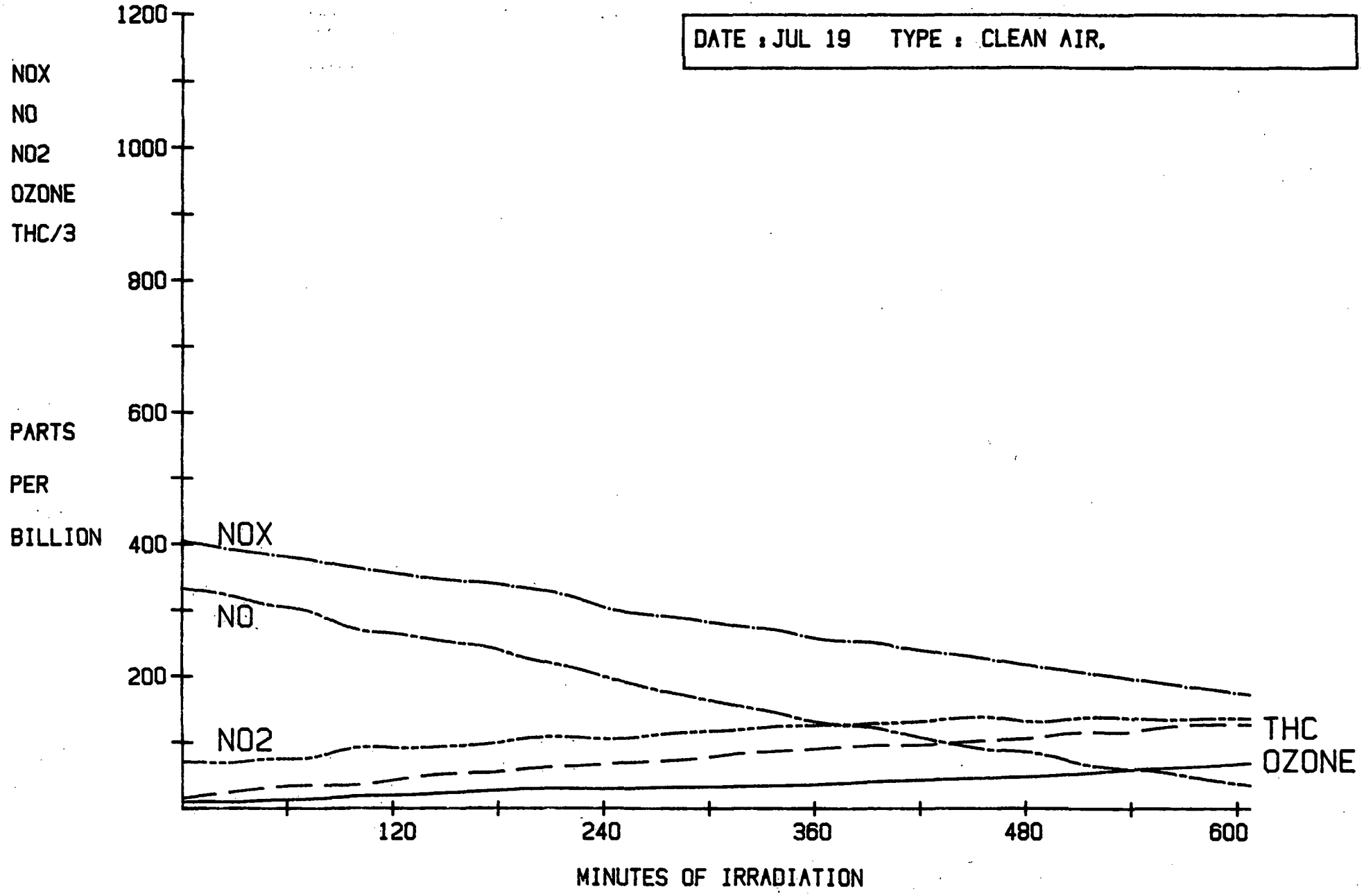

FIGURE VI.4 : CHARACTERIZATION EXPERIMENT USING CLEAN AIR AND NOX

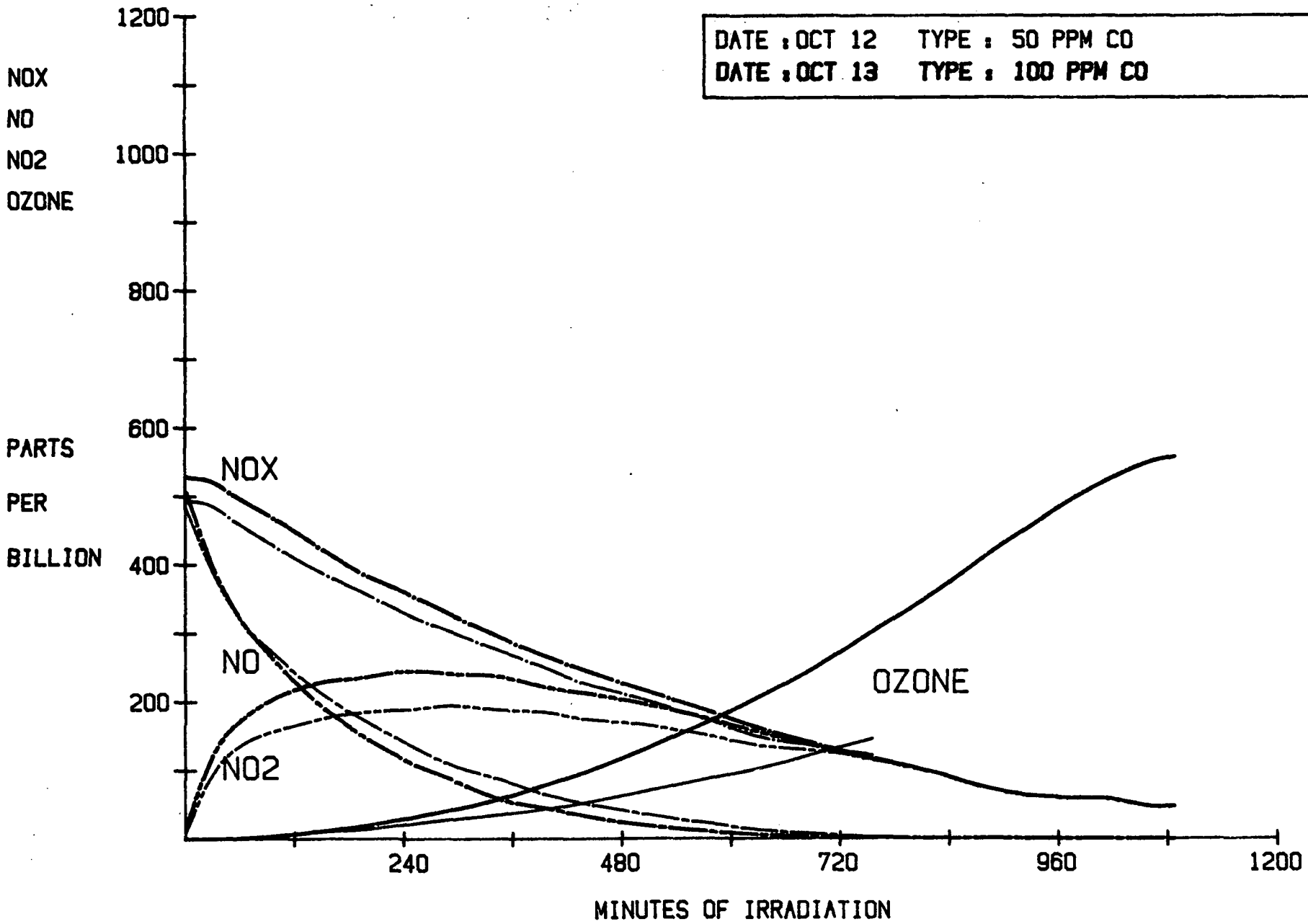

FIGURE VI.5 : CHARACTERIZATION EXPERIMENTS USING CARBON MONOXIDE AND NOX

well below the typical 1 ppb per minute or greater generated from the organics and their products used in the regular experiments.

A very important characteristic of the smog chamber is its ultraviolet light intensity. The solar simulation was provided by 84 blacklights (F30T8/350 Bl) and 18 sunlamps (FS20). The lamps were individually replaced over an 840 hour life cycle in order to control aging effects. The light must pass through "pyrex" glass windows which selectively attenuate the shorter wavelengths in the ultraviolet spectrum. The resulting spectral distribution of light intensity is analogous to that produced from sunlight after it passes through the earth's atmosphere.

Two photolysis reactions are of key importance in driving the photochemistry which produces urban ozone pollution. The first reaction is formaldehyde photolysis to yield radical products:

$$HCHO \xrightarrow{h\nu} 2HO_2 + CO \qquad \text{(VI.2)}$$

These products initiate radical chain reactions which further oxidize other hydrocarbons and eventually convert nitric oxide into nitrogen dioxide.

$$NO + HO_2 \longrightarrow NO_2 + OH \qquad \text{(VI.3)}$$

A series of propene/NOx characterization studies were performed in order to better understand the formaldehyde photolysis rate constant. Past modeling experience by SAI has shown this to be the most important factor for achieving a close simulation of observed chamber data (VI.3). Therefore, the formaldehyde photolysis constant was determined by fitting the propene experiments: these are shown in Fig. VI.6. The key formaldehyde constant for photolysis to radicals so determined was 0.0025 per minute, a fairly high value but not inconsistent with the mixture of blacklights and sunlamps used in this chamber. The photolysis constant to stable products from formaldehyde is not important to smog chemistry, but an equal value of 0.0025 per minute was used to be consistent. The smog chamber's formaldehyde photolysis rate constant is compared in Fig. VI.7 with the EPA's computed solar value for Los Angeles on June 26. There is a diurnal variation in sunlight intensity for formaldehyde photolysis which contrasts to the higher intensity but relatively constant chamber lights.

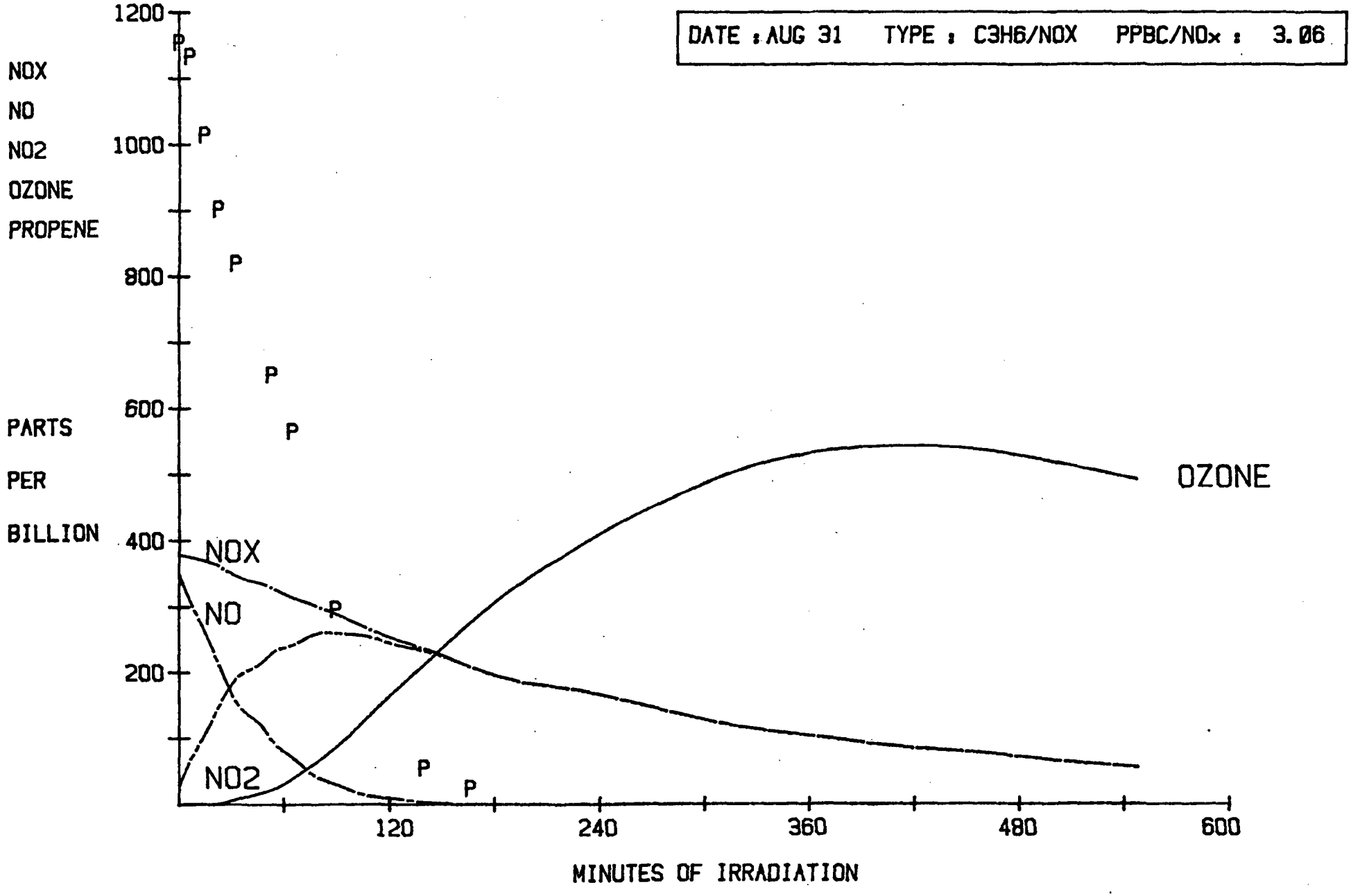

FIGURE VI.6 : PROPENE & NOX CHARACTERIZATION FOR FORMALDEHYDE PHOTOLYSIS

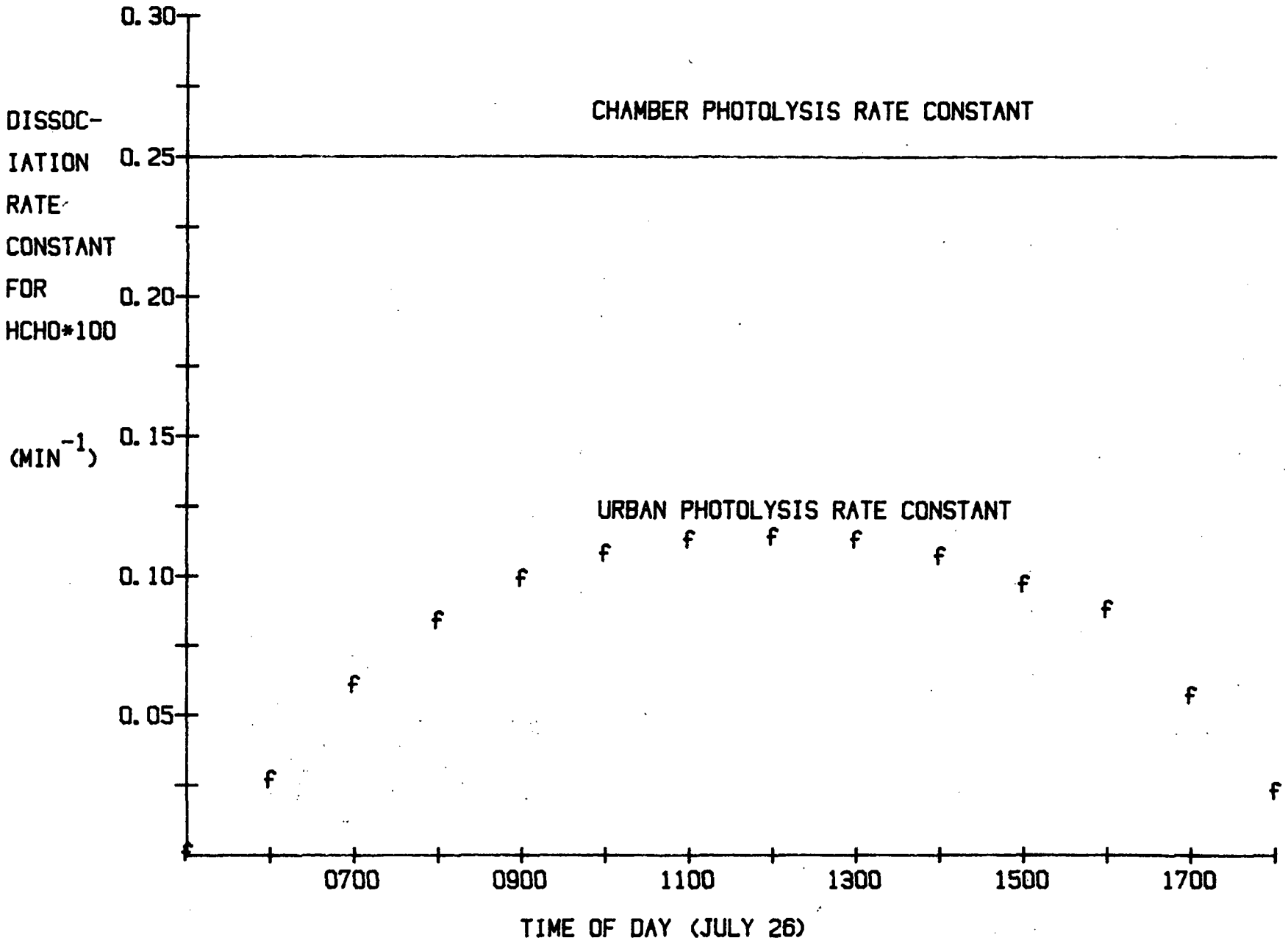

FIGURE VI.7 : EXPERIMENTAL & URBAN FORMALDEHYDE PHOTOLYSIS RATE CONSTANTS

The second photolysis characteristic of key importance is the dissociation rate constant for nitrogen dioxide:

$$NO_2 \xrightarrow{h\nu} NO + O \qquad \text{(VI.4)}$$

The method of Wu and Niki [VI.3] was used to determine the chamber's effective NO_2 dissociation rate. The measured value of 0.25 min^{-1} is compared in Figure VI.8 to the EPA's computed solar value for Los Angeles on June 26 [VI.4]. It is evident that the smog chamber's lights are less intense than mid-day urban sunlight for the photolysis of NO_2. The smog chamber, however, is used only to experimentally validate the chemistry of the hydrocarbon, alcohol and NOx surrogates under study. In this study the lower intensity but more constant chamber lights are treated accordingly when modeled. The chemical kinetic mechanism is subsequently used in an urban model which accurately represents the diurnal variations in the two photolysis rate constants discussed above.

The hydrocarbon surrogate mixture used in this study was designed to represent the current chemical classes of hydrocarbons in the South Coast Air Basin. It includes eight surrogate species rather than the two or four hydrocarbon surrogate blends used in previous studies. Table VI.1 lists the organic compounds and their relative carbon percentages within the surrogate mix.

Table VI.1 : Urban Hydrocarbon & Methanol Exhaust Surrogates

HYDROCARBON SURROGATES	CARBON %
ethene	5
propene	5
isobutene	15
n-butane	15
n-pentane	20
2,2,4-trimethyl pentane	15
toluene	12.5
m-xylene	12.5
METHANOL SURROGATES	
methanol	90
isobutene	10

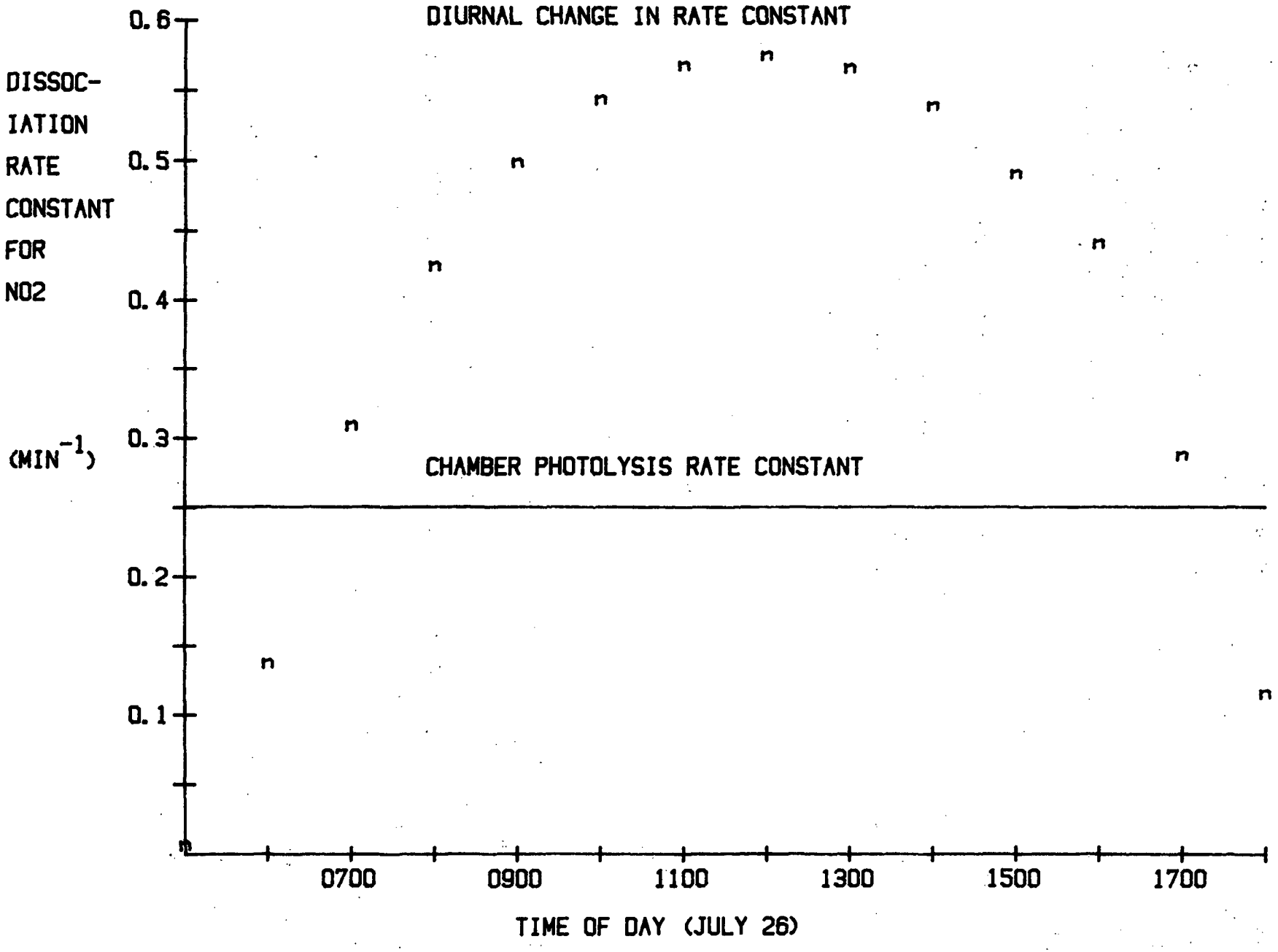

FIGURE VI.8 : EXPERIMENTAL & URBAN NITROGEN DIOXIDE PHOTOLYSIS RATE CONSTANTS

VI.5 EXPERIMENTATION

The experimental design is outlined in Table VI.2. The surrogate mixture of hydrocarbons was tested at three overall hydrocarbon (PPM carbon) to NOx ratios. Three sets of experiments were performed at each ratio: one with the full mixture (baseline), one with only two-thirds of the concentration (blank substitution), and one at two-thirds plus the remaining carbon concentraton substituted by a mixture of methanol and isobutene in a nine to one molar ratio (methanol substitution). Isobutene reacts rapidly to generate formaldehyde so the addition was equivalent to adding formaldehyde at the ten percent level to simulate exhaust from methanol vehicles.

Table VI.2 : Experimental Design & Initial Surrogate Concentrations

Experimental Conditions	PPM Carbon to Nox Ratio	NOx	8-Surrogate Urban Blend	Methanol Exhaust Surrogates
	3	1.2	3.6	0
Baseline	9	0.4	3.6	0
	27	0.4	10.8	0
Blank	2	1.2	2.4	0
Substitution	6	0.4	2.4	0
	18	0.4	7.2	0
Methanol	3	1.2	2.4	1.2
Substitution	9	0.4	2.4	1.2
	27	0.4	7.2	3.6

An example of a complete set of experimental measurements is plotted in Fig. VI.9. The initial reactant concentrations are shown at time zero on the left of the figure. Each of the eight urban surrogate hydrocarbons is represented by a letter symbol which is identified in the key at the upper right. Initial oxides of nitrogen (nitric oxide and nitrogen dioxide) are also plotted along with the photochemical products formaldehyde and ozone.

The observed change in concentration of each species is the result of both controlled dilution and photochemical reactions. The purpose of this experiment is to validate an evolving chemical kinetic mechanism which describes in detail the chemical reactions and their rates within the system under study. The chemical kinetic mechanism is then incorporated into a model of the physical

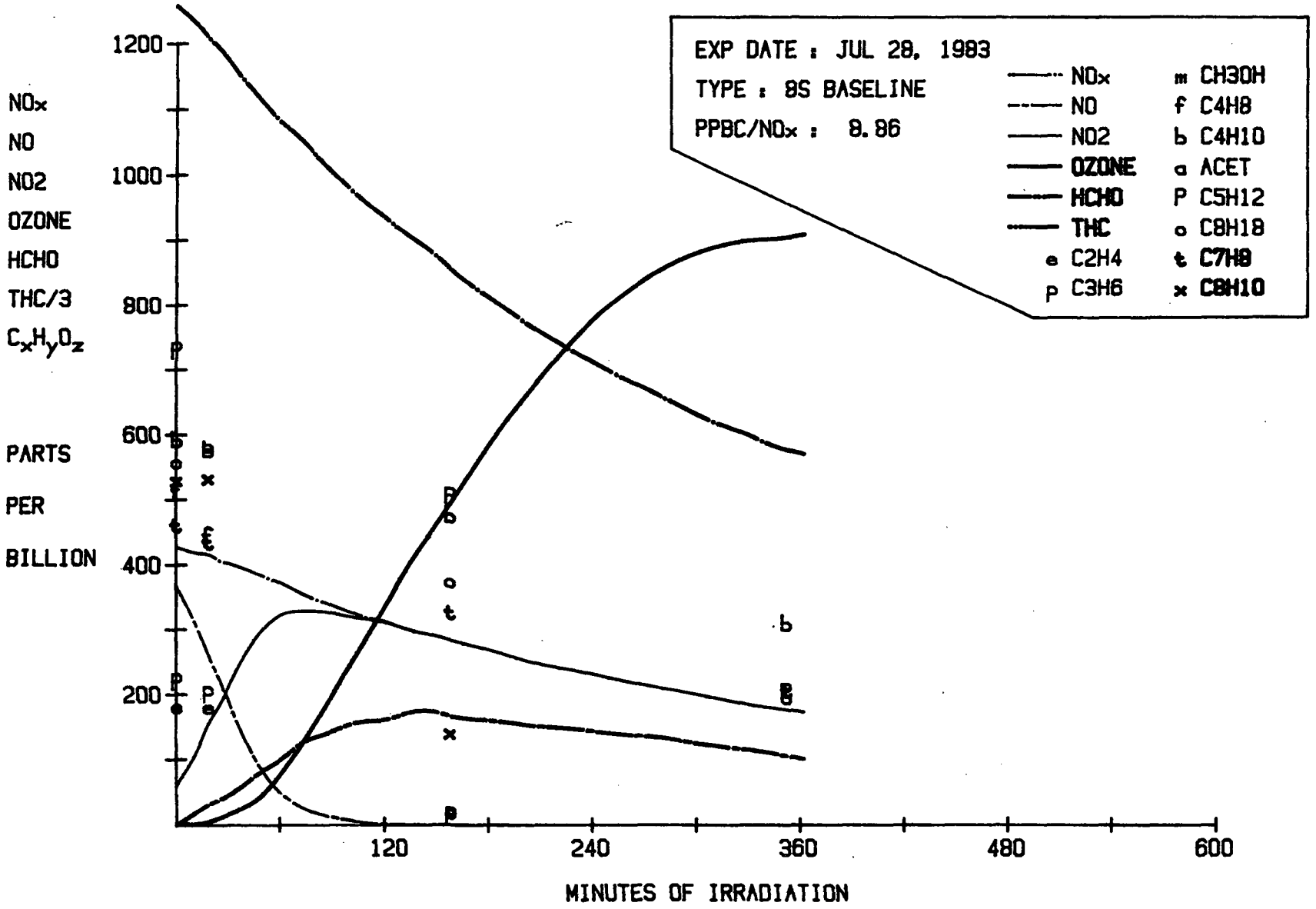

FIGURE VI.9 : REACTANT CONCENTRATIONS AND SMOG CHAMBER PRODUCTS OVER TIME

processes and emissions inventories of a specific urban setting for ozone modeling purposes. If the methanol substitution experiments produce results similar to the two-thirds level without methanol then one would conclude that methanol was inert. If the substitution experiments are the same or more reactive than the full concentration experiments then one should conclude that the methanol was as reactive or more reactive than the urban mixture.

The comparative set of experimental results at the lowest ppm carbon to NOx ratio concentration is presented in Fig. VI.10. Only nitric oxide, nitrogen dioxide and ozone are plotted for these experimental overlay comparisons. The evidence indicates that the methanol substitution experiment was very similar in reactivity to the blank substitution case. Therefore, at this low ppm carbon to NOx ratio the methanol exhaust surrogates were relatively inert and contributed very little to ozone production.

The nine to one ppm carbon to NOx ratio evidence is presented in Fig. VI. 11. The methanol substitution experiment was intermediate in reactivity at this reactant ratio. Methanol substitution contributed something to the conversion of nitric oxide into nitrogen dioxide and subsequently yielded more ozone than the blank substitution case. However, the substitution of methanol and isobutene (formaldehyde) produced a less reactive mixture and less ozone than the baseline urban surrogate case.

The twenty-seven to one ppm carbon to NOx ratio results are presented in Fig. VI.12. A very rapid conversion of nitric oxide into nitrogen dioxide was observed for both the baseline and the methanol substitution cases. After allowing for experimental uncertainties the ozone yield from the methanol substitution experiment was found not to be significantly greater than that from the baseline condition. Therefore, methanol substitution exhibited comparable reactivity at this very high reactant ratio. The pronounced effect of ppm carbon to NOx ratio on methanol's substitution reactivity is the subject of further analysis and future experimental work.

VI.6 CONCLUSIONS

The chemical kinetic mechanism derived from this experimental evidence is likely

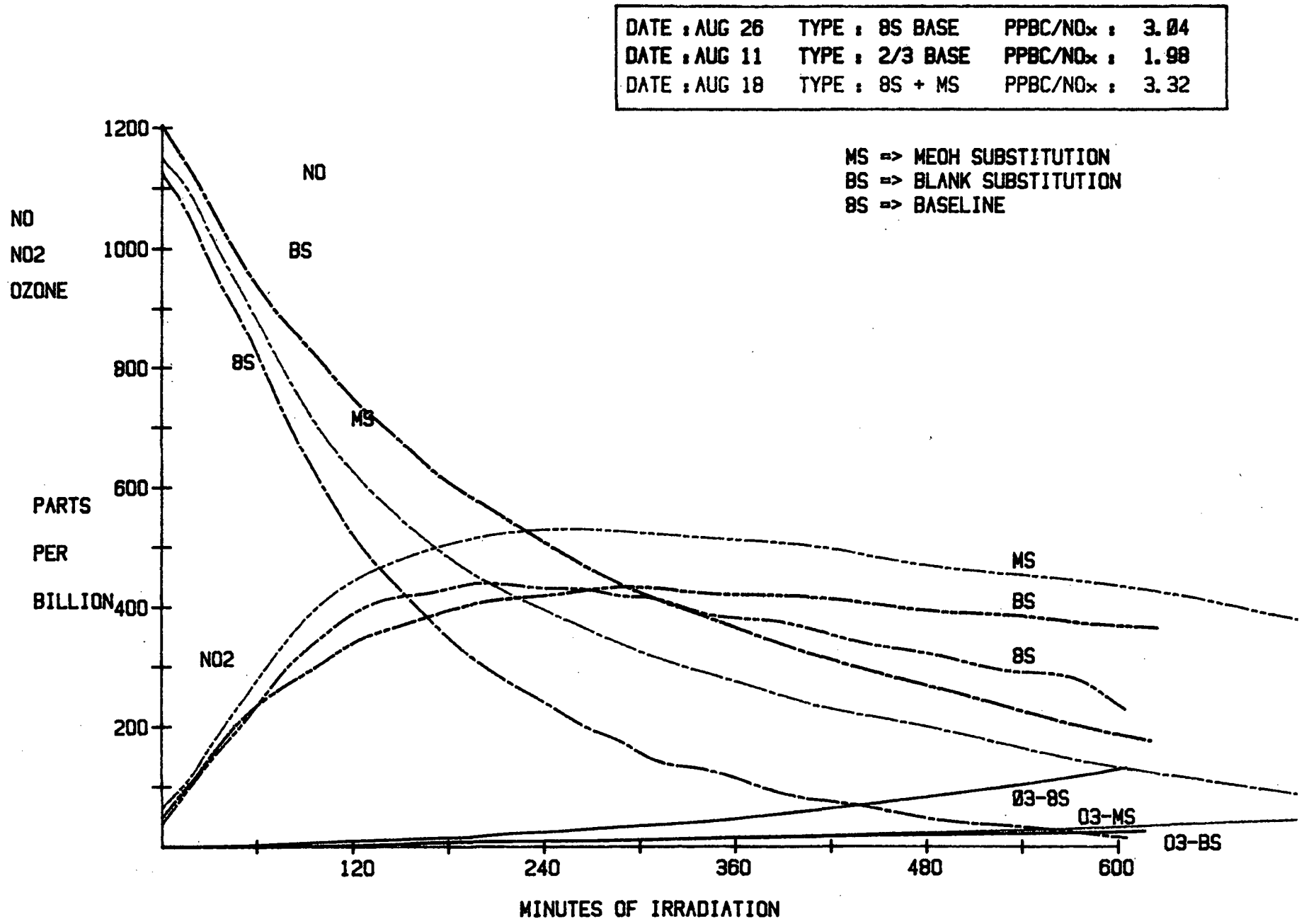

FIGURE VI.10 : BASELINE SURROGATES, 2/3 BASELINE & METHANOL SUBSTITUTION AT 3:1

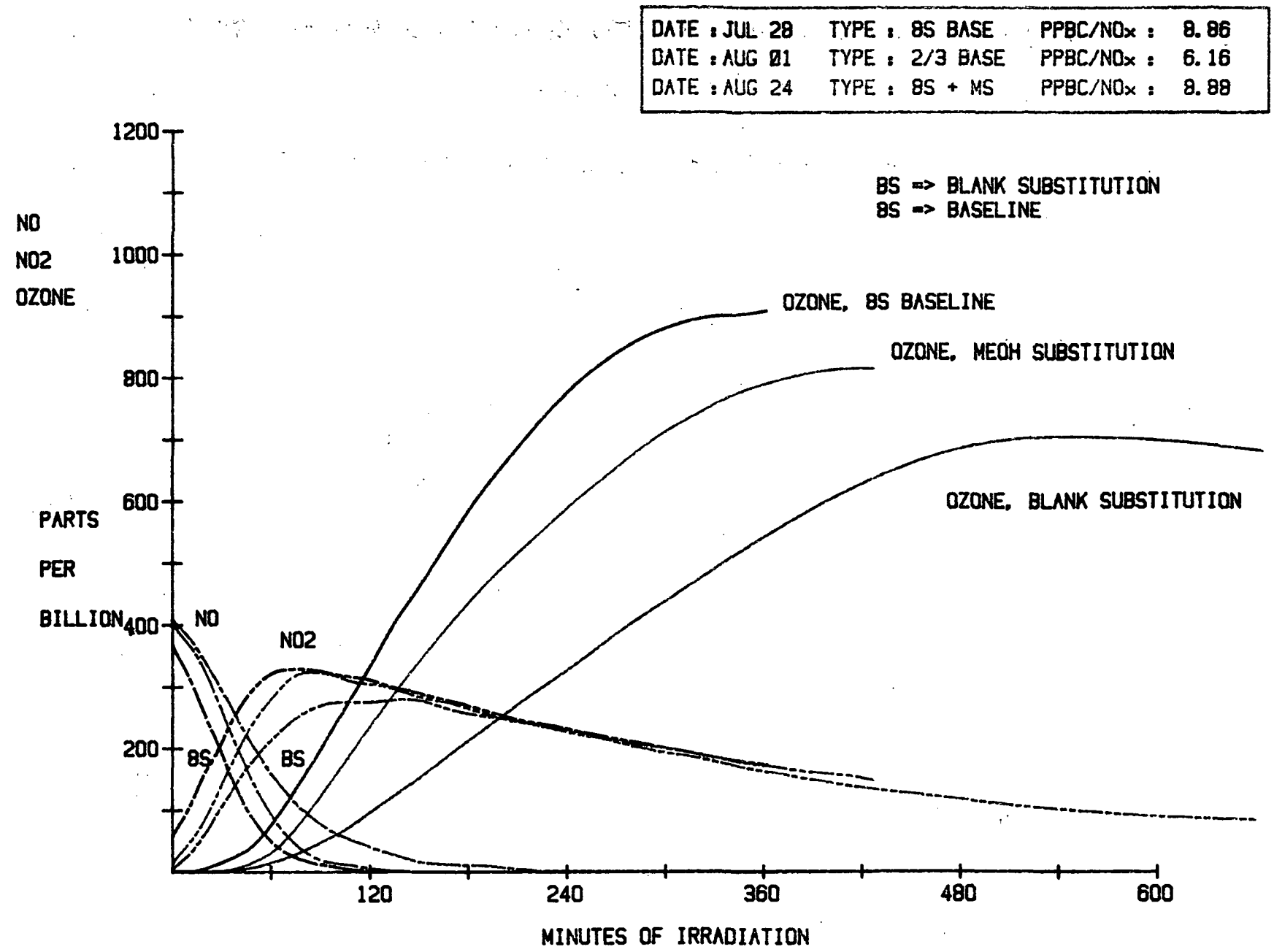

FIGURE VI.11 : BASELINE SURROGATES, 2/3 BASELINE & METHANOL SUBSTITUTION AT 9:1

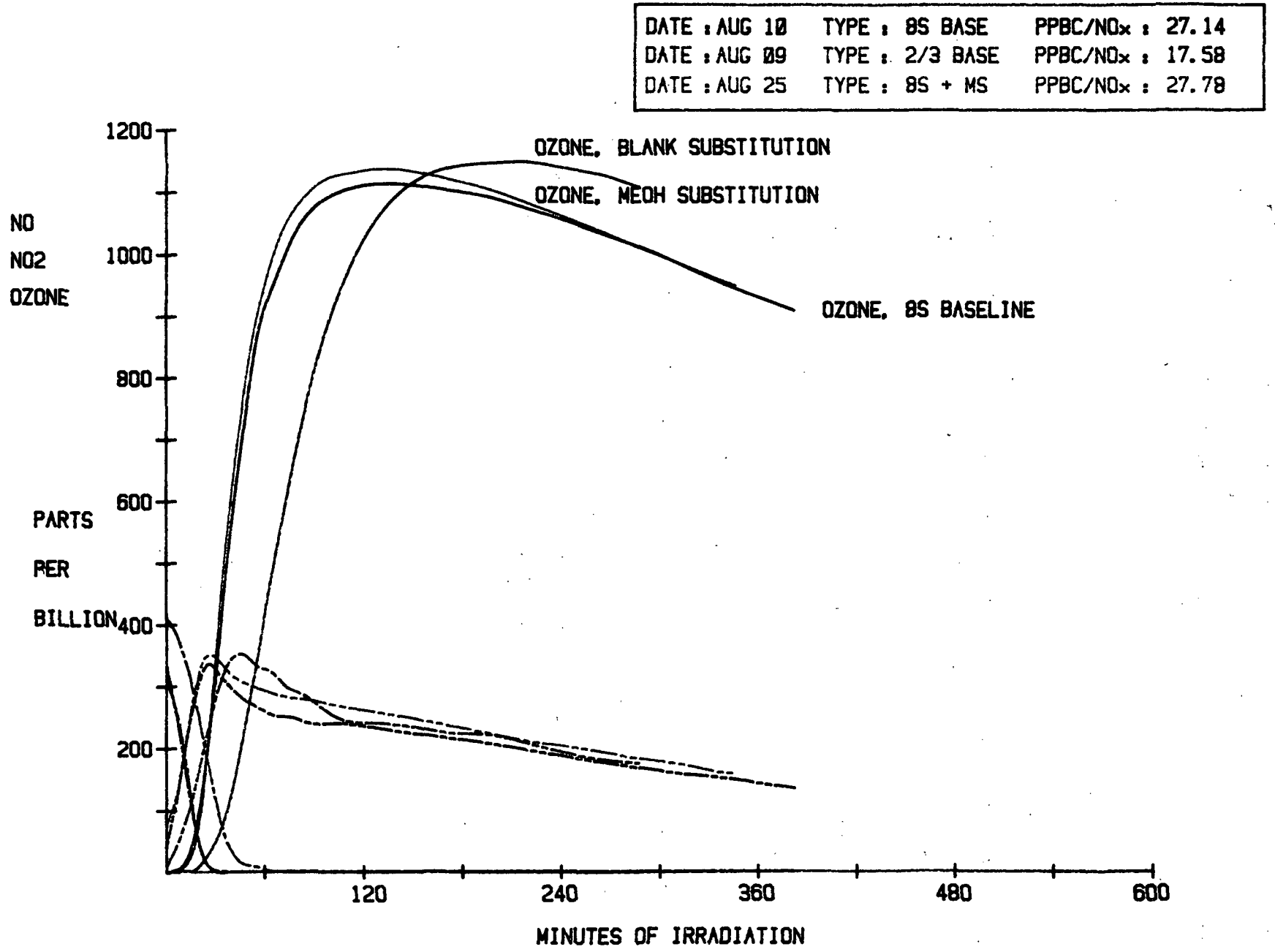

FIGURE VI.12 : BASELINE SURROGATES, 2/3 BASELINE & METHANOL SUBSTITUTION AT 27:1

to show strongly beneficial effects when incorporated into urban EKMA-type computer models. The reason is that, urban ppm carbon to NOx ratios in Los Angeles, for example, are currently in the nine to one range (the evidence in Fig. VI.11 is applicable). Existing plans and strategies for urban ozone control emphasize increased control of hydrocarbon emissions. Hence, the accelerated benefits of methanol sustitution at low ppm carbon to NOx ratios appears very promising as an urban ozone control strategy.

VI.7 REFERENCES

VI.1. Sakamaki, F., S. Hatakeyama and Y. Akimoto; "Formation of Nitrous Acid and Nitric Oxide in the heterogenous Dark Reaction of Nitrogen Dioxide and Water Vapor in a Smog Chamber," Int. J. Chem. Kinet., V.15, P.1013-1029; 1983.

VI.2. Whitten, G.Z., J.P. Killus and H. Hogo, "Modeling of Simulated Photochemical Smog with Kinetic Mechanisms," Vol 1. Final Report, EPA-600/3-80-028a, U.S. Enviornmental Protection Agency, Office of Research and Deelopment, Research Traingle Park, North Carolina, 1980.

VI.3. Wu, C.H. and H. Niki, "Methods for Measuring NO_2 Photolysis Rate," Environ. Sci. Technol., Vol. 9; P.46; 1975.

VI.4. Schere, K.L. and K.L. Demerjian, "Calculation of Selected Photolytic Rate Constants over a Diurnal Range," EPA-600/4-77-015, U.S.E.P.A., 1977.

1. Report No.	2. Government Accession No.	3. Recipient's Catalog No.

4. Title and Subtitle
Research and Development of Neat Alcohol Fuel Usage in Automobiles

5. Report Date
June 1984

6. Performing Organization Code

7. Author(s)
Pefley, R.K., Browning, L., Espanola, S., Pullman, B., Gururangan, R., Saito, N.

8. Performing Organization Report No.
ME84-1

10. Work Unit No.

9. Performing Organization Name and Address
The University of Santa Clara
Mechanical Engineering Research Department
Santa Clara, California 95053

SC188052

11. Contract or Grant No.
NASA Lewis Contract NAG-3-143

13. Type of Report and Period Covered

12. Sponsoring Agency Name and Address
NASA Lewis Research Center
21000 Brookpark Road
Cleveland, OH 44135

14. Sponsoring Agency Code

15. Supplementary Notes

16. Abstract

The study is an extension of previous work. Its topical coverage ranges from research in the forms of experimental operation of engines in cold chambers and a photochemical smog chamber with allied computer modeling of the thermofluid mechanics of cold engine starting and photochemical smog through engine corrosion and wear studies, to vehicle operation, which includes a description of the engineering development of after-market conversion kits to change Ford Pinto vehicles from gasoline to alcohol. Although further research is recommended, evidence presented contributes positively to the view that it is feasible to operate neat alcohol fleets in the range of 1000-10,000 vehicles, without major operational difficulties and without exacerbating the environmental, health and safety risks associated with petroleum fuels.

17. Key Words (Suggested by Author(s))
Methanol
Fuel
Cold Start
Emissions
Smog
Corrosion and Wear

18. Distribution Statement
Approved for public release; distribution unlimited

19. Security Classif. (of this report)	20. Security Classif. (of this page)	21. No. of Pages	22. Price*
Unclassified	Unclassified		

* For sale by the National Technical Information Service, Springfield, Virginia 22161

NASA-C-168 (Rev. 10-75)

* U.S. GOVERNMENT PRINTING OFFICE: 1984-461-208:11200

UNITED STATES
DEPARTMENT OF ENERGY
WASHINGTON, D.C. 20585

OFFICIAL BUSINESS
PENALTY FOR PRIVATE USE, $300

POSTAGE AND FEES PAID
U.S. DEPARTMENT OF ENERGY
DOE 350

THIRD CLASS MAI